

“A Macroscopic and Microscopic Investigation of the Magnesite – Otavite Solid Solution”

Von der Fakultät für Biologie, Chemie und Geowissenschaften der
Universität Bayreuth

Zur Erlangung des akademischen Grades
Doktor der Naturwissenschaften
-Dr. rer. nat.-

genehmigte Dissertation

vorgelegt von

Fiona Bromiley

Bayreuth, 2004

Table of Contents

Abstract	1
Zusammenfassung	5
1. Introduction	10
1.1 Carbonates in the Earth.....	11
1.1.1 Carbon Recycling and Carbonate Stability.....	11
1.1.2 Carbon Dioxide Sequestration.....	13
1.2 The Magnesite – Calcite System.....	14
1.3 The Magnesite – Otavite System as an Analogue.....	20
1.3.1 The Experimental Work.....	20
1.4 The Modelling Work.....	24
1.5 The Effects of Strain and Elasticity on Solid Solutions.....	30
1.5.1 Autocorrelation Studies.....	31
1.6 Aims of the Study.....	35
2. Synthesis and Experimental Techniques	37
2.1 Synthesis Techniques.....	37
2.1.1 Starting Materials.....	37
2.1.2 Addition of Silver Oxalate as a CO ₂ Source.....	38
2.1.3 Piston Cylinder Apparatus and Method.....	40
2.1.4 Synthesis Conditions.....	44
2.2 X-ray Powder Diffraction.....	45
2.3 Rietveld Analysis and Refinement.....	45
2.4 Infrared Powder Absorption Spectroscopy.....	47
2.4.1 Analysis of IR Powder Absorption Spectra.....	48
2.4.2 Autocorrelation Analysis.....	49
2.5 Quantitative Determination of Sample Composition.....	50

3. X-ray Diffraction and Rietveld Analysis	51
3.1 Results from X-ray Powder Diffraction.....	51
3.2 The Rietveld Analysis.....	55
3.2.1 Lattice Parameters.....	58
3.2.2 Atomic Position Parameters.....	65
3.2.3 Inter-atomic Distances.....	68
3.2.4 Site Occupancies.....	74
3.3 Degree of Order from X-ray Intensities.....	81
3.4 Order-Disorder Behaviour.....	84
4. Infra-red Powder Absorption Spectroscopy	86
4.1 IR Spectra.....	86
4.2 The Modal Behaviour.....	93
4.3 Carbonate Group Internal Modes.....	97
4.4 Autocorrelation Results.....	99
5. Discussion and Conclusions	107
5.1 Phase Stability in the Otavite – Magnesite System.....	107
5.2 Variation of Unit-cell Lattice Parameters, Atomic Positions and Inter-atomic Distances.....	111
5.2.1 Variation of Unit-cell Lattice Parameters.....	111
5.2.2 Variation of Atomic Positions.....	113
5.2.3 Variation of Inter-atomic Distances.....	115
5.3 The Order Parameter and the Order-Disorder Phase Transition.....	117
5.3.1 The Phase Transition.....	118
5.4 Macroscopic versus Microscopic Behaviour.....	121
5.5 Comparison of Mixing and Ordering Behaviour of Carbonates and Silicates.....	126
5.6 The Magnesite – Otavite System as an Analogue to the Magnesite – Calcite System.....	127

6. References	130
7. Appendices	137
Appendix 1: X-ray Diffraction Patterns and IR Spectra for Starting Materials.....	137
Appendix 2: Experiments Performed.....	139
Appendix 3: IR Powder Absorption Spectra to Establish Optimum Grinding Time.....	143
Appendix 4: X-ray Diffraction Pattern and IR Spectrum for Brucite.....	144
Appendix 5: Rietveld Refinement Patterns.....	145
Erklärung	163

Acknowledgements

There are many people I wish to thank for their help and support while I have been at the BGI. Doing my PhD at the BGI has been a great experience, as has living in Bayreuth, and I shall never forget my time here.

Part of the work for my PhD was done at the Earth Sciences Department at the University of Cambridge. I want to thank Ming Zhang for all his help while I was there, and for teaching me how to make great pellets! I would also like to thank Michael Carpenter for all the interesting and helpful discussions and suggestions.

Within the BGI there are several people I would very much like to thank;
Firstly, I would like to thank Fritz for being my official supervisor. I gained a lot from the discussions we had and your suggestions always helped me to go one step further.
I would like to thank Burkhard, who helped me get started with the syntheses and was always a mine of information regarding experimental problems and procedures.
Thanks to Diego, my “GSAS guru”, for always coming up with a solution.
Thanks to Geoff in a professional capacity for all your help in the piston cylinder lab.

The person I owe most to in the institute is Tiziana. I’m sorry that the system doesn’t recognise you for all the work you have put into being my supervisor!
You really have helped me to develop both as a scientist, and a person while I have been here, and I think, if it is possible, you have even made me less English! Grazie mille cara!

Finally, to Geoff. What would I do without you (and DBDFBM of course!)? You are always there for me and I am truly grateful for everything. I love you.

Vollständiger Abdruck der von der Fakultät für Biologie, Chemie und Geowissenschaften der Universität Bayreuth genehmigten Dissertation, zur Erlangung des akademischen Grades Doktors der Naturwissenschaften (Dr. rer. nat.).

Prüfungsausschuss:

Prof. J. Breu, Universität Bayreuth	(Vorsitzender)
Prof. F. Seifert, Universität Bayreuth	(1. Gutachter)
Prof. M.A. Carpenter, University of Cambridge	(2. Gutachter)
Dr. L.S. Dubrovinsky, Universität Bayreuth	
Prof. U. Galtzel, Universität Bayreuth	

Datum der Einreichung der Dissertation:	5. Juli 2004
---	--------------

Datum des wissenschaftlichen Kolloquiums:	9. Dezember 2004
---	------------------

Abstract

The magnesite (MgCO_3) – calcite (CaCO_3) system is the most geologically important of the carbonate minerals. At intermediate compositions a distinct ordered phase exists, dolomite [$\text{MgCa}(\text{CO}_3)_2$], which has $R\bar{3}$ symmetry. A complete, disordered ($R\bar{3}c$ symmetry) solid solution exists, but at temperatures in excess of 1400°C . The processes driving the order-disorder phase transition, and the effects of cation substitution, are important for elucidating the behaviour of the system. Unmixing and ordering processes that occur at high temperatures in the magnesite – calcite system make experimental work difficult. However, the use of an analogue system allows syntheses under more accessible experimental conditions. The effects of cation substitution and ordering in the magnesite (MgCO_3) – otavite (CdCO_3) solid solution have, therefore, been investigated using X-ray powder diffraction and Hard Mode Infrared Spectroscopy (HMIS). The samples studied have been synthesised in piston cylinder apparatus at 1 GPa in the temperature range $500\text{--}800^\circ\text{C}$ for run durations of 1–120 hours. A complete, disordered solid solution, with $R\bar{3}c$ symmetry, was obtained at 800°C , whereas ordered samples in the cadmium dolomite stability field, with $R\bar{3}$ symmetry, were obtained at intermediate compositions in the temperature range $500\text{--}650^\circ\text{C}$.

(1) X-ray powder diffraction and Rietveld analysis

The macroscopic behaviour of the magnesite – otavite solid solution has been characterised using X-ray powder diffraction. The results from Rietveld refinements of the X-ray powder diffraction data show that the variation of the a -axis is linear as a function of composition and is not affected by different degrees of order at intermediate compositions. However, the c -axis shows a positive deviation from linearity as a function of composition for the 800°C series. The observed deviation decreases with increasing degree of order for samples of composition $\text{Mg}_{0.5}\text{Cd}_{0.5}\text{CO}_3$.

Atomic positions, inter-atomic distances and site occupancies were also determined from Rietveld refinements. Oxygen-carbon-oxygen bond angles for samples with $R\bar{3}$ symmetry showed a decrease in bond angle from 120° (constrained by symmetry in

samples with the $R\bar{3}c$ structure) with increase in degree of order. Site occupancies were used to determine the long-range order parameter, Q , for samples with $R\bar{3}$ symmetry. The square of the order parameter varies linearly as a function of temperature, suggesting a second-order phase transition, and a critical transition temperature of $T_c = 719^\circ\text{C}$.

Intensity ratios between reflections present only in the low symmetry phase ($R\bar{3}$) and reflections present in both the low and high symmetry phases can be used to determine a value proportional to the square of the long-range order parameter, Q . Intensity ratios, between the (101) and (202) reflections for samples of composition $\text{Mg}_{0.5}\text{Cd}_{0.5}\text{CO}_3$, were determined from X-ray powder diffraction patterns and show a linear variation as a function of temperature, with a critical transition temperature, $T_c = 716^\circ\text{C}$. The linear relationship between the intensity ratio and the square of the long-range order parameter, Q , confirms the consistency of the results obtained and the quality of the site occupancies obtained from Rietveld refinements.

(2) Infrared Powder Absorption Spectroscopy

The local mixing and ordering behaviour of the magnesite – otavite solid solution has been characterised using infrared powder absorption spectroscopy. Potassium bromide and polyethylene pellets were used as matrix materials for the measurements taken over three spectral regions; $50\text{-}350\text{cm}^{-1}$ (PE pellets), $350\text{-}500\text{cm}^{-1}$ (KBr pellets), $500\text{-}4000\text{cm}^{-1}$ (KBr pellets). Vibrational modes due to cations on the octahedral sites are present at the lowest frequency of the spectral regions investigated. All other vibrational bands can be assigned to vibrations of the carbonate group.

Phonon bands due to cadmium-oxygen translations ($75\text{-}200\text{cm}^{-1}$), and magnesium-oxygen translations ($200\text{-}350\text{cm}^{-1}$) were both observed in the IR spectra for samples of intermediate composition. A Lorentzian peak fitting routine was used to determine band positions for both sets of bands. Band positions for cadmium-oxygen translations remained constant as a function of composition, whereas band positions for magnesium-oxygen translations showed a decrease in wavenumber as a function of composition. This suggests that the magnesite – otavite solid solution displays a combination of one-mode and two-mode behaviour at low frequencies, which may be due to the difference in atomic weight between magnesium and cadmium.

Vibrational bands in the spectral regions $350\text{-}550\text{cm}^{-1}$ (libration and translation of carbonate groups) and $650\text{-}900\text{cm}^{-1}$ (doubly degenerate in-plane bending and out-of-plane bending of carbonate groups) vary linearly as a function of composition and no effect of order on band position is observed. In the region $1000\text{-}1800\text{cm}^{-1}$, the phonon mode is due to doubly degenerate asymmetric stretching of the carbonate groups. The samples with $R\bar{3}c$ symmetry (800°C series) show a linear shift in band position as a function of composition, whereas, samples in the cadmium dolomite stability field, with $R\bar{3}$ symmetry, show a marked increase in frequency compared to their $R\bar{3}c$ symmetry counterparts. Since carbonate groups for samples with $R\bar{3}$ symmetry are non-planar, as determined from Rietveld refinements, it appears that more energy is required for asymmetric stretching, with a consequent shift in band position to higher wavenumbers with respect to the planar carbonate groups in samples with $R\bar{3}c$ symmetry.

(3) Autocorrelation Results

Cation substitution, or disordering causes broadening of IR vibrational bands for a given material. It is not always possible, however, to determine the line width of complex IR spectra using conventional fitting procedures. In this study an alternative method was used, which makes use of the autocorrelation function to establish average line widths for six spectral regions; $75\text{-}200\text{cm}^{-1}$, $200\text{-}350\text{cm}^{-1}$, $300\text{-}550\text{cm}^{-1}$, $700\text{-}800\text{cm}^{-1}$, $800\text{-}900\text{cm}^{-1}$ and $1000\text{-}1800\text{cm}^{-1}$. The autocorrelation results, Δcorr , can be interpreted in terms of local strain fields present in the structure due to cation substitution and disordering.

In the low frequency region, the Δcorr values show a positive deviation from linearity as a function of composition. For samples of composition $\text{Mg}_{0.5}\text{Cd}_{0.5}\text{CO}_3$ the Δcorr values are virtually all the same, independent of the degree of order. This suggests that the local heterogeneities within the samples, due to cation substitution, remain constant with varying degrees of order at a length scale of a few unit-cells. It also appears that the magnesite structure is able to accommodate cadmium atoms more readily than the otavite structure can accommodate magnesium atoms. Over all the spectral regions, the addition of 10mol% MgCO_3 (1 Mg atom every 2 unit cells) to the otavite results in a large

increase in line width. It is, therefore, suggested that the strain fields surrounding the substituting magnesium atoms into the otavite structure are on the order of 30\AA .

In the region $800\text{-}900\text{cm}^{-1}$ and at a composition of $\text{Mg}_{0.5}\text{Cd}_{0.5}\text{CO}_3$, an effect of order is observed as a reduction in Δcorr values with respect to the sample with $R\bar{3}c$ symmetry. The difference in Δcorr values between the ordered and disordered samples was used to determine the local-order parameter, q , which scales linearly with the long-range order parameter, Q , suggesting that the ordering process is the same on both macroscopic and microscopic length scales, since at low frequencies only cation substitution has a measurable effect on the line broadening.

Zusammenfassung

Das Magnesit (MgCO_3) – Kalzit (CaCO_3) System ist die geologisch wichtigste Mischkristallreihe der Karbonatminerale. Bei mittleren Zusammensetzungen existiert in diesem System eine bestimmte, geordnete Phase, Dolomit ($\text{CaMg}(\text{CO}_3)_2$), die die Kristallsymmetrie $R\bar{3}$ besitzt. Eine komplette, ungeordnete Mischkristallreihe (Kristallsymmetrie $R\bar{3}c$) existiert nur bei Temperaturen über 1400°C . Die Prozesse, die den Übergang von geordneten zu ungeordneten Phasen steuern, und die Auswirkungen der Kationensubstitution sind wichtig um das Verhalten dieses Systems zu verstehen. Entmischungen und Ordnungsvorgänge gehen im Magnesit – Kalzit System bei sehr hohen Temperaturen vor sich und machen daher eine experimentelle Arbeit schwierig. Die Untersuchung eines Analogsystems erlaubt jedoch die Synthese entsprechender Proben bei einfacher zugänglichen experimentellen Bedingungen. Die Auswirkungen der Kationensubstituierung und -ordnung wurden daher in der Magnesit (MgCO_3) – Otavit (CdCO_3) Mischkristallreihe mithilfe von Röntgenpulverdiffraktometrie und Hard Mode Infrarotspektroskopie (HMIS) untersucht. Die Proben wurden in der Stempel-Zylinder-Presse bei einem Druck von 1 GPa im Temperaturbereich von 500 bis 800°C für die Dauer von 1 bis 120 Stunden synthetisiert. Bei einer Temperatur von 800°C wurde eine komplette, ungeordnete Mischkristallreihe mit der Kristallsymmetrie $R\bar{3}c$ erzeugt, während im Temperaturbereich von 500 bis 650°C für gemischte Zusammensetzungen geordnete Kristalle im Cadmium-Dolomit Stabilitätsfeld mit der Symmetrie $R\bar{3}$ auftraten.

(1) Röntgenpulverdiffraktometrie und Rietveldanalyse

Das makroskopische Verhalten der Magnesit – Otavit Mischkristallserie wurde mithilfe von Röntgenpulverdiffraktometrie untersucht. Die Resultate der Rietveldanalyse der Röntgenpulverbeugungsdaten zeigen, dass die Änderung der a -Achse immer linear mit der Änderung der Zusammensetzung einhergeht, und nicht durch den unterschiedlichen Ordnungsgrad bei mittleren Zusammensetzungen beeinflusst wird. Die c -Achse jedoch zeigt eine positive Abweichung von der linearen Abhängigkeit von der Zusammensetzung bei der Temperatur von 800°C . Die beobachtete Abweichung

verringert sich mit ansteigendem Ordnungsgrad bei Proben der Zusammensetzung $\text{Mg}_{0.5}\text{Cd}_{0.5}\text{CO}_3$.

Die Atompositionen, interatomare Abstände und Gitterplatzbelegungen wurden ebenfalls anhand von Rietveldanalysen bestimmt. Sauerstoff-Kohlenstoff-Sauerstoff Bindungswinkel für Proben mit der Kristallsymmetrie $R\bar{3}$ zeigen eine Verringerung des 120° Winkels (der in der Kristallsymmetrie $R\bar{3}c$ festgeschrieben ist) mit ansteigendem Ordnungsgrad. Die Gitterplatzbelegungen wurden dazu benutzt, für Proben mit der Symmetrie $R\bar{3}$ den Fernordnungsparameter Q zu bestimmen. Das Quadrat dieses Fernordnungsparameters Q steht in linearer Beziehung zur Änderung der Temperatur, was für eine Phasenumwandlung zweiter Ordnung spricht, die bei einer kritischen Umwandlungstemperatur (T_c) von 719°C auftritt.

Intensitätsverhältnisse zwischen Röntgenbeugungsreflexen, die nur in der niedrig symmetrischen Phase ($R\bar{3}$) auftreten, und solchen, die sowohl in der niedrig als auch der höher symmetrischen Phase existieren, können dazu verwendet werden, einen Wert zu bestimmen, der proportional zum Quadrat des Fernordnungsparameters Q ist. Die Intensitätsverhältnisse der (101) und (202) Reflexe wurden daher aus den Röntgenpulverdiffraktogrammen bestimmt. Die Intensitätsverhältnisse ändern sich linear als Funktion der Temperatur, wobei die kritische Umwandlungstemperatur bei 716°C liegt. Die lineare Beziehung zwischen den Intensitätsverhältnissen und dem Quadrat des Fernordnungsparameters Q belegt die interne Übereinstimmung der Resultate sowie die Qualität der Werte für die Gitterplatzbelegung, die aus den Rietveldanalysen gewonnen wurden.

(2) Infrarotabsorptionsspektroskopie an Pulvern

Das lokale Mischungs- und Ordnungsverhalten in der Magnesit – Otavit Mischkristallreihe wurde mithilfe der Infrarotabsorptionsspektroskopie an Pulvern bestimmt. Für die Untersuchung der Proben wurden Kaliumbromid (KBr) und Polyethylen (PE) als Einbettungsmittel verwendet. Die Messungen wurden in drei Spektralbereichen durchgeführt: $50\text{-}350\text{cm}^{-1}$ (PE Presslinge), $350\text{-}500\text{cm}^{-1}$ (KBr Presslinge) und $500\text{-}4000\text{cm}^{-1}$ (KBr Presslinge). Phononschwingungen, die durch Kationen in oktaedrisch koordinierten Gitterplätzen verursacht werden, sind im nur im

Bereich der niedrigsten Frequenzen innerhalb der untersuchten Spektralbereiche vorhanden. All anderen beobachteten Schwingungsbanden können Vibrationen in der Karbonatgruppe zugeordnet werden.

Phononbande, die durch Cadmium-Sauerstofftranslationen ($75\text{-}200\text{cm}^{-1}$) und durch Magnesium-Sauerstofftranslationen ($200\text{-}350\text{cm}^{-1}$) erzeugt werden, wurden beide in den Infrarotspektren der Proben mit mittlerer Zusammensetzung beobachtet. Die Bandpositionen wurden mithilfe einer Anpassung an eine Lorentz Verteilungsfunktion bestimmt. Für die Cadmium-Sauerstoff-Translation bleibt die Bandposition als Funktion der Zusammensetzung konstant, während die Bandposition der Magnesium-Sauerstofftranslation eine Verringerung der Wellenzahl in Abhängigkeit von der Zusammensetzung zeigt. Das deutet darauf hin, dass die Magnesit – Otavit Mischkristallreihe eine Kombination von one-mode und two-mode Verhalten bei niedrigen Frequenzen zeigt, was wahrscheinlich durch die unterschiedlichen Atomgewichte von Magnesium und Cadmium verursacht wird.

Vibrationsbande in den Spektralbereichen $350\text{-}550\text{cm}^{-1}$ (Translation und Libration der Karbonatgruppen) und $650\text{-}900\text{cm}^{-1}$ (doppelt degenerierte Verbiegungen innerhalb und aus der Ebene der Karbonatgruppen) zeigen eine lineare Abhängigkeit von der Zusammensetzung und ihre Positionen werden durch den Ordnungsgrad nicht beeinflusst. Im Spektralbereich $1000\text{-}1800\text{cm}^{-1}$ sind die Phononbande durch doppelt degenerierte, asymmetrische Dehnung der Karbonatgruppen verursacht. Die Proben mit Kristallsymmetrie $R\bar{3}c$ zeigen hier eine lineare Verschiebung der Bandposition als Funktion der Zusammensetzung, während Proben des Cadmium-Dolomit Stabilitätsfeldes mit der Symmetrie $R\bar{3}$ durch einen deutlichen Anstieg in der Frequenz – verglichen mit ihren Äquivalenten der Symmetrie $R\bar{3}c$ – charakterisiert sind. Da, wie die Rietveldanalysen zeigen, die Karbonatgruppen in den Proben mit der Symmetrie $R\bar{3}$ nicht planar sind, muss offenbar in diesem Fall mehr Energie für die asymmetrische Dehnung aufgewendet werden, so dass die Bandposition zu entsprechend höheren Wellenzahlen im Vergleich zu den Proben mit Symmetrie $R\bar{3}c$ verschoben werden.

(3) Resultate der Autokorrelation

Kationensubstitution oder Unordnungsphänomene verursachen Verbreiterungen von Vibrationsbanden in der Infrarotspektroskopie. Es ist jedoch nicht immer möglich, die Linienbreite von komplexen Infrarotspektren mit herkömmlichen Anpassungsmethoden zu bestimmen. In der vorliegenden Arbeit wurde deshalb eine alternative Methode benutzt, die es mithilfe der Autokorrelationsfunktion ermöglicht, die durchschnittlichen Linienbreiten für sechs Spektralbereiche zu bestimmen: $75\text{-}200\text{cm}^{-1}$, $200\text{-}350\text{cm}^{-1}$, $300\text{-}550\text{cm}^{-1}$, $700\text{-}800\text{cm}^{-1}$, $800\text{-}900\text{cm}^{-1}$ und $1000\text{-}1800\text{cm}^{-1}$. Die Resultate der Autokorrelation, Δ_{corr} , können im Bezug auf die lokalen Deformationsfelder interpretiert werden, die in der Kristallstruktur durch Kationensubstitution und -unordnung entstehen. Im Niederfrequenzbereich zeigen die Δ_{corr} Werte eine positive Abweichung von der linearen Abhängigkeit von der Zusammensetzung und werden nur leicht durch den Ordnungsgrad beeinflusst. Für Proben der Zusammensetzung $\text{Mg}_{0.5}\text{Cd}_{0.5}\text{CO}_3$ sind die Δ_{corr} Werte unabhängig von ihrem Ordnungsgrad praktisch identisch. Dies deutet darauf hin, dass lokale Heterogenitäten innerhalb der Proben auch bei unterschiedlichem Ordnungsgrad bei einer Grössenordnung von einigen Einheitszellen bleiben. Ebenso erscheint es, dass die Magnesitstruktur leichter Cadmium Atome aufnehmen kann als die Otavit-Struktur Magnesium Atome. In allen Spektralbereichen führt die Hinzunahme von 10mol% MgCO_3 (das entspricht einem Magnesium Atom pro zwei Einheitszellen) in Otavit zu einem starken Anstieg in der Linienbreite. Daraus ergibt sich, dass die Deformationsfelder um die jeweiligen Magnesium Atome eine Grössenordnung von 30 Å haben.

Bei der Zusammensetzung $\text{Mg}_{0.5}\text{Cd}_{0.5}\text{CO}_3$ ist im Spektralbereich $800\text{-}900\text{cm}^{-1}$ ein Ordnungseffekt zu beobachten, der sich in der Erniedrigung der Δ_{corr} Werte relativ zu denen der Proben mit der Kristallsymmetrie $R\bar{3}c$ widerspiegelt. Dieser Unterschied in Δ_{corr} Werten zwischen den geordneten und ungeordneten Phasen wurde benutzt, um den Nahordnungsparameter q zu berechnen. Dieser steht mit dem Fernordnungsparameter Q in linearer Beziehung, was bedeutet, dass der Ordnungsmechanismus im makroskopischen und mikroskopischen Massstab der gleiche ist.

Die Resultate der vorliegenden Arbeit verdeutlichen die strukturellen Unterschiede zwischen Karbonat- und Silikatmaterialien. Es scheint, dass die $R\bar{3} \rightarrow R\bar{3}c$ Phasenumwandlung in der Magnesit – Otavit Mischkristallreihe nicht durch einen Relaxationsprozess des Gitters angetrieben wird, da bei niedriger Frequenz nur die Kationensubstitution einen messbare Wirkung auf die Linienverbreiterung hat.

1: Introduction

The temperature and pressure at which mineral assemblages form has always been of great interest and importance to Earth-scientists in an attempt to understand and elucidate large-scale processes that occur deep within the Earth. Such processes are closely related to the structure and physical properties of the rock forming minerals. Most minerals in the Earth display varying degrees of cation substitution, which require systematic studies in order to determine mixing behaviour. It is therefore necessary to determine better constraints on the thermodynamic properties of these minerals. It has been shown that comparison of microscopic and macroscopic behaviour is particularly useful in understanding the properties of solid solutions and describing, quantitatively, phase transitions and cation ordering processes [Malcherek *et al.*, 1995; Boffa-Ballaran *et al.*, 1998a&b; Boffa-Ballaran *et al.*, 1999; Boffa-Ballaran *et al.*, 2001; Tarantino *et al.*, 2002; Tarantino *et al.*, 2003]. These studies, however, are related to silicate, or silicate-analogue type structures. Others mineral groups, such as oxides and carbonates, may be expected to display a significantly different response to cation substitution than that observed for silicates.

Among carbonates, the magnesite (MgCO_3) – calcite (CaCO_3) solid solution is the geologically most significant system, but certain ordering and unmixing processes occur at high temperatures and make experimental work for this system difficult. The magnesite (MgCO_3) – otavite (CdCO_3) solid solution may be taken as an analogue, allowing studies at much lower temperatures.

This project aims to investigate the mixing behaviour and structural changes of carbonate minerals as a function of temperature and pressure in order to generate thermodynamic data relating to phase transitions and cation ordering in solid solutions.

1.1 Carbonates in the Earth

Carbonates are one of the most abundant materials within the Earth after silicates. The most abundant carbonates found in the Earth are calcite (CaCO_3), magnesite (MgCO_3) and the ordered compound found at intermediate compositions between these two end-members, dolomite [$\text{MgCa}(\text{CO}_3)_2$]. The formation of carbonates occurs in several different ways; from weathered landmass that is deposited and lithified, calcite (CaCO_3) can be precipitated from super saturated seawater, or from the decomposition of aquatic life. The formation of dolomite, $\text{MgCa}(\text{CO}_3)_2$, can occur after sedimentation of calcite by the addition of magnesium ions from seawater or from ground water, in contact with the calcite or by direct precipitation from brines.

Carbonate materials are important not only as geologic materials but also as a possible means for understanding the CO_2 cycle in the Earth, as well as where and how carbon is stored within the mantle. The role of carbonates as materials for sequestration has also become very important over the last decade as global warming becomes more of an issue and companies realise the financial implications of the production of large amounts of greenhouse gases.

1.1.1 Carbon Recycling and Carbonate Stability

Increasing attention is being given to carbonate materials as work is directed towards understanding the depth to which carbonates are stable in the Earth, and how carbonates contribute to CO_2 recycling. It has been suggested that subduction of carbonates may provide a CO_2 source within the upper-mantle, so allowing further reactions to occur [Edmund and Huh, 2003; Molina and Poli, 2000; Kerrick and Connolly, 2001; Bebout, 1995; Holl *et al.*, 2000].

Although water is far more important in terms of recycling of volatiles in the mantle, it has been suggested by Molina and Poli (2000) that oceanic crust is not only a H_2O reservoir, but also a CO_2 reservoir, so establishing a relationship between shallow and

deep recycling of CO₂. Volatiles found at depths of greater than 15 km, are thought to be produced primarily from those bound in minerals within subducting slabs, e.g. carbonates. It is thought that the volatiles are then released by way of metamorphic devolatilisation [Bebout, 1995; Kerrick and Connolly, 2001]. Release of CO₂ volatiles can play an important part in affecting the stability and phase relations of minerals within the mantle, as well as controlling genesis of carbonatitic and kimberlitic magmas.

Keppler *et al.* (2003) studied the solubility of carbon in olivine in an attempt to elucidate the mode of carbon storage within the Earth's mantle. It was found that the solubility of carbon in olivine was, in fact, much lower than originally thought, 0.1 to 1 ppm by weight. It is therefore hypothesised that carbon must be present in some other form, most probably a carbonate phase, and hence the depth to which carbonate materials are stable is of great importance. Work by Isshiki *et al.* (2004), shows that magnesite, in a high-pressure form, is stable at temperatures and pressures of the lower-mantle, and approaching core-mantle boundary conditions (~115GPa and 2,100-2,200K). Investigation of the high-pressure behaviour of calcite has shown that several polymorphs exist, even at modest pressures. The first phase transition in calcite was observed by Bridgman in 1939, this being, firstly, the transition from calcite to calcite II at 1.44GPa, and then the transition from calcite II to calcite III at 1.77GPa, the phases increasing in density with increasing pressure [Smyth and Ahrens, 1997]. The stable high-pressure phase of calcite is aragonite, stable to at least 40GPa. It is thought to be metastable up to pressures of 70GPa, but beyond that the structure is uncertain. It is thought, however, that the stability of a carbonate phase will depend on the divalent cations present in the structure. For example, calcium is a large cation compared to magnesium, and hence calcite becomes structurally unstable at lower pressures than magnesite [Santillán and Williams, 2004]. The stability of dolomite has also been investigated by Santillán *et al.* (2003), who found that dolomite is likely to transform to a high-pressure phase, with the calcite III structure at pressures of 20-30GPa.

Therefore it may be seen that the stability, structure, and behaviour of carbonate materials is paramount in elucidating the recycling of carbon in the Earth.

1.1.2 Carbon Dioxide Sequestration

The subject of climate change due to an increase in greenhouse gases in the atmosphere is currently of great interest within the scientific community. The drive to reduce greenhouse gases has also led to increased interest and the need for a better understanding of carbonate materials. The amount of CO₂ in the atmosphere, it has been estimated, has increased by 30% since the use of fossil fuels began [Lackner *et al.* 1998]. Over the past 200 years, it is estimated that the amount of CO₂ in the atmosphere has increased from 280ppm to 365ppm, hence causing changes in climate. A global call for a reduction in greenhouse gases has led to the need for some kind of CO₂ trapping, or extraction from the air. The use of stable mineral complexes to trap CO₂ has been investigated over the last 20 years [Lackner *et al.*, 1998; O'Connor *et al.*, 2000 and Haywood *et al.*, 2001].

Reaction of carbon dioxide with mineral oxides is an exothermic process, so making carbon thermodynamically more stable at ambient conditions, a fact that can be exploited in order to sequester carbon dioxide. The amount of CO₂ that can be sequestered is dependent on the mineral formations present at a particular location. The Sleipner facility, a company with an off-shore gas rig in the Norwegian sector of the North Sea, set up a sequestration plant at a cost of \$80 million [Walter, 2001]. The rig produces 1 million tons of CO₂ per year, so the tax imposed upon the company by the government would cost \$55 million per year. Since 1996 the company has sequestered some of the CO₂ produced, so saving the company \$195 million. The CO₂ is stored in a highly porous, fluid saturated sandstone, sealed by shale. The CO₂ displaces the water, and reacts with the plagioclase present, precipitating calcite. Mineral trapping at this site accounts for 4% of CO₂ sequestered. Although, this number is small, the effectiveness of the process is wholly dependent on the formations present, so with different mineralogy this figure could be greatly increased.

The use of olivine (Mg_2SiO_4), and serpentine [$\text{Mg}_3\text{Si}_2\text{O}_5(\text{OH})_4$] have also been considered in terms of mineral trapping [O'Connor *et al.*, 2000]. The high MgO content allows a large percentage of the material to be transformed to carbonate. Possible sequestration methods must not, however, have a detrimental effect on the environment. Haywood *et al.* (2001) suggests six methods for CO_2 sequestration but all six are discounted as having an adverse effect on the environment, by way of energy use for processing and disposal of by-products, most notably acid.

Knowledge of the physical properties of carbonates is essential for studies on CO_2 sequestration and the environmental impact of the associated with the techniques employed.

1.2 The Magnesite – Calcite System

The Magnesite – Calcite system is very important to both sedimentary and metamorphic aspects of geology, and hence, much work has been carried out to study this system. Dolomite, the ordered phase observed at intermediate compositions in this system, was one of the first minerals to be investigated by X-ray diffraction, by Wyckoff and Merwin in 1924 [Steinfink and Sans, 1959]. This early investigation by Wyckoff and Merwin showed, using Laue photographs, that dolomite was a distinct compound from the two constituent end-members (magnesite and calcite) due to the lower symmetry it displayed ($R\bar{3}$ as opposed the $R\bar{3}c$ of the two end-members). This study also determined the unit cell dimensions of dolomite and showed that four atomic parameters were required in order to determine the structure. It was not until the 1950's that further work was carried out on dolomite to determine the atomic positions of the carbonate group [Bradley *et al.*, 1953; Steinfink and Sans, 1959]. It was also at this time that work was done on the magnesite – dolomite - calcite system to gain insight into how it might be used in terms of a geologic thermometer. Graf and Goldsmith (1955), Harker and Tuttle (1955), Goldsmith and Heard (1960), Goldsmith and Newton (1969), Irving and

Wyllie (1975) and Byrnes and Wyllie (1981) mapped the sub-solidus phase relations within the calcite – magnesite solid solution (Figure 1.1). It may be seen from Figure 1.1 that the complete solid solution is only stable at high temperatures. At lower temperatures a miscibility gap exists between the end-members and an ordered phase superimposed at intermediate compositions (this phase being dolomite). Cation ordering within the dolomite structure was indicated by the presence of reflections not observed for the magnesite and calcite end-members, both of which have the $R\bar{3}c$ space group. The dolomite structure has $R\bar{3}$ symmetry and may be thought of as consisting of alternating layers of magnesium and calcium ions between carbonate group layers (Figure 1.2).

Harker and Tuttle (1955) first suggested the presence of the high temperature disordered dolomite, but it was not until 1960 that Goldsmith and Heard actually proved the existence of such a phase. The runs performed at 1200°C showed the presence of two phases by way of X-ray powder diffraction; a dolomite and a magnesite-rich material, which is thought to have been exsolved upon cooling. It was noted that the dolomite lines appeared “spread out and diffuse”, so suggesting that the rate of quench was not sufficient to prevent reversion to the stoichiometric composition, as well as unmixing of the magnesite – rich material, which is rapid due to fast diffusion of the small Mg^{2+} ions. In order to check that the material was indeed homogeneous at 1200°C, comparison was made with powder diffraction patterns taken from natural, annealed dolomites. Patterns taken from samples of the dolomite heated to below 1000°C were indistinguishable from patterns from the original samples. It was also observed that patterns collected for a synthetic mixture reacted below 1000°C were indistinguishable from a natural dolomite. All the samples were then heated to temperatures above 1000°C, so providing evidence of substitutional disorder. The degree of order was also seen to decrease with increase in temperature. This observation was made from the gradual weakening of reflections due to ordering, most notably the (101), (015) and the (021). The same study also found there to be an effect of cation disorder on the lattice constants. An increase along the c -axis was observed as the sample became increasingly disordered. The overall effect was found to be relatively small, but the unit cell volume of the disordered dolomite was found to be larger than that of the ordered phase.

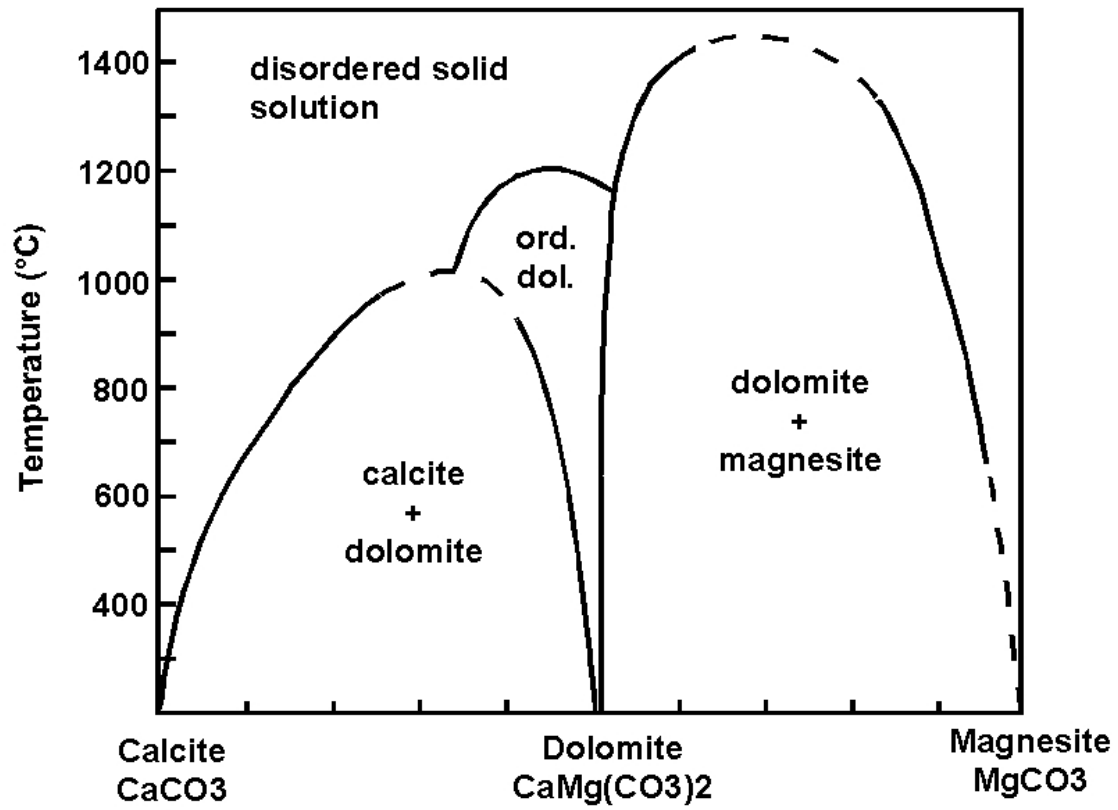


Figure 1.1: Phase diagram for the calcite-magnesite system

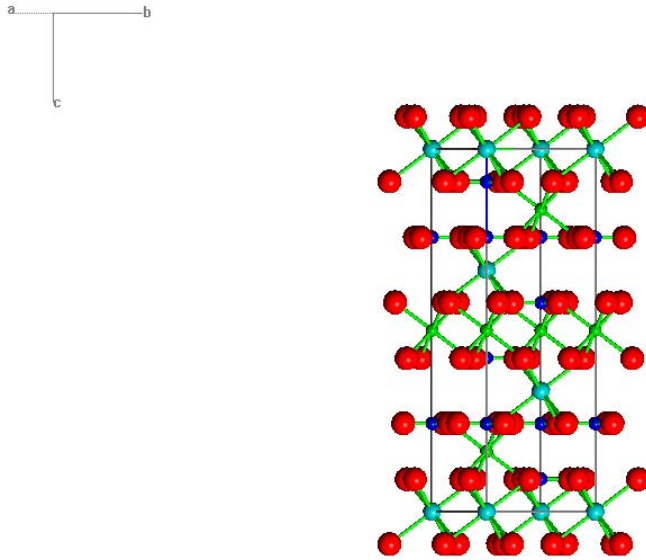


Figure 1.2: The ordered $R\bar{3}$ carbonate structure from Reeder and Markgraf (1986). The atoms are attributed as being red = oxygen, blue = carbon, green = magnesium and turquoise = calcium. Alternating layers of calcium and magnesium cations may be seen to be sandwiched between planar CO_3 groups.

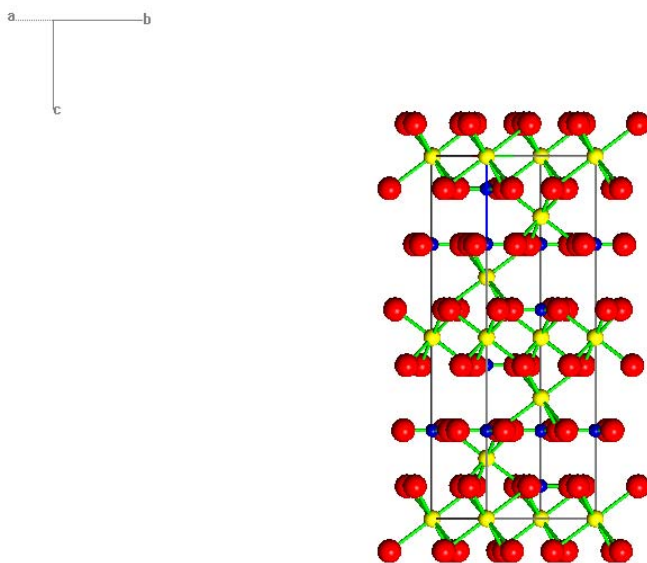


Figure 1.3: The disordered $R\bar{3}c$ carbonate structure from Reeder and Markgraf (1986). Atoms may be attributed as; red = oxygen, blue = carbon, yellow = random arrangement of calcium and magnesium atoms.

Goldsmith and Heard (1960) also concluded that the mechanism of disorder must be substitutional due to the way in which the samples disordered. It was observed that although the reflections due to ordering became weaker, they remained sharp, so suggesting simple substitutional disorder. If disorder of the carbonate material was due to the formation of domains of disorder, the reflections due to ordering would be seen as diffuse, becoming more so with increasing disorder. If domain disorder is thought of in terms of mixed layering, as is found in dolomite, then the affected planes would be those from planes in the disturbed sequence (in this case the *c*-axis), or at angles close to it. All the reflections due to ordering observed in the Goldsmith and Heard study were at planes steeply inclined to the *c*-axis, so they could not observe any diffuse peak effects. However, samples from the Goldsmith and Heard (1960) study that were partially disordered and that deviated from the ideal Ca:Mg 50:50 ratio did show obvious spreading and diffuseness of those reflections near the *c*-axis.

In order to prove the existence of an intermediate ordered phase over a compositional range Graf and Goldsmith (1955) used a calcareous algal material, containing approximately 20mol% MgCO_3 in solid solution for the basis of solid state synthesis. It was thought that cation migration would occur more readily than “reorganisation” of two distinct phases i.e. magnesite and calcite. From the published results they observed that one of the reflections due to ordering displayed a deviation from ideal stoichiometry. It was estimated that up to 5mol% excess CaCO_3 could be incorporated into the ordered structure at 800°C.

It is interesting to note that all the studies used the same method for ascertaining the composition of the sample synthesised. The method was first used by Harker and Tuttle (1955). They noted a shift in the calcite peaks towards those for magnesite with the inclusion of Mg^{2+} ions into the structure. They concluded that the shift was a function of magnesium content and so devised a semi-quantitative approach to ascertaining composition. A standard was added to the samples and the angular distance between the standard peak and the carbonate peak was measured. The difference in 2θ between the position of the standard and the carbonate peak were plotted against carbonate

compounds from this system of known composition. This produced a series of points extremely close to a straight line. Therefore, using this line, the compositions of the samples were estimated to within $\pm 1\%$. Further studies by Goldsmith and Newton (1969), Irving and Wyllie (1975) and Byrnes and Wyllie (1981) utilised this technique using the intense (104) peak, which is present in both structures, to ascertain the composition to within $\pm 1\text{mol}\%$.

Constraint of the order-disorder transition and phase relations within the magnesite – calcite system is difficult due to the required experimental conditions. Quenching from 1400°C results in the reversion of the disordered phase to some degree of partial ordering at intermediate compositions. Therefore, attention was turned to the possibility of there being an analogue system which would allow synthesis at lower temperatures, and which could be used to elucidate the thermodynamic behaviour of this solid solution.

1.3 The Magnesite – Otavite System as an Analogue

It was in 1958 that Goldsmith suggested that the magnesite (MgCO_3) – otavite (CdCO_3) system might be used as an analogue to the geologically important magnesite – calcite system (Graf, 1961). Due to the very low abundance of cadmium, the end-member, Otavite, is a very rare mineral, found only in the Tsusmeh mine in Namibia, whereas “cadmium dolomite” $[\text{MgCd}(\text{CO}_3)_2]$ has never been found in nature. Therefore all the work done on this system has been on synthetic samples.

1.3.1 The Experimental work

Experimental work by Goldsmith (1972) and Capobianco *et al.* (1987) showed that the phase diagram for the MgCO_3 - CdCO_3 system did indeed mirror that of the magnesite – calcite system, but at significantly lower temperatures. Graf (1961) published an extensive study on crystallography for the rhombohedral carbonates,

including data for both ordered and disordered “cadmium dolomite”. Neither Goldsmith (1972) nor Capobianco *et al.* (1987) reported the variation of lattice parameters along the join.

Goldsmith (1972) synthesised a series of samples across the magnesite – otavite solid solution using squeezer apparatus at 1 GPa between 500-600°C for the ordered $R\bar{3}$ phase, and 800-850°C for disordered $R\bar{3}c$ phase. Runs at lower temperatures were carried out to map the phase boundaries of the miscibility gaps that flank the ordered “cadmium dolomite”. Run durations were between 3-4 hours and run products were characterised by way of X-ray powder diffraction. From the experiments carried out Goldsmith produced a phase diagram for the system (Figure 1.4). Comparison of Figure 1.1 with Figure 1.4 shows a similar topology, there being a intermediate ordered phase superimposed on the miscibility gap at lower temperature, and a continuous solid solution at higher temperatures. Goldsmith reports the onset of disorder at 675°C, and completion between 800-850°C, depending on composition of the sample. The degree of order within the samples was ascertained using X-ray powder diffraction. As with the work by Goldsmith and Heard (1960) on the magnesite – calcite system, only the three most intense reflections due to ordering were observed. Goldsmith observed that samples synthesised or annealed at 675°C began to show weakening of the reflections due to ordering, as observed by Goldsmith and Heard (1960) for the magnesite – calcite system. The disappearance of the reflections due to ordering was similar to the work done by Goldsmith and Heard (1960), the reflections weakened with a decrease of intensity, no diffuseness or spreading was observed, although no comment is made regarding reflections normal to the c -axis, and how the transition effects the sharpness of these reflections. Goldsmith, therefore, concludes that the $\text{MgCd}(\text{CO}_3)_2$ system displays gradual equilibrium thermal disordering, as reported by Goldsmith and Heard (1960) for $\text{MgCa}(\text{CO}_3)_2$. The degree of order within the samples was determined by eye from X-ray films. The assumption was therefore made that the sample with the most intense reflections due to ordering was fully ordered, although there was no way to quantitatively ascertain the degree of order within the samples. Goldsmith (1972) notes that the maximum compositional deviation for cadmium dolomite occurs at 700°C, at which point 10% excess Cd can be contained within the ordered $\text{Mg}_{0.5}\text{Cd}_{0.5}\text{CO}_3$ phase.

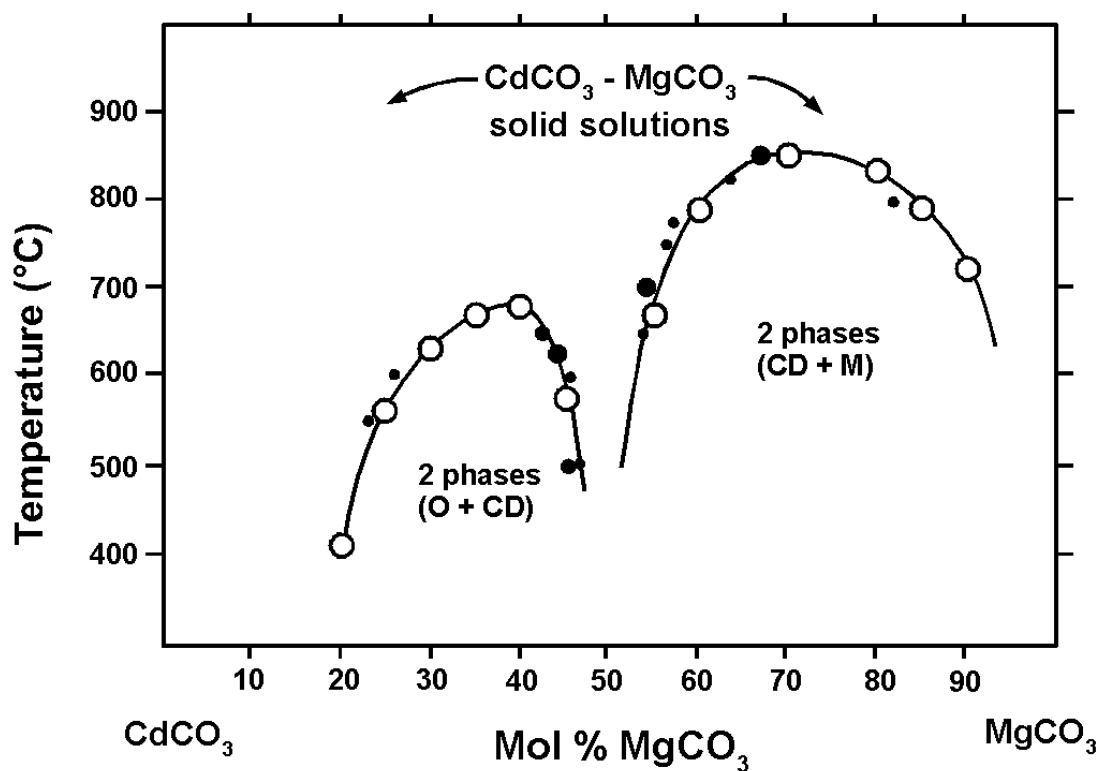


Figure 1.4: Phase diagram of the otavite-magnesite system, as determined by Goldsmith (1972). Open circles are plotted at temperatures above which a single phase is observed, and below which a two-phase assemblage is produced. Solid circles are compositions determined by spacings of selected X-ray reflections. A dashed line may be added at intermediate compositions to delimit the region of detectable order, although no quantitative results were obtained by Goldsmith to accurately constrain the stability of the ordered phase.

Capobianco *et al.* (1987) did a more extensive study, combining experimental and modelling techniques in order to investigate the $\text{MgCd}(\text{CO}_3)_2$ system further. The modelling techniques employed will be discussed in section 1.4. The experimental work was carried out at 0.1 GPa in hydrothermal apparatus and at 600°C, with run durations of 4 days for samples of composition $\text{Mg}_{0.5}\text{Cd}_{0.5}\text{CO}_3$, thereby ordering the material. Once synthesised, the samples were subjected to an annealing process within the disorder temperature range published by Goldsmith (1972). For annealing experiments piston cylinder apparatus was used in order to prevent dissociation of carbonate materials. Samples were annealed between 600-850°C, at 0.1-1.5 GPa, for durations of 1.5-168 hours. The degree of order, as with the Goldsmith (1972) study was ascertained from the X-ray powder diffraction data. Intensity data from the reflections due to ordering were obtained for the annealed samples and compared with that of the same reflections in the ordered starting material. Again, the assumption was made that the sample having the most intense reflections due to ordering was fully ordered. The experimental results obtained from the study were not used to derive a phase diagram for the system, but to calculate long-range order parameters from X-ray intensity data for partially disordered dolomites. With the assumption that at 600°C samples were fully ordered, they found that at 850°C samples were almost completely disordered. Ordered samples annealed at 750 and 775°C have calculated long-range cation order parameters (s) of between 0.6 and 0.7 (a fully ordered sample having $s = 1$, and a completely disordered sample having $s = 0$).

In neither experimental study were the lattice parameters across the solid solution accurately determined, or the effect of cation substitution on lattice strain investigated.

The most recent experimental study was done by Bromiley (2002). A series of samples were synthesised, in 10mol% increments, across the solid solution at 600°C for 3 hours at 1 GPa. All the experiments were carried out in piston cylinder apparatus. The results of the study showed a miscibility gap at compositions of $\text{Mg}_{0.7}\text{Cd}_{0.3}\text{CO}_3$ and $\text{Mg}_{0.8}\text{Cd}_{0.2}\text{CO}_3$. Rietveld analysis of the samples synthesised allowed refinements of the two phases to the compositions $\text{Mg}_{0.6}\text{Cd}_{0.4}\text{CO}_3$ and $\text{Mg}_{0.9}\text{Cd}_{0.1}\text{CO}_3$. An intermediate ordered phase was found over a compositional range of $\text{Mg}_{0.4}\text{Cd}_{0.6}\text{CO}_3$ to $\text{Mg}_{0.6}\text{Cd}_{0.4}\text{CO}_3$,

broader than found in the previous experimental studies. At 600°C no miscibility gap was observed in the cadmium-rich half of the phase diagram. It was suggested that the miscibility gap may exist at temperatures below 600°C, or at a composition between those synthesised by Bromiley (2002). Refinements for all the samples showed a linear trend for unit cell volume as a function of composition across the solid solution. Bond lengths and atomic positions were refined. Transmission Electron Microscopy (TEM) was employed to show the presence of two phases in the samples within the miscibility gap. Selected Area Electron Diffraction (SAED) was used to show specific crystallographic orientations only observed in the $R\bar{3}$ structure, and compositional micro-analysis (EDX) was used to show qualitatively that two distinct compositions existed within the same sample.

1.4 The Modelling Work

Over the last 20 years several studies have been done concentrating on modelling of both the magnesite – calcite system and the magnesite – otavite system. Burton and Kikuchi (1984) used the tetrahedron approximation of the cluster variation method to thermodynamically model the $\text{CaCO}_3\text{-MgCO}_3$ system. The model takes into account the separation of two different atoms onto different planes (an intersublattice pairwise energy parameter), so modelling the ordering within the system, but also considers interactions related to exsolution (intrasublattice interactions). The tetrahedron approximation model in this study was shown to better predict the phase diagram, as it not only considers long-range order, but also short-range order both above and below the order - disorder transition temperature. Results obtained were seen to be in semi-quantitative agreement with experimental results published by Goldsmith and Heard (1961). The differences observed between the model and experimental data may be due to assumptions made regarding the energetics of the system based on the M-O_6 octahedra, and the consideration of atomic interactions within the system. Most of the modelling work done only considered pairwise interactions, not many body interactions.

In 1987 both Burton and Capobianco *et al.* published models for the magnesite – otavite system. The work of Burton used the same technique as that by Burton and Kikuchi (1984) for the work on the magnesite – calcite system, a tetrahedron approximation in the cluster variation model. The phase diagram derived from this study may be seen in Figure 1.5. Burton notes that the topology of the calculated diagram is in good agreement with experimental work by Goldsmith (1972) (Figure 1.4).

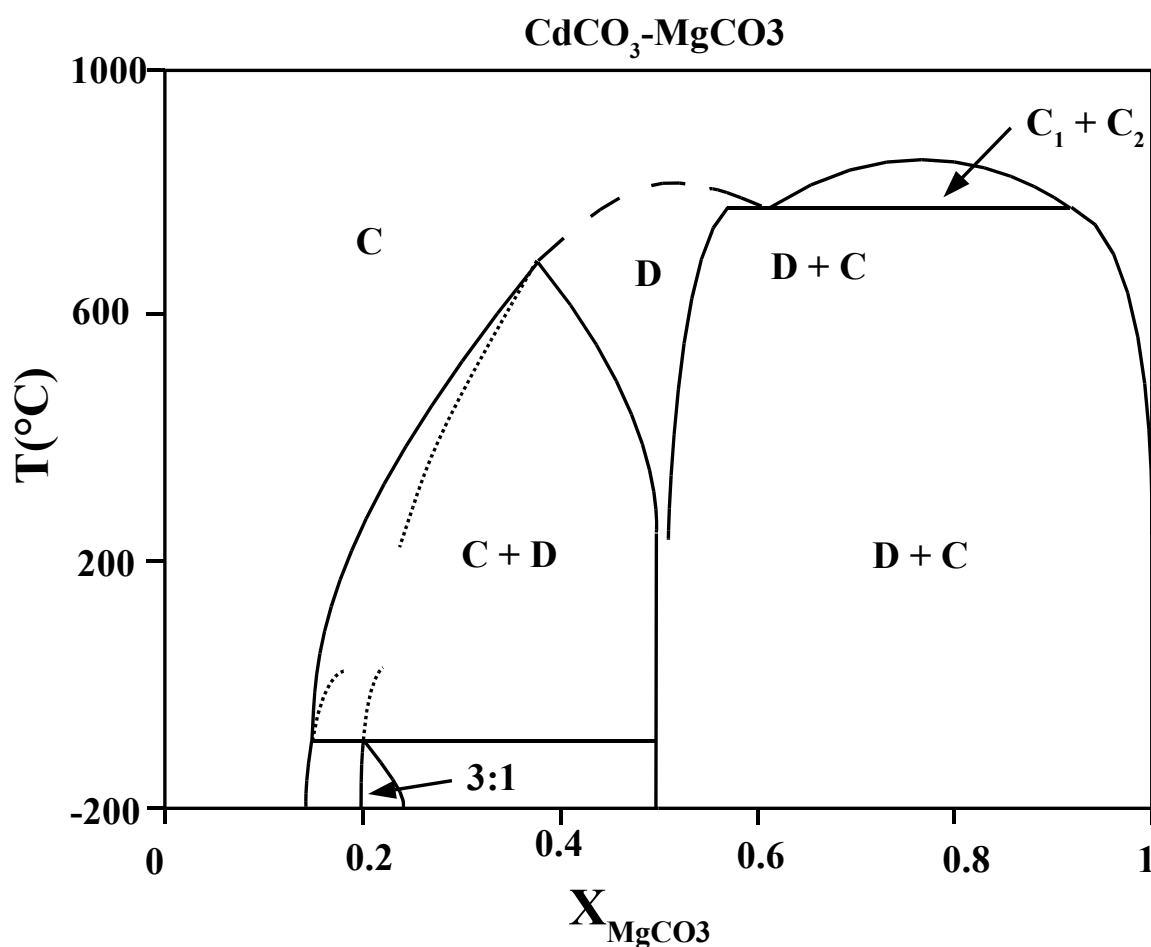


Figure 1.5: A theoretical model for the otavite - magnesite phase diagram, taken from Burton (1987). C denotes a calcite-type structure ($R\bar{3}c$), D denotes a dolomite-type structure ($R\bar{3}$).

Capobianco *et al.* (1987) derived models using several different techniques, namely a Bragg-Williams approximation, a generalised point approximation and a tetrahedron approximation in the cluster variation method. The Bragg-Williams approximation cannot account for positive enthalpies of mixing in disordered solid solutions, due to an energy parameter, W , which is related to the long-range order parameter, so this energy parameter must be negative for ordering. Therefore, using this model, calculations for disordered phases still show a negative enthalpy of mixing. The generalised point approximation model takes into account an attractive interaction (interlayer – unlike pair formation) and a repulsive interaction (intralayer - segregation). By having these two energy parameters, the enthalpy of mixing will be negative at lower temperature, but as the long-range order parameter (s) goes to zero, the enthalpy of mixing becomes positive. The asymmetry of the miscibility gap observed in the experimental phase diagram of Goldsmith (1972) (Figure 1.4) was not observed so it was concluded that thermochemical and phase equilibria data should be considered separately in order to introduce asymmetry into the phase diagram. The tetrahedron approximation in the cluster variation method is the same method used by Burton (1987), and gives results that are in good agreement. Figure 1.6 shows the three phase diagrams, derived from different models. The first point approximation model diagram (PA_1) in Figure 1.6 was fit to phase equilibrium data only, whereas the second point approximation model (PA_2) was first optimised in terms of thermochemical data, then to phase equilibrium data.

The tetrahedron approximation in the cluster variation method includes short-range order by considering clusters of atoms. As with the second model from the generalised point approximation technique, the tetrahedron approximation was also fit in terms of both thermochemical and phase equilibrium data. The phase diagram topologies for the different modelling techniques can be compared in Figure 1.6. It may be seen from this diagram that the tetrahedron approximation gives by far the best agreement with the experimental data from Goldsmith (1972).

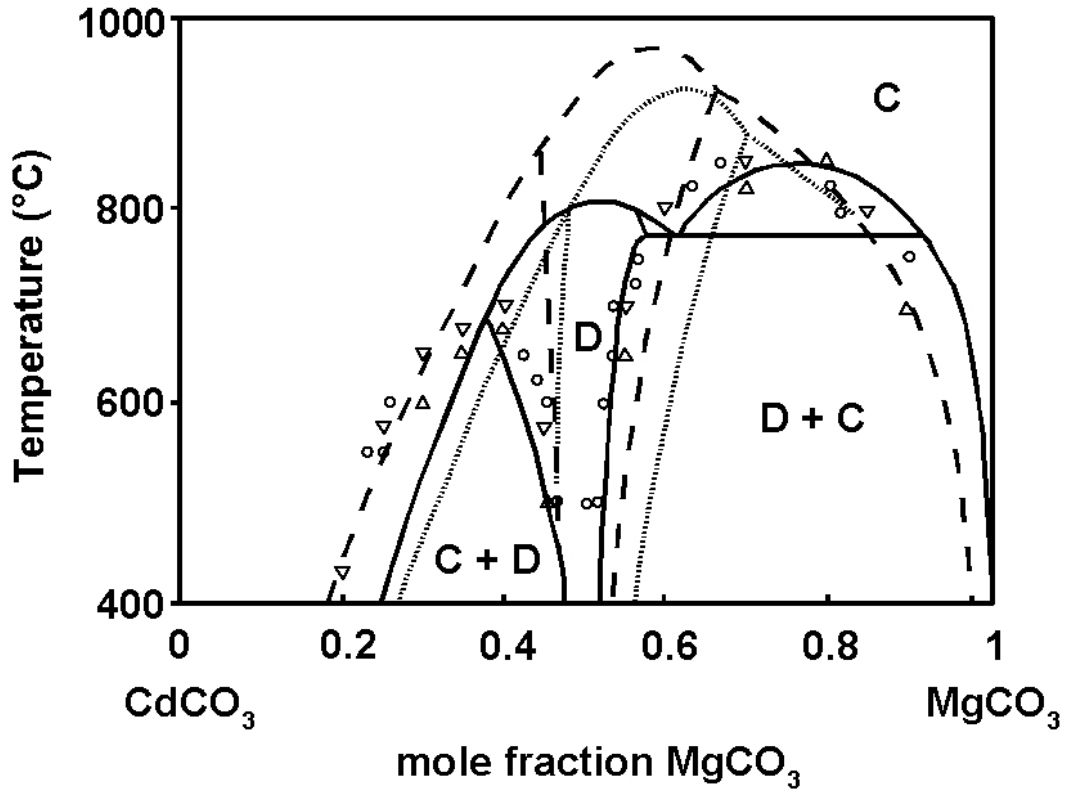


Figure 1.6: Phase diagrams, as produced by Capobianco *et al.* (1987). The first point approximation model (PA₁) is coarsely dashed, the second point approximation model (PA₂) is finely dashed, and the solid line is the result of the tetrahedral approximation in the cluster variation method model. Open circles and triangles correspond to experimental data from Goldsmith (1972).

The most recent modelling work done on the magnesite – otavite system was by Burton and Van de Walle (2003) in which the phase diagram is calculated from first principles. The model uses planewave pseudopotential calculations of supercell energies to derive the energy of the system from first principles, so giving better constraints than in the previous models [Burton and Kikuchi, 1984; Burton, 1987; Capobianco *et al.*, 1987]. Figure 1.7 shows the calculated phase diagram published by Burton and Van de Walle (2003) for the magnesite – otavite system. It is noted in the article that the results are only in qualitative to semi-qualitative agreement to experimental data, and the authors also note that first-principle phase diagram calculations overestimate transition temperatures when vibrational effects are ignored, as is the case with their work.

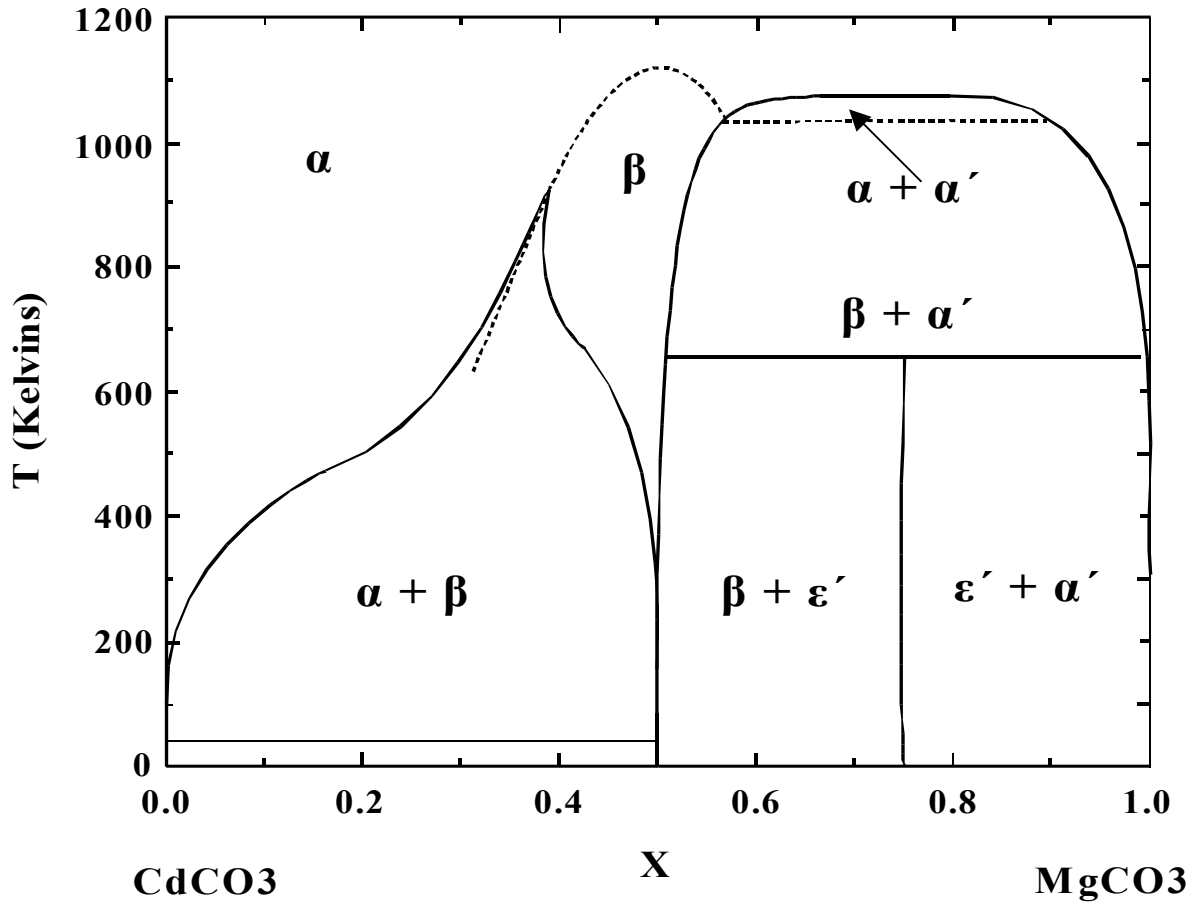


Figure 1.7: Phase diagram derived from first-principle-based calculations, taken from Burton and Van de Walle (2003). The phase diagram not only predicts the expected intermediate ordered phase, flanked by miscibility gaps, but also several metastable phases, yet to be observed experimentally. α denotes the otavite structure, β denotes cadmium dolomite, α' denotes the magnesite structure. ϵ and ϵ' are phases calculated for the system, but which have not been observed experimentally.

1.5 The Effects of Strain and Elasticity on Solid Solutions

From many studies on structural phase transitions in minerals it is known that strain and elasticity play a fundamental role in controlling the thermodynamic behaviour of silicates [Bratkovsky *et al.*, 1984; Carpenter *et al.*, 1998; Dove, 1997, 2001]. Bratkovsky *et al.* (1984) noted that disordering transformations often have characteristic length scales far exceeding the unit cell itself, so showing the effect of long range elastic forces. Phase transitions can, therefore, be understood as the correlation between small local distortions that impact over large distances, hence causing a break in symmetry.

In the last few decades Raman spectroscopy and Infrared (IR) spectroscopy have been used successfully as the primary tool for investigating phase transitions. In particular, Hard Mode Infrared Spectroscopy (HMIS) utilises phonon energies to determine the evolution of a structure as a function of temperature, pressure or composition [Salje, 1992; Salje and Bismayer, 1997; Salje *et al.* 2000; Boffa-Ballaran and Carpenter, 2003]. It is noted by Salje (1992) that the relative changes of the phonon frequencies are below 2% of their total energy, therefore allowing a coupling between phonon frequency, ω , linewidth, Γ , and absorbance, A , with the order parameter, Q , associated with a phase transformation.

Linewidths of IR spectra have been observed to correlate with local strain heterogeneities, showing a decrease when local strains present in the high-symmetry phase are reduced in the low-symmetry phase [Salje, 1992; Salje and Bismayer, 1997]. Analogous changes in linewidth may also be expected in spectra from samples, for which the only variable is composition, if strain fields develop during the formation of the solid solution. This appears to be a valid assumption for silicates. Several mineral families have been investigated by means of HMIS and the use of a systematic methodology to collect and analyse IR spectra allowed detailed studies of variation in linewidth due to cation substitution and ordering effects across the solid solution [Boffa Ballaran *et al.*, 1998; Carpenter *et al.*, 1999; Boffa Ballaran *et al.*, 1999; Salje *et al.*, 2000; Boffa Ballaran *et al.*, 2001; Carpenter and Boffa Ballaran, 2001; Boffa Ballaran *et al.*, 2001; Tarantino *et al.*, 2002; Boffa Ballaran and Carpenter, 2003; Tarantino *et al.*, 2003]

1.5.1 Autocorrelation Studies

The autocorrelation method [Salje *et al.*, 2000] has been used to follow effective linewidth (Δcorr) variations of phonon bands in a given spectral region [Boffa Ballaran *et al.*, 1998; Carpenter *et al.*, 1999; Boffa Ballaran *et al.*, 1999; Carpenter and Boffa Ballaran, 2001; Boffa Ballaran *et al.*, 2001; Tarantino *et al.*, 2002; Tarantino *et al.*, 2003]. The following section discusses briefly two of the aforementioned studies to illustrate how local strain heterogeneities can explain solid solution mechanisms for structures that differ as greatly as garnets and pyroxenes.

Boffa Ballaran *et al.* (1998) investigated cation ordering in the augite-jadeite system. This system contains an ordered phase at intermediate compositions with the $P2/n$ symmetry, which disorders with increase in temperature to the $C2/c$ symmetry of the end-members. The disordering process gives rise to an increase in bandwidth of the IR spectra. The Δcorr results presented in the study, as revised by Boffa Ballaran and Carpenter (2003), are shown in Figure 1.8 for the three regions of the IR spectra. In the FIR region ($100\text{-}200\text{cm}^{-1}$) an increase in bandwidth is observed at intermediate compositions of disordered samples with the $C2/c$ structure (Figure 1.8a). The positive deviation from ideality appears to be related to the enthalpy of mixing, ascertained for the system using solution calorimetry [Wood *et al.*, 1980]. The ordered $P2/n$ samples, in comparison, show a decrease in bandwidth indicating that cation ordering causes a decrease in local strain heterogeneities. At higher frequencies ($210\text{-}800\text{cm}^{-1}$) the linewidth of IR spectra is still sensitive to cation ordering, whereas in the region $800\text{-}1400\text{cm}^{-1}$ the effect of ordering is relatively small and erratic. The $C2/c$ data in both ranges can be interpreted in terms of two linear segments for augite-rich and jadeite-rich compositions. This suggests a substantial difference in the local structure of augite with respect to jadeite, despite their similarity on a macroscopic scale. The structural mechanism for the order – disorder phase transition involves adjustment of cation coordination at the M sites by tilting of basal faces of SiO_4 tetrahedra, which appear relatively rigid.

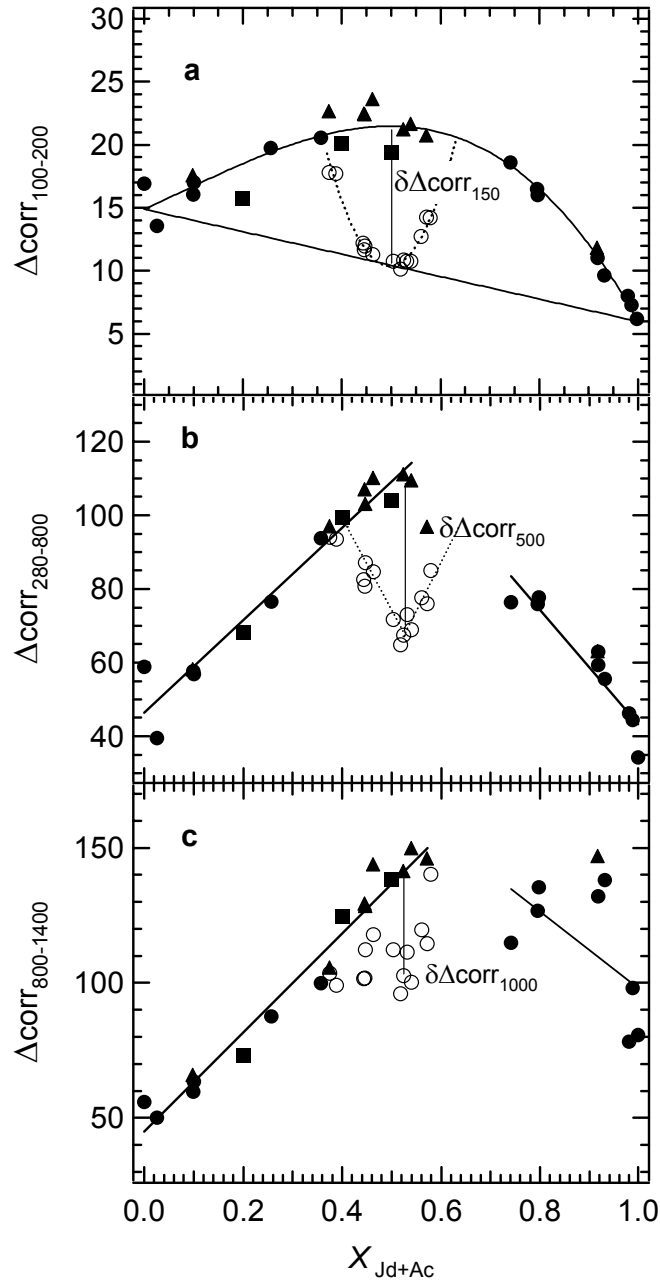


Figure 1.8a-c: Autocorrelation results taken from Boffa-Ballaran *et al.* (1998), and subsequently updated in Boffa-Ballaran and Carpenter (2003) for the augite-jadeite solid solution.

a) For the $100\text{-}200\text{cm}^{-1}$ region. b) For the $280\text{-}800\text{cm}^{-1}$ region, and c) For the $800\text{-}1400\text{cm}^{-1}$ region. Filled symbols are for $C2/c$ samples and circles for natural ordered $P2/n$ samples. $\delta\Delta\text{corr}_{150}$, $\delta\Delta\text{corr}_{500}$ and $\delta\Delta\text{corr}_{1000}$ are the difference between $C2/c$ and $P2/n$ data in the three different regions.

Boffa Ballaran *et al.* (1999) conducted a study on three garnet solid solutions, pyrope-almandine, almandine-grossular and pyrope-grossular. The main difference between the structure of garnets and that of pyroxenes is that there are no rigid unit modes. This means that there are no distortion mechanisms of relatively rigid units to accommodate the substitution of cations into the structure, e.g the out-of-plane tilting of the rigid SiO_4 tetrahedra in the augite-jadeite system. Results from the study showed that the line broadening variation was essentially the same over the different regions investigated (Figure 1.9, reproduced from Boffa Ballaran *et al.*, 1999). The almandine-grossular and pyrope grossular systems show a positive deviation from linearity, whereas the linewidth variation of the pyrope-almandine solid solution appears linear. This suggests that the pyrope-grossular system is the most heterogeneous on a local length scale, and pyrope-almandine, the most homogeneous.

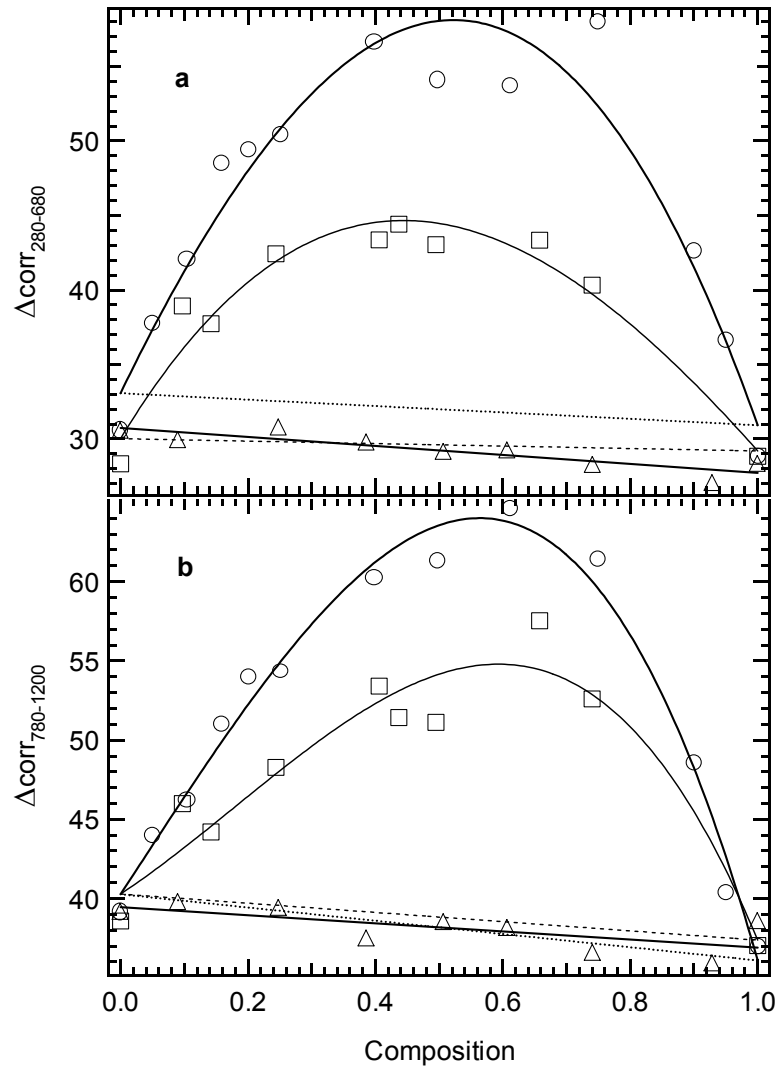


Figure 1.9: Autocorrelation results for the pyrope-grossular (circles), pyrope-almandine (triangles) and almandine-grossular (squares) systems, taken from Boffa-Ballaran *et al.* (1999). The pyrope-almandine system shows linear behaviour across the solid solution. The maximum deviation from linearity is shown by the pyrope-grossular system, which has a $\delta(\Delta\text{corr}) \sim 26$, whereas the almandine-grossular system has a $\delta(\Delta\text{corr}) \sim 15\text{-}16$.

1.6 Aims of the Study

The work conducted by Harker and Tuttle (1955) and Goldsmith and Heard (1960) on the calcite – magnesite system and the experimental work by Goldsmith (1972) and Capobianco *et al.* (1987) has answered many questions with regard to the topology of the phase diagrams of these two systems, but has invited many more questions concerning the order-disorder phase transition and cation substitution mechanisms within the system. This work has been undertaken in an attempt to characterise the macroscopic and microscopic behaviour of the magnesite – otavite system as an analogue to the magnesite – calcite system.

Moreover, this solid solution constitutes an ideal system for testing if strain and elasticity play a substantial role in determining cation substitution and ordering mechanisms in carbonates. The work carried out by Boffa Ballaran *et al.* (1998) on the augite-jadeite system, which presents an analogue phase diagram with an ordered phase at intermediate compositions, will provide an opportunity for a direct comparison between carbonate and silicate structures.

This project entails:

- Relating the behaviour of the otavite – magnesite system to that of the calcite – magnesite system;
- Studying the relationship between substitution of cations of different sizes and variation of lattice parameters of samples synthesised at different temperatures and run durations;
- Studying the relationship between lattice parameters of samples with different structures, the ordered $R\bar{3}$ structure, and the disordered $R\bar{3}c$ structure;
- Quantifying lattice strain associated with cation substitution, and ordering, as well as ascertaining the origin of such a strain;
- Quantifying the degree of order within samples with the ordered $R\bar{3}$ structure, and in turn relating that to the conditions of synthesis, equilibrium conditions of the system, and the kinetics of the system;

- Studying the origin of the order-disorder phase transition via Hard Mode Infrared Spectroscopy (HMIS), and hence relating the results obtained to local structural occurrences within the material.

Synthesis of the samples will be carried out using piston cylinder apparatus. The samples will be characterised using X-ray powder diffraction, Rietveld analysis and Hard Mode Infrared Spectroscopy. Details of the experimental work completed, and the results obtained, are outlined in the following chapters.

2: Synthesis and Experimental Techniques

The techniques used for synthesising and characterising samples along the magnesite – otavite join are outlined in the following chapter.

2.1. Synthesis Techniques

In order to synthesise a complete series of samples across the solid solution the experimental methods from the previous studies were used as a starting point. As reported in Bromiley (2002), several problems were encountered with the hydrothermal pressure vessel, namely, dissociation of the carbonate material. Large cadmium oxide crystals were observed at cadmium-rich compositions, as well as significant amounts of brucite $[\text{Mg}(\text{OH})_2]$ at magnesium-rich compositions. Neither Goldsmith nor Capobianco *et al.* reported major problems with dissociation. Capobianco *et al.* simply report that during the annealing experiments the loss of CO_2 was prevented by increasing pressure to 10-15 kbar and Goldsmith reports that a few runs yielded small amounts of cadmium oxide, so runs were repeated at 20 kbar. It was therefore decided that increased pressure and the addition of a CO_2 source to the capsule might prevent dissociation.

2.1.1 Starting Materials

The starting materials used in this study were mixed from magnesium carbonate (MgCO_3), produced by Alfa Aesar, with a purity of 99.996% and cadmium carbonate (CdCO_3), produced by Aldrich Chemicals, with a purity of 99.999%. Full characterisation of the starting materials was done using both X-ray powder diffraction and Infrared spectroscopy, the X-ray diffraction patterns and IR spectra for which may be found in Appendix 1. Powders were weighed in appropriate amounts to give 2g batches

and nominal compositions between the end-members, as given in Table 2.1. The powders were ground under acetone with an agate pestle and mortar, before being dried at 150°C for 24 hours.

Table 2.1: Nominal compositions for samples mixed between the MgCO_3 and CdCO_3 end-members. Weights given in grams for 2g batches.

Composition	Weight MgCO_3 (g)	Weight CdCO_3 (g)
MgCO_3	2	0
$\text{Mg}_{0.9}\text{Cd}_{0.1}\text{CO}_3$	1.6297	0.3703
$\text{Mg}_{0.8}\text{Cd}_{0.2}\text{CO}_3$	1.3234	0.6766
$\text{Mg}_{0.7}\text{Cd}_{0.3}\text{CO}_3$	1.0659	0.9341
$\text{Mg}_{0.6}\text{Cd}_{0.4}\text{CO}_3$	0.8463	1.1537
$\text{Mg}_{0.55}\text{Cd}_{0.45}\text{CO}_3$	0.7482	1.2518
$\text{Mg}_{0.5}\text{Cd}_{0.5}\text{CO}_3$	0.6568	1.3432
$\text{Mg}_{0.45}\text{Cd}_{0.55}\text{CO}_3$	0.5715	1.4283
$\text{Mg}_{0.4}\text{Cd}_{0.6}\text{CO}_3$	0.4917	1.5083
$\text{Mg}_{0.3}\text{Cd}_{0.7}\text{CO}_3$	0.3465	1.6535
$\text{Mg}_{0.2}\text{Cd}_{0.8}\text{CO}_3$	0.2179	1.7821
$\text{Mg}_{0.1}\text{Cd}_{0.9}\text{CO}_3$	0.1031	1.8969
CdCO_3	0	2

2.1.2 Addition of Silver Oxalate as a CO_2 source

The use of direct CO_2 pressure poses several problems. If CO_2 gas is used in a Titanium-Zirconium-Molybdenum (TZM) autoclave, firstly the maximum pressure that can be reached is only in the range of 1-1.5 kbar, which was not sufficient to prevent

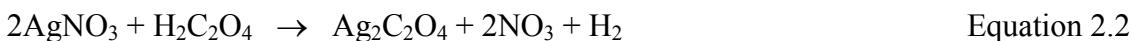
dissociation, and secondly, CO₂ becomes a supercritical fluid at 32°C and 75 bar, so making pressurisation of the experiment difficult.

A technique was investigated which is reported by Chai and Navrotsky (1993), in which a clamped, but unwelded, capsule was placed in a cold seal vessel which was then packed with dry ice, so giving a direct CO₂ pressure. Chai and Navrotsky (1993) report that although the pressure within the vessel could not be measured, it was estimated to be between 1-2 kbar, and that this was sufficient to prevent dissociation of the carbonate materials. The same set-up was used for this investigation and an internal pressure sensor did allow the pressure to be monitored as the vessel was heated. Two runs were performed, a test run, without a capsule, designed to monitor the pressure, and an experimental run, with a capsule. Despite crushing the dry ice to a fine powder and packing it tightly into the vessel, the maximum pressure obtained was between 700-900 bar. The run products from the capsule contained in the experimental run were examined using X-ray powder diffraction, but it was found that complete dissociation of the carbonate material had occurred and the patterns obtained were those for cadmium oxide and magnesium oxide.

An alternative CO₂ source, which can be added directly to the capsule, is silver oxalate (Ag₂C₂O₄), which has been used in studies by Sterner and Bodnar (1991), Koziol and Newton (1998), Jendrzewski *et al.* (1997) and Frost and Wood (1997). Upon heating the silver oxalate decomposes to produce carbon dioxide and silver, Equation 2.1:



The silver oxalate was precipitated from reagent grade silver nitrate and oxalic acid before being washed in distilled water and methanol, then dried for three days in a vacuum desiccator and stored in a light opaque container, Equation 2.2:



Care was taken that the silver oxalate did not decompose prematurely when the capsule was being welded, by continuous cooling of the capsule with water during the weld. To prevent the contamination of the run product with silver from the decomposition process, the silver oxalate was added to the capsule in a platinum foil envelope, which was removed, intact, from the capsule once the run had been quenched.

2.1.3 Piston Cylinder Apparatus and Method

The piston cylinder provided a logical solution for sample synthesis, as higher pressures could be obtained (up to 5 GPa and 1800°C [Boyd and England, 1960]), and therefore shorter run durations used, thus allowing less time for dissociation.

The piston cylinder is a solid pressure medium apparatus, within which the pressure is generated via pressure amplification from a small force on a large piston to a large force on a small piston. The hydraulic bridge transfers the load from the ram to the piston, which in turn pushes up into the bomb, and hence applies pressure to the sample. The larger $\frac{3}{4}$ inch bomb allows for a larger sample volume and was used for all the experiments in this study.

The assembly into which the sample is inserted consists of a pressure transferring medium, which in these experiments was talc, a graphite resistance furnace, and the sample volume in the middle, Figure 2.1. For this study a pyrex glass cylinder was used between the graphite and the talc as it not only acts as an electrical insulator, but also traps excess water. It had been reported by both Goldsmith and Newton (1969) and Byrnes and Wyllie (1981) that dehydration of the talc assembly led to the presence of brucite within the sample, as well as a coating of graphite around the sample, both of which were avoided with the use of the pyrex glass sleeve. It may be seen from Fig 2.1 that the graphite resistance heater is tapered, so allowing a symmetrical temperature

gradient to be achieved, and hence the maximum offset from the set temperature is only 5°C [Watson *et al.*, 2002].

The powder sample is loaded into a cylindrical platinum capsule, along with the envelope containing the silver oxalate. The geometry of the capsule is important in order that it can fit tightly into the graphite furnace, so circular end-caps are welded top and bottom on the capsule. This not only keeps the correct geometry, but also prevents the loss of volatiles from the capsule. The excess space within the furnace is filled with unsintered alumina spacer discs, Figure 2.1. The assemblage is wrapped in a thin lead foil that provides lubrication at temperature and pressure. The assemblage is inserted into the bomb and a thin steel disc is inserted below to ensure good electrical contact. A steel piston ring prevents the extrusion of lead down towards to piston once the assembly is at temperature and pressure. A steel base plug with a pyrophalite jacket is inserted into the top of the bomb. This contains a hole, through which the thermocouple can be inserted. The bomb sits on the bridge and a thermocouple plate sits on top. The thermocouple used was a Pt Pt/Rh S-type thermocouple. A thin sintered alumina ceramic containing two holes is used to house the thermocouple, which is threaded through the two holes and welded at the base to form a junction. This in turn is pushed through the plate and bomb until it sits just above the sample. A spacer plate is then placed on top and moved into place in the press. The system is water cooled through the bridge, bomb, thermocouple plate and spacer plate, Figure 2.2.

Temperature is monitored by a Eurotherm power controller, which operates in a feedback loop with the thermocouple. This allows temperature fluctuations to be kept to a minimum, $\pm 1^\circ\text{C}$. Once the assembly is in place within the press and the water and power have been connected, the pressure can be increased by alternating between pumping of the upper and lower rams. Once the pressure is 10% below the desired pressure, the sample can be heated to the final temperature. It is only once the temperature is stable that the pressure can be increased to the final pressure. The pressure can be controlled automatically and is increased or decreased about a set point by a worm screw.

Switching off the power that heats the assembly quenches the sample. The cooling water continues to circulate, so cooling the assembly rapidly. A quench from 800°C takes approximately 10-15 seconds.

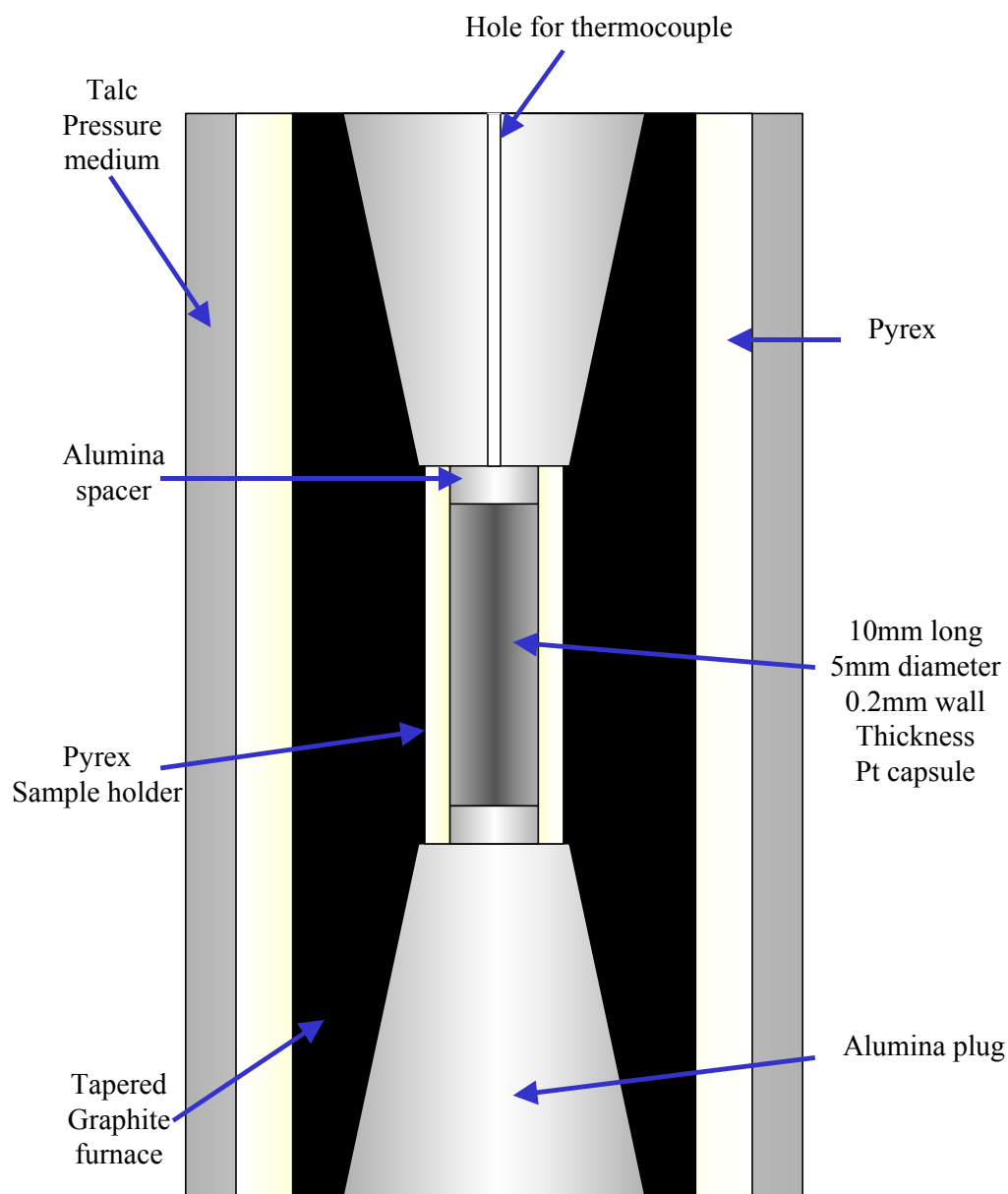


Figure 2.1: Cross-sectional schematic diagram of the piston cylinder assemblage. Not to scale.

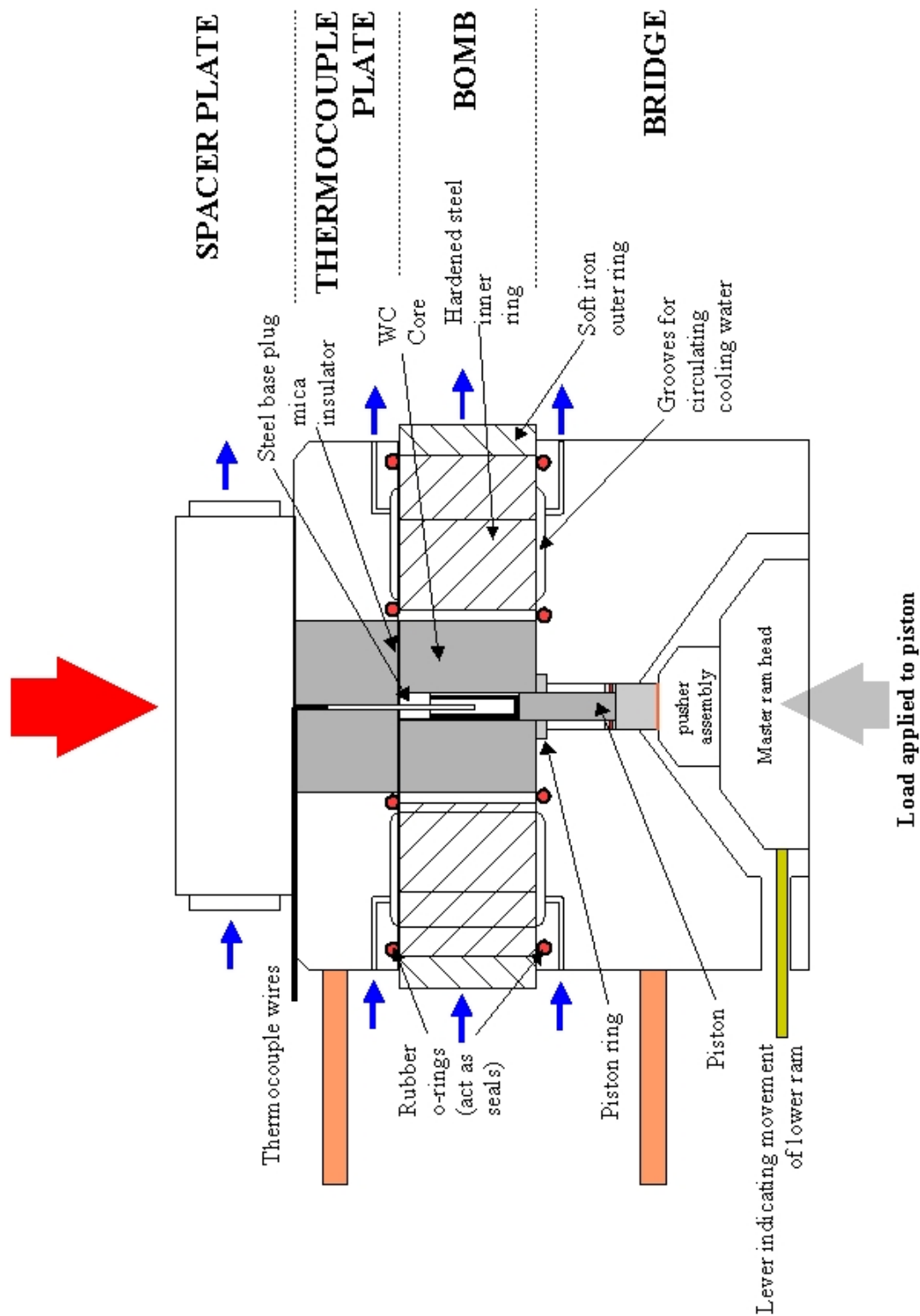


Figure 2.2: Schematic diagram of the piston cylinder apparatus.

2.1.4 Synthesis Conditions

All syntheses for this study were performed using piston cylinder apparatus. Care was taken to ensure that sufficient time was allowed for the reaction to occur, but that run durations were not too long that the CO₂ source from the silver oxalate was exhausted. In order to obtain an idea of the rate of reaction and effect of pressure, several experiments were run and optimum run conditions were ascertained. As reported in Bromiley (2002), a set of samples were synthesised at 10 kbar, 600°C for 3 hours. For samples of intermediate composition this yielded ordered samples, as well as two-phase samples at magnesium-rich compositions.

The synthesis of a complete set of disordered samples was more difficult and much more time was required to determine the optimum run conditions. Initially, the same run conditions as Bromiley (2002) were used and following work by Capobianco *et al.* (1987) and Goldsmith (1972), run temperatures of 850 and 900°C were used. The resultant run products were often brown in appearance and X-ray diffraction of the run products showed them to have a very low degree of crystallinity. A run pressure of 10 kbar was used, but with a lower temperature, 800°C. The run duration was only 1 hour as it was assumed that at increased temperature the reaction kinetics would be faster, and hence a reduction in run time was beneficial in terms of the CO₂ source. It was found that these run conditions were sufficient to synthesise a complete set of disordered samples across the entire solid solution. It is interesting to note at this point that both Capobianco *et al.* and Goldsmith both observed some degree of order up to 825°C.

Samples of composition Mg_{0.5}Cd_{0.5}CO₃ were synthesised at 500, 650 and 700°C in order to study the evolution, with temperature, of the order parameter associated with the order – disorder transformation. Samples of the same composition (Mg_{0.5}Cd_{0.5}CO₃) were also synthesised at different run durations (3, 19, 24, 48, 72, 96 and 120 hours) at 500, 600 and 650°C to determine equilibrium conditions. Although the ordered phase within the system only constitutes a small part of the phase diagram, it was very important for this study that this section of the phase diagram was investigated as

thoroughly as possible. A complete list of experiments carried out during this study may be found in Appendix 2.

2.2 X-ray Powder Diffraction

All samples synthesised were characterised by means of X-ray powder diffraction. This was done using a Philips X'Pert Pro X-ray diffraction system operating in reflection mode, using Co-K α_1 ($\lambda = 1.78892\text{\AA}$) radiation selected with a focusing monochromator, a symmetrically cut curved Johansson Ge₍₁₁₁₎ crystal. The K α_2 line was reduced by the monochromator to <2% of the intensity of the K α_1 line. A Philips X'celerator detector was used. This is a detector based on RTMS (Real Time Multiple Strip) technology capable of simultaneously measuring intensities of a range of 2θ . The active length of the X'celerator detector was $2.123^\circ 2\theta$.

Samples were ground under acetone with an agate pestle and mortar. A small amount of silicon (NBS standard material no.640) was added as an internal standard. A silicon sample holder was used, upon which the powder was deposited from a suspension of ethanol. The diffractometer was set with a step size of 0.2° , a step time of 1000 seconds and a scan speed of $0.002^\circ/\text{sec}$ with a spinning platform rotating at 1 rotation/sec. Data were collected from $2\theta = 20^\circ$ to 120° .

2.3 Rietveld Analysis and Refinement

Once the data had been collected the X-ray diffraction pattern was calibrated using STOE Win XPOW (Version 1.08, STOE & Cie GmbH) software. Rietveld analysis and subsequent refinements were performed using EXPGUI [Toby, 2001] and GSAS [Larsen and Von Dreele, 1994]. The parameters refined during the Rietveld analysis were as follows:

- 12 coefficients for the “Chebyshev polynomial of the first kind” background function [GSAS manual p.132, Larson and Van Dreele]
- Scale factors for each phase present in the diffraction pattern, normally one for silicon and one for the carbonate phase.
- Lattice parameters
- Gaussian and Lorentzian broadening coefficients of the pseudo-Voigt profile function [GSAS manual p.161, Larson and Van Dreele]

For the carbonate phases it was also possible to refine the following parameters for the carbonate phase:

- Atomic position
- March-Dollase preferential orientation
- Mg and Cd occupancies, constrained to the nominal composition for each sample

Atomic positions and lattice parameters were reported by Reeder (1983) for both magnesite and otavite, by Reeder and Wenk (1983), Paquette and Reeder (1990), Althoff (1977), Ross and Reeder (1992) and Steinfink and Sans (1959) for dolomites with varying degrees of order. Markgraf and Reeder (1985) and Oh *et al.* (1973) reported lattice parameters, atomic positions and bond distances for single crystals of magnesite. The results from all these studies were used as starting parameters for the refinements of the ordered and disordered carbonate structures in this study.

The term used to determine the “goodness-of-fit” for each refinement for a weighted pattern, R_{wp} , is expressed as;

$$R_{wp} = \left\{ \frac{\sum w_i (y_i(obs) - y_i(calc))^2}{\sum w_i (y_i(obs))^2} \right\}^{1/2}$$

where w_i is the weight, which is equal to $1/y_i$, and y_i is a term that incorporates all the information regarding the scale factor and geometry factor from the instrument, as well as the structure factor, peak position and background from the sample. The terms *obs* and *calc* are for the observed and calculated patterns respectively. The weighted refinement term, R_{wp} , and the Lorentzian line width for each refinement can be found in Appendix 5.

2.4 Infra-red Powder Absorption Spectroscopy

Powder samples from all the experiments carried out were analysed by means of Hard Mode Infra-red Spectroscopy (HMIS) at the University of Cambridge, England. In order to obtain very high quality IR spectra, the homogeneity of the grain size is of paramount importance for the preparation of the pellets. Two different grinding times (5 and 10 minutes) were used on the otavite starting material in order to ascertain the optimum grinding time, the results of which are presented in Appendix 3. Each sample was then hand ground under acetone in an agate pestle and mortar for 5 minutes before the pellets were prepared.

Two types of matrix were used, selected according to their IR transparency, in order to collect spectra across a broad frequency range. Potassium bromide was used as a matrix material at higher frequencies ($250\text{-}4000\text{cm}^{-1}$), whereas a polyethylene matrix was used at low frequencies ($50\text{-}350\text{cm}^{-1}$).

Potassium bromide was mixed with the sample powder in a ratio of 500:1 to obtain the desired absorbance. Sample and matrix were accurately weighed in appropriate quantities and then mixed thoroughly in an agate pestle and mortar, 200mg of the mixture was weighed in order to make a pellet of the desired thickness. Pellets were prepared in a 13mm die under vacuum, which was left to pump down for 10 minutes. The die was then subjected to a pressure of 9 tonnes in a small press, and again left for 10 minutes. The vacuum was then released and after 5 minutes the load was removed slowly to prevent cracking of the pellets. The KBr pellets were kept in a drying oven before the IR experiments, due to the hygroscopic nature of the KBr.

Polyethylene was mixed with the sample powder in a ratio of 50:1. Due to the fineness of the PE powder, it was necessary to ballmill the sample powder with the PE

powder for 5 minutes to ensure homogeneity of the pellet. 100mg of the powder was weighed and pressed in the die, using the same method as for the KBr pellets.

Spectra were collected under vacuum at room temperature using a Bruker 113v FT-IR spectrometer. All measurements taken were averaged over 512 scans with an instrumental resolution of 2cm^{-1} . Spectra were collected in three different regions, $50\text{--}400\text{cm}^{-1}$, $200\text{--}500\text{cm}^{-1}$ and $400\text{--}4000\text{cm}^{-1}$. For the MIR ($400\text{--}4000\text{cm}^{-1}$) a Globar source was used with a KBr beamsplitter and a DTGS detector with a KBr window. For the KBr FIR region ($200\text{--}500\text{cm}^{-1}$) the Globar source was used once again, but with a Ge-coated 6 micrometer Mylar beamsplitter and a DTGS detector with a polyethylene window. For the FIR ($50\text{--}400\text{cm}^{-1}$ measured using the PE pellets), a mercury lamp source was used with the Ge-coated 6 micrometer Mylar beamsplitter and DTGS detector with polyethylene window.

Two reference pellets, one of pure PE and one of pure KBr were made and spectra from these reference pellets were collected. The reference spectra collected were subtracted from the sample spectra. Some samples of magnesium-rich compositions were observed to have small amounts of brucite ($\text{Mg}(\text{OH})_2$) present. Therefore a spectrum of brucite was taken, and subtracted from spectra of samples that contained brucite. The X-ray powder diffraction pattern and IR spectrum for brucite may be found in Appendix 4.

Spectra were loaded into Igor Pro 4.09A software before autocorrelation and peak position values were obtained.

2.4.1 Analysis of IR Powder Absorption Spectra

Analysis of IR spectra was done using Igor Pro 4.09A software. In order to determine the variation of vibrational band position across the solid solution two different routines were used. The band positions of well-defined bands, such as those in the MIR region of the spectra, were determined using the “Find Peak” routine in Igor Pro, which identifies peak maxima by analysing the first and second derivative of absorption signals.

Overlapping bands at low frequencies were resolved using a Lorentzian profile fit (Equation 2.3). Six Lorentzian profiles where K_0 , K_l and K_2 are intensity, position and

fullwidth at half maximum respectively, were used in the range 75-200cm⁻¹, while five were used in the region 200-350cm⁻¹.

$$L = \frac{2K_0}{\pi K_2} * \frac{1}{\left[1 + 4\left(\frac{x - K_1}{K_2}\right)^2\right]} \quad \text{Equation 2.3}$$

2.4.2 Autocorrelation Analysis

The autocorrelation function, as defined by Equation 2.4, where $\alpha(\omega)$ represents the spectrum, and $\alpha(\omega + \omega')$ represents the same spectrum moved by a value ω' , was used to quantify the variation in effective linewidth of vibrational bands over a given spectral range [Salje *et al.*, 2000].

$$\text{Corr}(\alpha, \omega') = \int_{-\infty}^{\infty} \alpha(\omega + \omega') \alpha(\omega) d\omega \quad \text{Equation 2.4}$$

By correlating the spectrum with itself, it is possible to determine the area of overlap between the two spectra at different values of ω' , and hence produce a renormalized spectrum, which has a maximum of $\Delta\omega' = 0$. A Gaussian function, of the form in Equation 2.5, can then be fitted to the central peak of the autocorrelation spectrum to extract information about the original linewidth of the IR spectra.

$$G = k_0 \exp\left[-\left(\frac{x - k_1}{k_2}\right)^2\right] \quad \text{Equation 2.5}$$

k_0 , k_1 and k_2 are intensity, position and full width at half maximum respectively.

2.5 Quantitative Determination of Sample Composition

Several methods were investigated in an attempt to quantitatively determine the composition of samples synthesised for this study. It was not possible to use Inductively Coupled Plasma-Mass Spectroscopy (ICPMS) as the amount of carbon present in the atmosphere fluctuates, hence giving inaccurate compositional analyses.

Powder products recovered from piston cylinder runs were very fine (1-5 μ m), making powder mounting for electron microprobe analysis impossible. An alternative method, originally investigated by Bromiley (2002), was the use of Transmission Electron Microscopy (TEM) to do Energy Dispersive X-ray (EDX) analysis. The use of this method to obtain quantitative information was not possible, as it required a cadmium standard to quantify the amount of cadmium present in each sample. Cadmium carbonate proved to be very beam sensitive and other cadmium compounds introduced too great a safety risk.

3: X-ray Diffraction and Rietveld Analysis

X-ray powder diffraction was used to obtain lattice parameters, atomic positions, bond lengths and to determine, quantitatively, the degree of order as a function of temperature and composition.

3.1 Results from X-ray Powder Diffraction

X-ray powder diffraction patterns for the series of carbonates synthesised at 600°C, 1 GPa for 3 hours were reported by Bromiley (2002). Figure 3.1 shows a selected part of the diffraction patterns collected for 10mol% increment composition samples synthesised at 800°C. The 2θ positions of the diffraction signals are clearly decreasing as a function of substitution of cadmium, indicating a decrease in unit-cell parameters across the magnesite – otavite solid solution. All these samples have the $R\bar{3}c$ structure and consist of a single carbonate phase, indicating that at such conditions there is a complete, disordered solid solution between the two end-members. This is particularly clear when comparing the $\text{Mg}_{0.5}\text{Cd}_{0.5}\text{CO}_3$ diffraction pattern with that of the same composition from Bromiley (2002), the only variable in synthesis conditions being the temperature at which the samples were synthesised (Figure 3.2). Note that in Figure 3.1 the samples of composition $\text{Mg}_{0.7}\text{Cd}_{0.3}\text{CO}_3$ and $\text{Mg}_{0.8}\text{Cd}_{0.2}\text{CO}_3$ show significantly broader peaks than all the other samples. It is suggested that at 800°C these two samples lie on the solvus between the complete, disordered solid solution and the miscibility gap, and hence these samples may show some degree of exsolution, which in turn would lead to broadening of X-ray diffraction reflections.

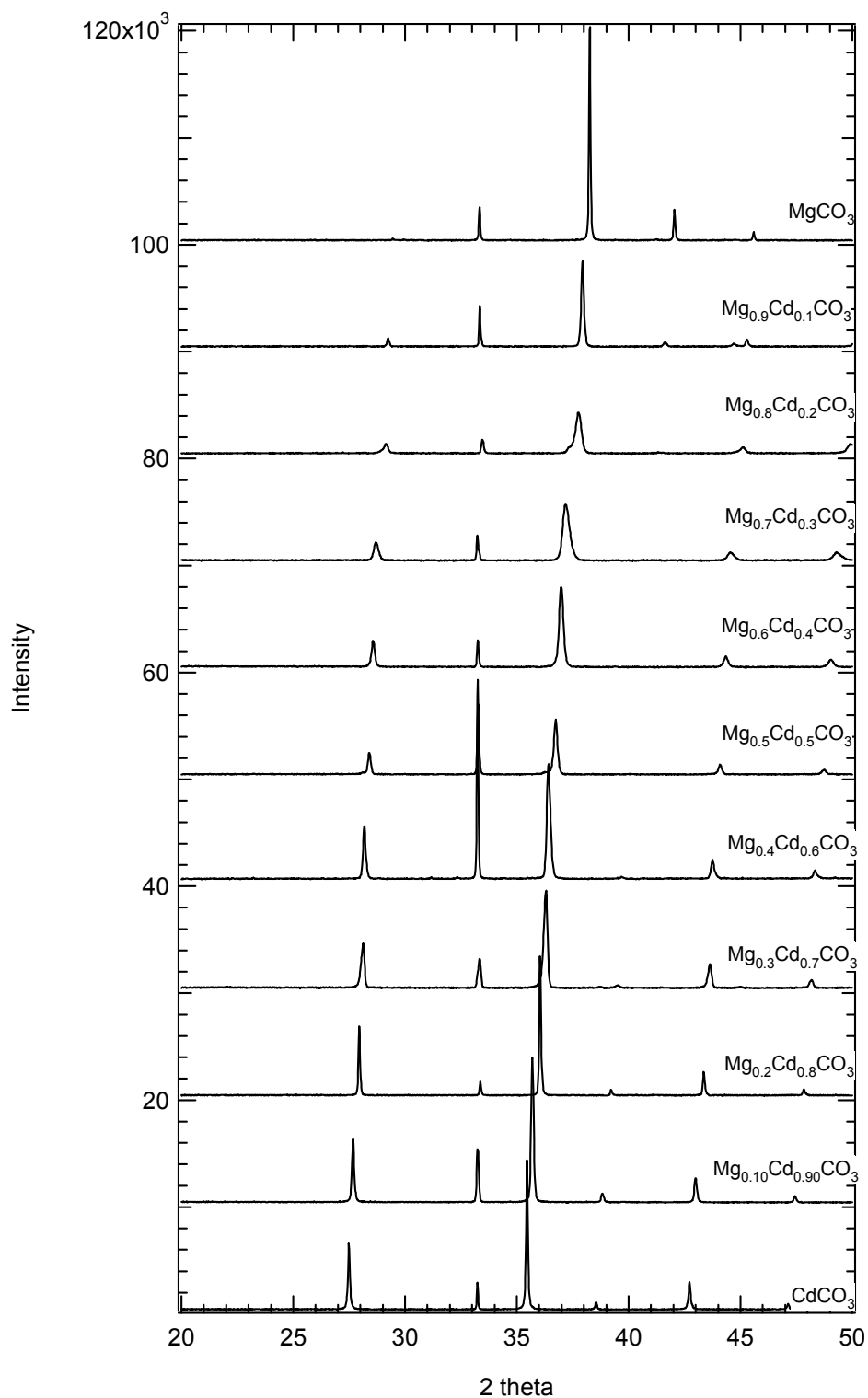


Figure 3.1: Selected region of stacked X-ray powder diffraction patterns for a complete set of samples synthesised at 800°C, 1GPa, 1 hour. Note that the peak at $2\theta = 33.15^\circ$ is due to the internal Si standard.

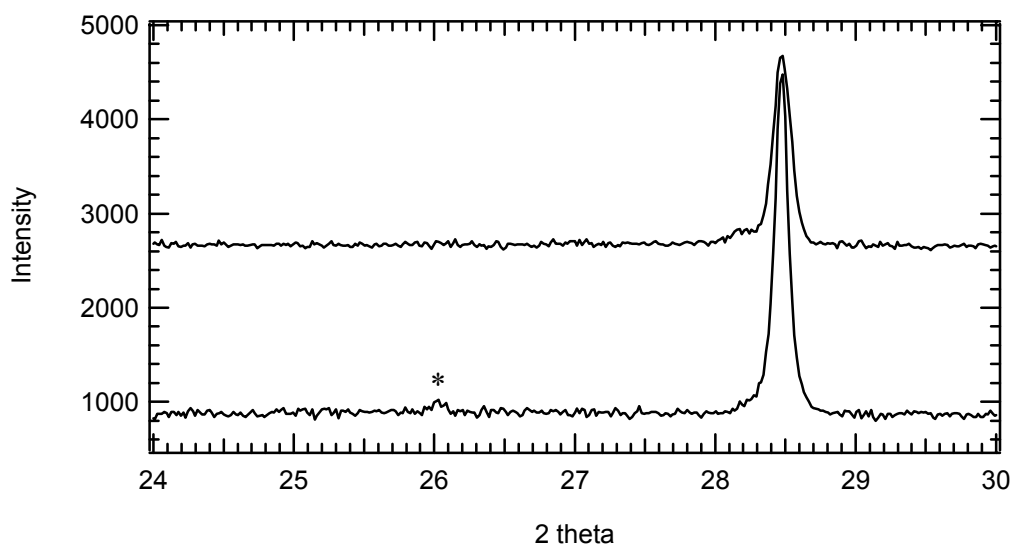


Figure 3.2: Comparative XRD patterns for $\text{Mg}_{0.5}\text{Cd}_{0.5}\text{CO}_3$ samples synthesised at 600°C from Bromiley (2002) (bottom), and 800°C from this study, (top). Note the small, but present, peak at $2\theta = 26^\circ$ (indicated by *) for the ordered phase from Bromiley (2002) (bottom).

Comparison of the two patterns reveals a subtle, but essential, difference at $2\theta \sim 26^\circ$. In the ordered sample from Bromiley (2002) a small peak is observed, which is not present in the sample synthesised for this study. This reflection is the (101) and is present only in the ordered $R\bar{3}$ samples. In the study by Bromiley (2002) the (101) reflection was observed for all samples of intermediate compositions, indicating, therefore, the presence of a cadmium dolomite structure. However, in the diffraction patterns of the same compositions synthesised at 800°C , the (101) peak is absent, confirming the $R\bar{3}c$ symmetry of these samples.

Several samples with composition $\text{Mg}_{0.5}\text{Cd}_{0.5}\text{CO}_3$ were synthesised at different temperatures and run durations. A region of the X-ray diffraction patterns for these samples is shown in Figure 3.3.

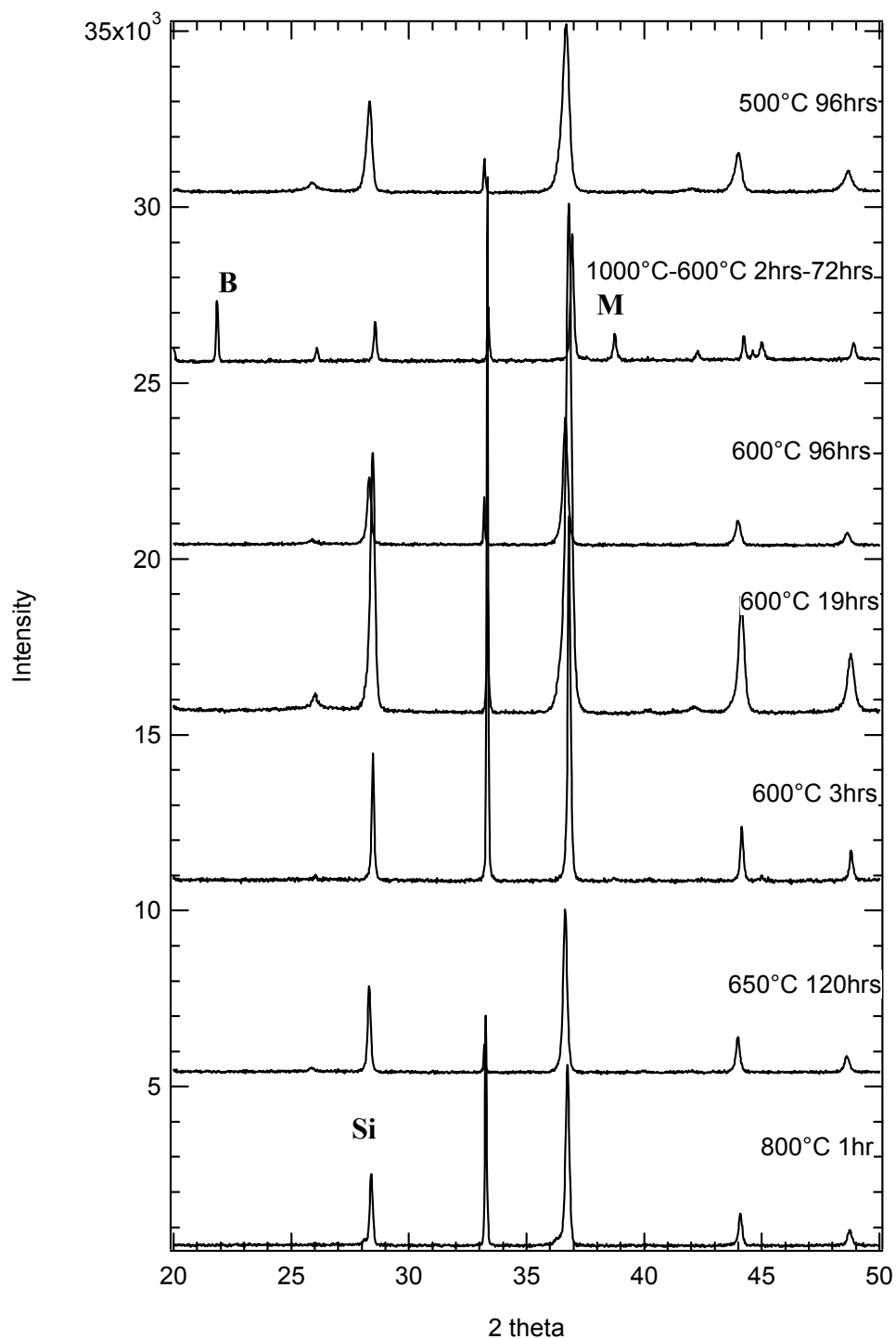


Figure 3.3: Selected region of stacked powder XRD patterns for $\text{Mg}_{0.5}\text{Cd}_{0.5}\text{CO}_3$ samples synthesised at 1GPa. B = brucite, M = monteponite, Si = silicon standard.

The sample synthesised at 600°C for 3 hours is taken from Bromiley (2002).

Comparison of the patterns in Figure 3.3 reveals the presence of the (101) peak at $2\theta = 26^\circ$, for the samples with $R\bar{3}$ symmetry. The samples synthesised at 700 and 800°C show $R\bar{3}c$ symmetry. The sample synthesised at 1000°C for two hours, then at 600°C for 72 hours was an experiment designed to grow a single crystal from a melt. No silver oxalate source was used in the capsule, so it may be seen that products due to carbonate dissociation are present in the diffraction pattern, namely a peak due to brucite $[\text{Mg}(\text{OH})_2]$ at $2\theta = 21^\circ$, and a peak due to monteponite $[\text{CdO}]$ at $2\theta = 38^\circ$.

3.2 The Rietveld Analysis

Rietveld refinements for all samples synthesised for this study were done using GSAS [Larson and Von Dreele, 1994] and the windows interface, Expgui [Toby, 2001] (see Section 2.3). From the refinements it was possible to ascertain accurate lattice parameters, and to determine bond lengths and angles and site occupancies, although with lower accuracy than is obtainable by way of single crystal structure refinements. The results for the refinements are presented in this section. Results for the series synthesised at 600°C, which have been published in Bromiley (2002) will be given again here, as since the time of publication the refinements have been improved due to the addition of a preferential orientation parameter. Given the form of the otavite crystals (rhombohedral, due to their cleavage direction), the likelihood of preferential orientation being present in reflection X-ray powder diffraction patterns is high. It has been found in the carbonates studied that this parameter can correspond to between 20-30% of preferential orientation along the $[104]$. To illustrate the improvement of the refinements presented in this study, the Rietveld refinements for the otavite end-member, synthesised at 600°C, are compared, with the preferential orientation being refined (Figure 3.4) and without it being refined from Bromiley (2002) (Figure 3.5).

The purple line shows the difference between the observed and calculated intensities and clearly shows better agreement once preferential orientation is taken into account. A better fit of observed intensities from the diffraction pattern does not,

however, modify unit-cell parameters, which are the same as those reported by Bromiley (2002). However, other parameters, such as cation-oxygen bond lengths, are better constrained, and their values are now in better agreement to those obtained from single-crystal data refinements [Borodin *et al.*, 1979].

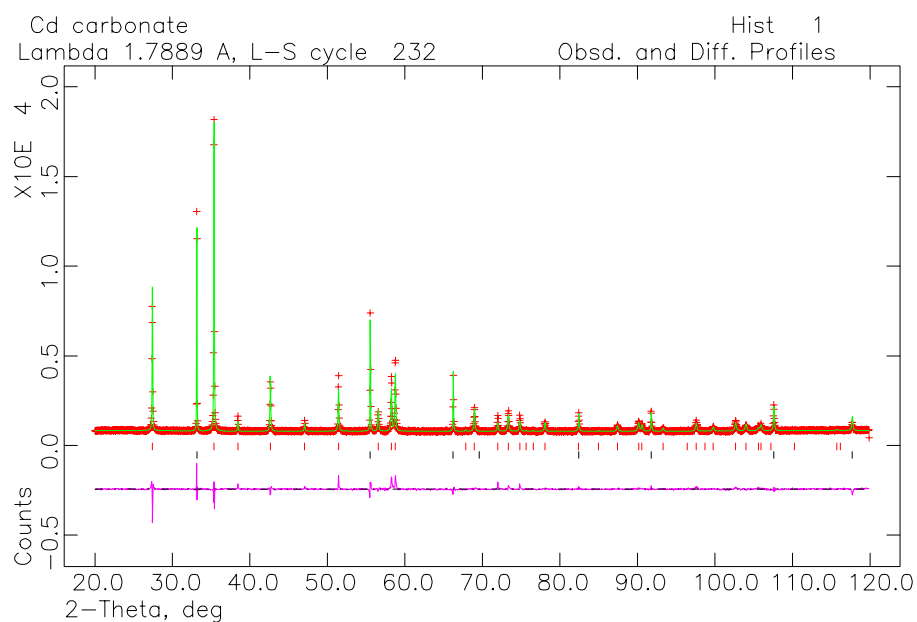


Figure 3.4: Rietveld refinement of the diffraction pattern for CdCO_3 with Si standard. Preferential orientation refined (27%). Where $R^2 = 0.0503$, $\Gamma = 0.1651 \times 10^2$.

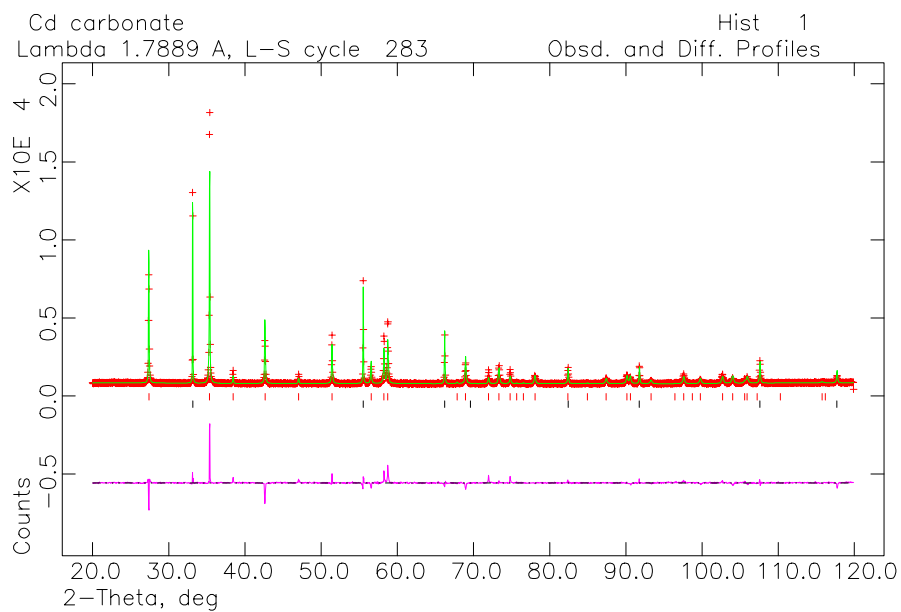


Figure 3.5: Rietveld refinement of the same diffraction pattern for CdCO_3 with Si standard, taken from Bromiley (2002). Preferential orientation was not refined for this sample. Where $R^2 = 0.0758$, $\Gamma = 0.1808 \times 10^2$.

The series of samples synthesised at 800°C were all refined as having the $R\bar{3}c$ structure, with cadmium and magnesium cations being randomly arranged within the structure. Therefore only one cation site is present within the refined structure and Mg and Cd occupancies at this site was constrained to be equal to the nominal composition. For the samples synthesised at intermediate compositions and temperatures below 700°C, refinements were made using the $R\bar{3}$ symmetry with two distinct cation sites, M1 and M2. Mg and Cd occupancies were refined as follows: the total occupancy of each site was constrained to be equal to one, and the total amount of Cd and Mg were constrained to be equal to the nominal composition.

Rietveld refinements of diffraction patterns for all samples synthesised for this study may be found in Appendix 5, along with values of R^2 (the statistical term for the “goodness of fit” for a weighted pattern) and Γ (the Lorentzian linewidth).

3.2.1 Lattice Parameters

Unit-cell parameters for samples synthesised for this study are presented in Table 3.1. Lattice parameters for the 600°C series of samples [Bromiley, 2002], are reported in Table 3.1 for comparison. Variations of the unit-cell lattice parameters as a function of composition are shown in Figure 3.6a-c. Note that for samples of composition $\text{Mg}_{0.7}\text{Cd}_{0.3}\text{CO}_3$ and $\text{Mg}_{0.8}\text{Cd}_{0.2}\text{CO}_3$ two values are present in Figure 3.6 for the 600°C series. This is due to the coexistence of two distinct phases, an $R\bar{3}$ ordered phase, and an $R\bar{3}c$ disordered phase in the run products, indicating the presence of a miscibility gap at this temperature [Bromiley, 2002]. There is no noticeable difference between the 600°C and 800°C series, except with respect to the c -axis (Figure 3.6b). Whereas the a -axis varies linearly with composition (Figure 3.6a), a small positive deviation from linearity can be seen for the disordered $R\bar{3}c$ series for the c -axis. Samples of composition $\text{Mg}_{0.5}\text{Cd}_{0.5}\text{CO}_3$, and with varying degrees of order lie between the polynomial fit through the 800°C series of data and the ideal behaviour for a completely ordered solid solution. The strain associated with the order-disorder phase transition for samples of composition $\text{Mg}_{0.5}\text{Cd}_{0.5}\text{CO}_3$ can be calculated assuming that a completely ordered sample would have

a c value that lies on a straight line between the end-members, so displaying ideal behaviour. This assumption is justified if the behaviour of the magnesite – calcite system is considered. Single-crystal c -axis lattice parameters for magnesite [Oh et al., 1973] and calcite [Markgraf and Reeder, 1985] were plotted as a function of composition and the theoretical c -axis length for dolomite was determined from a straight line between the end-members. The value obtained for a fully ordered dolomite was $c = 16.042\text{\AA}$. Reeder and Wenk (1983) reported a value of $c = 16.006\text{\AA}$ for an ordered dolomite from Eugui. The strain is defined in Equation 3.1 and is reported for sample synthesised for this study in Table 3.2.

$$\varepsilon = \frac{c - c_0}{c_0} \quad \text{Equation 3.1}$$

Where c is the c -axis length of the sample, and c_0 is the reference c -axis length.

Table 3.1: Unit-cell lattice parameters, volume strain (see p.64) and symmetry for all samples synthesised in the otavite – magnesite solid solution. (Standard deviations are in parentheses). Note that GSAS Rietveld refinements tend to underestimate errors.

Nominal Composition	Length a-axis (Å)	Length c-axis (Å)	Unit-cell Volume (Å ³)	Volume Strain (Vs)	Space Group
600°C Series. Synthesised at 1GPa for 3 hours [Bromiley, 2002]					
CdCO ₃	4.9204(5)	16.296(2)	341.687(5)	0.22335	$R\bar{3}c$
Mg _{0.1} Cd _{0.9} CO ₃	4.8954(2)	16.1958(14)	336.137(3)	0.20348	$R\bar{3}c$
Mg _{0.2} Cd _{0.8} CO ₃	4.8674(4)	16.0811(20)	329.956(4)	0.18135	$R\bar{3}c$
Mg _{0.3} Cd _{0.7} CO ₃	4.8402(7)	15.964(4)	323.902(7)	0.15968	$R\bar{3}c$
Mg _{0.4} Cd _{0.6} CO ₃	4.8115(8)	15.8366(5)	317.517(8)	0.13682	$R\bar{3}$
Mg _{0.5} Cd _{0.5} CO ₃	4.7791(7)	15.6888(4)	310.335(7)	0.11110	$R\bar{3}$
Mg _{0.6} Cd _{0.4} CO ₃	4.7595(11)	15.5950(6)	305.944(10)	0.09538	$R\bar{3}$

Nominal Composition	Length a-axis (Å)	Length c-axis (Å)	Unit-cell Volume (Å ³)	Volume Strain (Vs)	Space Group
Mg _{0.7} Cd _{0.3} CO ₃	4.7616(2)	15.6050(8)	306.417(14)	0.09707	$R\bar{3}$
Mg _{0.7} Cd _{0.3} CO ₃	4.658(1)	15.189(5)	285.41(8)	0.02186	$R\bar{3}c$
Mg _{0.8} Cd _{0.2} CO ₃	4.7595(2)	15.6046(9)	306.130(16)	0.09605	$R\bar{3}$
Mg _{0.8} Cd _{0.2} CO ₃	4.6653(4)	15.189(2)	286.32(3)	0.02512	$R\bar{3}c$
Mg _{0.9} Cd _{0.1} CO ₃	4.6618(15)	15.1659(6)	285.438(10)	0.02196	$R\bar{3}c$
MgCO ₃	4.6338(5)	15.0197(2)	279.304(4)	0	$R\bar{3}c$
800°C Series. Synthesised at 1GPa for 1 hour					
CdCO ₃	4.9204(4)	16.2957(3)	341.680(5)	0.22341	$R\bar{3}c$
Mg _{0.1} Cd _{0.9} CO ₃	4.8905(6)	16.1781(4)	335.095(7)	0.19983	$R\bar{3}c$
Mg _{0.2} Cd _{0.8} CO ₃	4.8642(4)	16.0703(2)	329.291(4)	0.17905	$R\bar{3}c$
Mg _{0.3} Cd _{0.7} CO ₃	4.8334(7)	15.9429(4)	322.564(7)	0.15496	$R\bar{3}c$
Mg _{0.4} Cd _{0.6} CO ₃	4.8098(5)	15.8385(2)	317.325(5)	0.13620	$R\bar{3}c$
Mg _{0.5} Cd _{0.5} CO ₃	4.7785(8)	15.6975(4)	310.418(8)	0.11147	$R\bar{3}c$
Mg _{0.6} Cd _{0.4} CO ₃	4.7512(8)	15.5773(4)	304.537(7)	0.09042	$R\bar{3}c$
Mg _{0.7} Cd _{0.3} CO ₃	4.7254(1)	15.4607(6)	298.985(11)	0.07054	$R\bar{3}c$
Mg _{0.8} Cd _{0.2} CO ₃	4.6973 (2)	15.3488(9)	293.306(15)	0.05020	$R\bar{3}c$
Mg _{0.9} Cd _{0.1} CO ₃	4.6636(6)	15.1723 (3)	285.796(5)	0.02331	$R\bar{3}c$
MgCO ₃	4.6337(2)	15.01964(9)	279.285(2)	0	$R\bar{3}c$
Samples synthesised for 19 hours at 600°C and 1GPa					
Mg _{0.4} Cd _{0.6} CO ₃	4.8118(1)	15.8311(7)	317.442(12)	0.13655	$R\bar{3}$
Mg _{0.45} Cd _{0.55} CO ₃	4.7965(1)	15.7672 (5)	314.157(9)	0.12479	$R\bar{3}$
Mg _{0.5} Cd _{0.5} CO ₃	4.78204 (8)	15.7069 (5)	311.064(8)	0.11371	$R\bar{3}$
Mg _{0.55} Cd _{0.45} CO ₃	4.7748(1)	15.6772(7)	309.541(12)	0.10826	$R\bar{3}$
Mg _{0.6} Cd _{0.4} CO ₃	4.7638(1)	15.6109(8)	306.810(13)	0.09848	$R\bar{3}$

Nominal Composition	Length a-axis (Å)	Length c-axis (Å)	Unit-cell Volume (Å ³)	Volume Strain (Vs)	Space Group
Sample synthesised for 96 hours at 600°C and 1GPa					
Mg _{0.5} Cd _{0.5} CO ₃	4.7819(1)	15.7037(5)	310.986(9)	0.11343	$R\bar{3}$
Sample synthesised at 650°C for 120 hours and 1GPa					
Mg _{0.5} Cd _{0.5} CO ₃	4.7830(7)	15.7113(4)	311.282(7)	0.11449	$R\bar{3}$
Samples synthesised at 500°C for 96 hours and 1GPa					
Mg _{0.2} Cd _{0.8} CO ₃	4.8658(6)	16.0791(3)	329.693(6)	0.18040	$R\bar{3} c$
Mg _{0.3} Cd _{0.7} CO ₃	4.8424(2)	15.9717(9)	324.353(17)	0.16129	$R\bar{3} c$
Mg _{0.5} Cd _{0.5} CO ₃	4.7829(1)	15.7015(6)	311.079(11)	0.11376	$R\bar{3}$
Samples synthesised at 700°C for 24 hours at 1GPa					
Mg _{0.4} Cd _{0.6} CO ₃	4.8090(7)	15.8361(4)	317.172(8)	0.13566	$R\bar{3} c$
Mg _{0.5} Cd _{0.5} CO ₃	4.7829(7)	15.7157(4)	311.349(7)	0.11481	$R\bar{3} c$
Samples disordered from 500°C sample with $R\bar{3}$ symmetry at 600°C					
Mg _{0.5} Cd _{0.5} CO ₃ 20min	4.7821(1)	15.691(8)	310.74(1)	0.1126	$R\bar{3}$
Mg _{0.5} Cd _{0.5} CO ₃ 48 hours	4.782(1)	15.697(7)	310.87(1)	0.1130	$R\bar{3}$

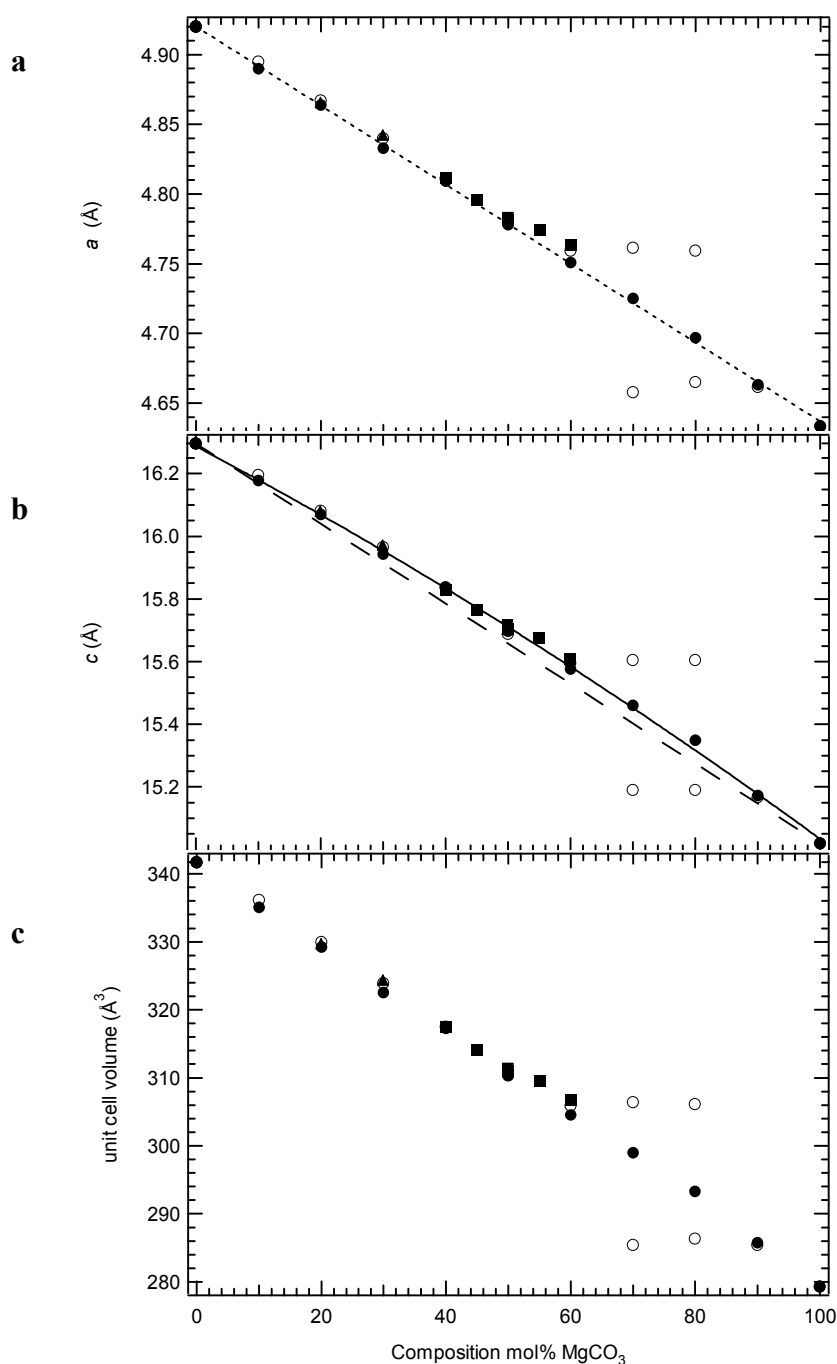


Figure 3.6a-c: Unit-cell lattice parameters as function of composition (mol% MgCO₃) Symbols: open circle = 600°C, 3 hours [Bromiley, 2002], solid circle = 800°C, 1 hour, inverted solid triangle = 700°C, 24 hours, solid triangle = 500°C, 96 hours, inverted open triangle = 650°C, 120 hours, Black square = 600°C, 19 hours, and open triangle = 600°C, 96 hours. 3a) Dashed line is a linear fit through the 800°C series, given by $y = 4.9206 - 0.00283x$ 3b) Dashed line is a linear fit through the end-member values from the 800°C series data, given by $y = 16.288 - 0.010527x$. Note the small deviation from linearity of the c parameter. The solid curve is a fit through the 800°C series using a second order polynomial, $c = 16.288 - 0.010527x - 2.0121 \times 10^{-2}x^2$. Where $x = \text{mol\% MgCO}_3$. Uncertainties are in the order of the symbol size.

Table 3.2 reports the strain for samples of composition $\text{Mg}_{0.5}\text{Cd}_{0.5}\text{CO}_3$ synthesised at equilibrium conditions using Equation 3.1. The variation of strain as a function of temperature is shown in Figure 3.7. The linear fit between the two end-members from the 800°C series (Figure 3.6b) was used to obtain a value for c_0 for a completely ordered sample at $\text{Mg}_{0.5}\text{Cd}_{0.5}\text{CO}_3$. Table 3.2 shows that there is less than 1% strain associated with the $R\bar{3} \rightarrow R\bar{3}c$ phase transition. This value is consistent with spontaneous strains associated with phase transition reported by Carpenter *et al.* (1998).

Table 3.2: Shear strain of $\text{Mg}_{0.5}\text{Cd}_{0.5}\text{CO}_3$ samples.

Synthesis Conditions	<i>c</i> -axis length (Å)	Shear Strain (ε)
500°C, 96 hours	15.7016	0.00278
600°C, 19 hours	15.7069	0.00312
600°C, 96 hours	15.7038	0.00293
650°C, 120 hours	15.7113	0.00340
700°C, 24 hours	15.7157	0.00368
Linear fit, c_0	15.658	0

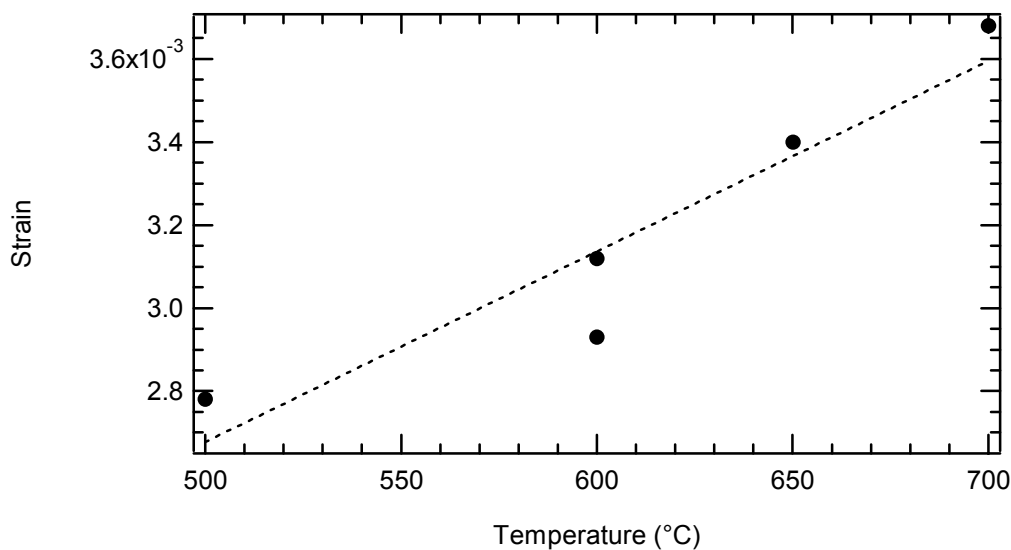


Figure 3.7: Shear strain along the c -axis as a function of temperature for samples of composition $\text{Mg}_{0.5}\text{Cd}_{0.5}\text{CO}_3$. Note that c_0 is theoretical, and is calculated from the linear fit in Figure 3.6b between the two 800°C series end-members, and represents the c -axis length for a completely ordered sample.

Volume strain associated with substituting larger cadmium cations in the magnesite structure is calculated according to Equation 3.2.

$$V_S = \frac{V - V_0}{V_0} \quad \text{Equation 3.2}$$

where V is unit-cell volume of different compositions, and V_0 is the reference volume of magnesite (Table 3.1). Substituting magnesium with cadmium gives rise to a linear increase in volume strain from magnesite to otavite (Figure 3.8).

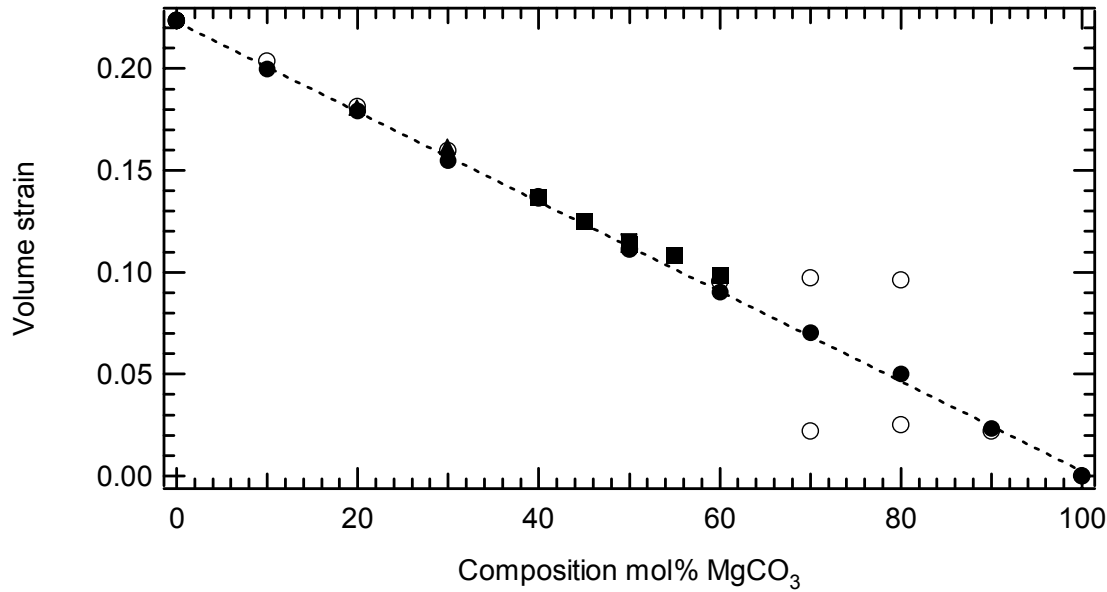


Figure 3.7: Volume strain (V_s) versus composition for all samples synthesised at 1GPa. Symbols as in Figure 3.6a-c. Dashed line is the fit through the 800°C data series ($V_s = 0.22341 \text{ mol\% MgCO}_3$). Note that all data show such variation regardless of temperature of synthesis or ordering processes.

3.2.2 Atomic Position Parameters

All positions of atoms within the disordered $R\bar{3}c$ phase are constrained by symmetry, except for the x -coordinate of the oxygen atoms. There is one cation site, which is at the origin (0,0,0), and the carbon atom is at $0,0,\frac{1}{4}$. The phase transformation from the disordered $R\bar{3}c$ to the ordered $R\bar{3}$ structure results in the loss of a c -glide, and the diad axes in the $R\bar{3}c$ structure due to ordering of the cations. Therefore two cation sites exist in the $R\bar{3}$ structure, one at 0,0,0 and the other at $0,0,\frac{1}{2}$. In the disordered structure, $R\bar{3}c$, these sites are equivalent. The carbon is not constrained by symmetry in the $R\bar{3}$ structure, and can move to be slightly out of plane with respect to the usually planar carbonate group. Moreover, the oxygen atoms are in general positions. The refined

atomic positions for the $R\bar{3}c$ and $R\bar{3}$ symmetries for all the samples studied are reported in Table 3.3. Note that the results reported in Table 3.3 for the 600°C series synthesised by Bromiley (2002) are significantly different from those reported by the author, due to improvement of the Rietveld refinements.

Table 3.3: Positional parameters as a function of composition for samples across the otavite – magnesite solid solution. (Standard deviations are in parentheses). Note that GSAS Rietveld refinements tend to underestimate errors.

Nominal Composition	Space Group	Position of Oxygen			Position of carbon on the z-axis
		x	y	z	
600°C Series. Synthesised at 1GPa for 3 hours					
CdCO ₃	$R\bar{3}c$	0.246(1)	0	0.25	0.25
Mg _{0.1} Cd _{0.9} CO ₃	$R\bar{3}c$	0.2511(7)	0	0.25	0.25
Mg _{0.2} Cd _{0.8} CO ₃	$R\bar{3}c$	0.2592(5)	0	0.25	0.25
Mg _{0.3} Cd _{0.7} CO ₃	$R\bar{3}c$	0.2592(6)	0	0.25	0.25
Mg _{0.4} Cd _{0.6} CO ₃	$R\bar{3}$	0.249(1)	0.021(3)	0.2574(9)	0.235(1)
Mg _{0.5} Cd _{0.5} CO ₃	$R\bar{3}$	0.266(2)	0.006(4)	0.254(2)	0.238(2)
Mg _{0.6} Cd _{0.4} CO ₃	$R\bar{3}$	0.255(1)	0.024(2)	0.250(1)	0.243(2)
Mg _{0.7} Cd _{0.3} CO ₃	$R\bar{3}$	0.255(1)	0.030(2)	0.241(1)	0.246(4)
Mg _{0.7} Cd _{0.3} CO ₃	$R\bar{3}c$	0.274(2)	0	0.25	0.25
Mg _{0.8} Cd _{0.2} CO ₃	$R\bar{3}$	0.273(2)	0.011(4)	0.259(1)	0.266(2)
Mg _{0.8} Cd _{0.2} CO ₃	$R\bar{3}c$	0.2769(7)	0	0.25	0.25
Mg _{0.9} Cd _{0.1} CO ₃	$R\bar{3}c$	0.2761(4)	0	0.25	0.25
MgCO ₃	$R\bar{3}c$	0.2798(8)	0	0.25	0.25
800°C Series. Synthesised for 1 hour at 1GPa					
CdCO ₃	$R\bar{3}c$	0.2486(9)	0	0.25	0.25
Mg _{0.1} Cd _{0.9} CO ₃	$R\bar{3}c$	0.251(1)	0	0.25	0.25

Nominal Composition	Space Group	Position of Oxygen			Position of carbon on the z-axis
		x	y	z	
Mg _{0.2} Cd _{0.8} CO ₃	$R\bar{3}c$	0.262(1)	0	0.25	0.25
Mg _{0.3} Cd _{0.7} CO ₃	$R\bar{3}c$	0.2515(9)	0	0.25	0.25
Mg _{0.4} Cd _{0.6} CO ₃	$R\bar{3}c$	0.2562(7)	0	0.25	0.25
Mg _{0.5} Cd _{0.5} CO ₃	$R\bar{3}c$	0.2637(8)	0	0.25	0.25
Mg _{0.6} Cd _{0.4} CO ₃	$R\bar{3}c$	0.2696(5)	0	0.25	0.25
Mg _{0.7} Cd _{0.3} CO ₃	$R\bar{3}c$	0.2728(5)	0	0.25	0.25
Mg _{0.8} Cd _{0.2} CO ₃	$R\bar{3}c$	0.2723(6)	0	0.25	0.25
Mg _{0.9} Cd _{0.1} CO ₃	$R\bar{3}c$	0.2779(5)	0	0.25	0.25
MgCO ₃	$R\bar{3}c$	0.2790(3)	0	0.25	0.25
Samples synthesised for 19 hours at 600°C and 1GPa					
Mg _{0.4} Cd _{0.6} CO ₃	$R\bar{3}$	0.268(2)	0.008(4)	0.246(1)	0.237(2)
Mg _{0.45} Cd _{0.55} CO ₃	$R\bar{3}$	0.273(1)	0.025(3)	0.241(1)	0.263(1)
Mg _{0.5} Cd _{0.5} CO ₃	$R\bar{3}$	0.2709(9)	0.011(2)	0.249(1)	0.252(1)
Mg _{0.55} Cd _{0.5} CO ₃	$R\bar{3}$	0.277(1)	0.028(2)	0.240(8)	0.272 (1)
Mg _{0.6} Cd _{0.4} CO ₃	$R\bar{3}$	0.276(1)	0.019(2)	0.2404(8)	0.227(1)
Sample synthesised for 96 hours at 600°C and 1GPa					
Mg _{0.5} Cd _{0.5} CO ₃	$R\bar{3}$	0.273(1)	0.009(2)	0.254(1)	0.249(2)
Sample synthesised at 650°C for 120 hours at 1GPa					
Mg _{0.5} Cd _{0.5} CO ₃	$R\bar{3}$	0.271(1)	0.010(2)	0.247(1)	0.255(2)
Sample synthesised at 500°C for 96 hours at 1GPa					
Mg _{0.2} Cd _{0.8} CO ₃	$R\bar{3}c$	0.2543(7)	0	0.25	0.25
Mg _{0.3} Cd _{0.7} CO ₃	$R\bar{3}c$	0.2617(7)	0	0.25	0.25
Mg _{0.5} Cd _{0.5} CO ₃	$R\bar{3}$	0.273(9)	0.015(2)	0.2438(8)	0.261(1)

Nominal Composition	Space Group	Position of Oxygen			Position of carbon on the z-axis
		x	y	z	
Samples synthesised at 700°C for 24 hours at 1GPa					
Mg _{0.4} Cd _{0.6} CO ₃	$R\bar{3}$	0.2238(7)	0	0.25	0.25
Mg _{0.5} Cd _{0.5} CO ₃	$R\bar{3}$	0.2623(5)	0	0.25	0.25

3.2.3 Inter-atomic Distances

Determination of cation-oxygen bond lengths provides information regarding the effect of cadmium substitution into the magnesite structure. Although the inter-atomic distances refined from powder samples generally show larger uncertainties than those determined from single-crystal structure refinements, they still provide important information when single-crystal data are not available. Table 3.4 presents mean bond lengths for carbon-oxygen and magnesium- and cadmium-oxygen bonds across the solid solution for the two series synthesised at 600°C and 800°C, as well as experiments at intermediate compositions, synthesised to study the order within the system.

As already noted, samples having $R\bar{3}$ symmetry have two different cation sites, one preferentially occupied by magnesium (M1) and the other by cadmium (M2). Therefore, for such samples, two different bond distances, $\langle\text{M1-O}\rangle$ and $\langle\text{M2-O}\rangle$ are given in Table 3.3, as well as their mean value. For the Mg_{0.7}Cd_{0.3}CO₃ and Mg_{0.8}Cd_{0.2}CO₃ samples synthesised at 600°C for 3 hours, three $\langle\text{M}^{2+}\text{-O}\rangle$ bond distances exist, two for the $\langle\text{M2-O}\rangle$ and $\langle\text{M1-O}\rangle$ bonds in the ordered $R\bar{3}$ phase, and one for the $\langle\text{M}^{2+}\text{-O}\rangle$ bond present in the disordered $R\bar{3}c$ phase, both present in these samples [Bromiley, 2002]. Also presented in Table 3.4 are oxygen-carbon-oxygen bond angles. In the samples with $R\bar{3}$ symmetry the loss of the c -glide enables the carbon to move on the

z-coordinate, as reported in Section 3.2.2. This in turn allows the carbonate group to become non-planar, so the O-C-O bond angles deviate from 120° , a value dictated by symmetry in the disordered samples. Non-planar CO_3 groups have been reported by Beran and Zemmann (1977) and Zemmann (1981) for dolomites, in some cases being described as CO_3 tetrahedra.

In Figure 3.9 bond length distances are plotted as a function of composition. For ordered samples, only the mean value for $\langle \text{M1-O} \rangle$ and $\langle \text{M2-O} \rangle$ is shown. Note that distances follow a linear trend between the two end-members. The small scatter of the data about the linear fit is indicative of the quality the Rietveld refinements. Figure 3.10 shows average cation-oxygen bond lengths for $\langle \text{M1-O} \rangle$ and $\langle \text{M2-O} \rangle$ sites as a function of temperature for samples of composition $\text{Mg}_{0.5}\text{Cd}_{0.5}\text{CO}_3$. Note that as temperature increases, the average bond lengths for the two distinct sites converge to the $\langle \text{M-O} \rangle$ value of the disordered phase.

Table 3.4: Mean bond lengths for $\langle \text{C-O} \rangle$ and $\langle \text{M}^{2+}\text{-O} \rangle$ bonds across the otavite – magnesite solid solution. (Standard deviations are in parentheses). Note that GSAS Rietveld refinements tend to underestimate errors.

Nominal Composition	$\langle \text{C-O} \rangle$ (Å)	$\langle \text{M1-O} \rangle$ (Å)	$\langle \text{M2-O} \rangle$ (Å)	$\langle \text{M}^{2+}\text{-O} \rangle$ (Å)	O-C-O Bond Angle ($^\circ$)
600°C Series. Synthesised for 3 hours at 1GPa					
CdCO_3	1.211(5)	-	-	2.328(3)	120
$\text{Mg}_{0.1}\text{Cd}_{0.9}\text{CO}_3$	1.229(4)	-	-	2.3029(19)	120
$\text{Mg}_{0.2}\text{Cd}_{0.8}\text{CO}_3$	1.262(3)	-	-	2.2679(14)	120
$\text{Mg}_{0.3}\text{Cd}_{0.7}\text{CO}_3$	1.255(3)	-	-	2.2539(17)	120
$\text{Mg}_{0.4}\text{Cd}_{0.6}\text{CO}_3$	1.265(6)	2.221(13)	2.256(14)	2.238(2)	119.5(6)
$\text{Mg}_{0.5}\text{Cd}_{0.5}\text{CO}_3$	1.284(7)	2.152(17)	2.27(2)	2.211(8)	116.6(10)
$\text{Mg}_{0.6}\text{Cd}_{0.4}\text{CO}_3$	1.274(7)	2.203(10)	2.237(11)	2.22(1)	119.99(7)
$\text{Mg}_{0.7}\text{Cd}_{0.3}\text{CO}_3$	1.297(5)	2.032(8)	2.341(9)	2.1865(9)	118.6(10)
$\text{Mg}_{0.7}\text{Cd}_{0.3}\text{CO}_3$	1.276(11)	-	-	2.126(5)	120

Nominal Composition	<C-O> (Å)	<M1-O> (Å)	<M2-O> (Å)	<M ²⁺ -O> (Å)	O-C-O Bond Angle (°)
Mg _{0.8} Cd _{0.2} CO ₃	1.279(4)	2.073(12)	2.314(13)	2.1935(13)	117.7(14)
Mg _{0.8} Cd _{0.2} CO ₃	1.292(4)	-	-	2.121(2)	120
Mg _{0.9} Cd _{0.1} CO ₃	1.287(2)	-	-	2.1207(11)	120
MgCO ₃	1.297(4)	-	-	2.0969(3)	120
800°C Series. Synthesised for 1 hour at 1GPa					
CdCO ₃	1.222(5)	-	-	2.322(3)	120
Mg _{0.1} Cd _{0.9} CO ₃	1.245(7)	-	-	2.291(3)	120
Mg _{0.2} Cd _{0.8} CO ₃	1.277(5)	-	-	2.258(3)	120
Mg _{0.3} Cd _{0.7} CO ₃	1.252(5)	-	-	2.270(2)	120
Mg _{0.4} Cd _{0.6} CO ₃	1.250(4)	-	-	2.246(2)	120
Mg _{0.5} Cd _{0.5} CO ₃	1.261(4)	-	-	2.210(2)	120
Mg _{0.6} Cd _{0.4} CO ₃	1.2814(26)	-	-	2.1826(13)	120
Mg _{0.7} Cd _{0.3} CO ₃	1.2893(27)	-	-	2.1617(13)	120
Mg _{0.8} Cd _{0.2} CO ₃	1.2795(29)	-	-	2.1490(14)	120
Mg _{0.9} Cd _{0.1} CO ₃	1.296(2)	-	-	2.1175(12)	120
MgCO ₃	1.2932(17)	-	-	2.0985(8)	120
Samples synthesised for 19 hours at 600°C and 1GPa					
Mg _{0.4} Cd _{0.6} CO ₃	1.277(9)	2.219(18)	2.238(19)	2.228(11)	118.6(5)
Mg _{0.45} Cd _{0.55} CO ₃	1.308(8)	2.164(13)	2.272(14)	2.218(16)	116.8(5)
Mg _{0.5} Cd _{0.5} CO ₃	1.275(3)	2.179(11)	2.240(11)	2.209(17)	116.511(7)
Mg _{0.55} Cd _{0.45} CO ₃	1.301(7)	2.203(10)	2.237(11)	2.22(11)	117.5(8)
Mg _{0.6} Cd _{0.4} CO ₃	1.292(4)	2.174(11)	2.251 (12)	2.213(1)	119.3(3)
Sample synthesised for 96 hours at 600°C and 1GPa					
Mg _{0.5} Cd _{0.5} CO ₃	1.290(4)	2.160(7)	2.249(8)	2.2125(3)	116.51(3)
Sample synthesised at 650°C for 120 hours at 1GPa					
Mg _{0.5} Cd _{0.5} CO ₃	1.280(5)	2.204(15)	2.212(14)	2.208(12)	117.9(8)
Sample synthesised at 500°C for 96 hours at 1GPa					
Mg _{0.2} Cd _{0.8} CO ₃	1.262(3)	-	-	2.267(1)	120

Nominal Composition	<C-O> (Å)	<M1-O> (Å)	<M2-O> (Å)	<M ²⁺ -O> (Å)	O-C-O Bond Angle (°)
Mg _{0.3} Cd _{0.7} CO ₃	1.286(4)	-	-	2.233(2)	120
Mg _{0.5} Cd _{0.5} CO ₃	1.301(6)	2.130(7)	2.294(8)	2.212(6)	114.5(9)
Samples synthesised at 700°C for 24 hours at 1GPa					
Mg _{0.4} Cd _{0.6} CO ₃	1.265(4)	-	-	2.318(1)	120
Mg _{0.5} Cd _{0.5} CO ₃	1.276(3)	-	-	2.214(1)	120

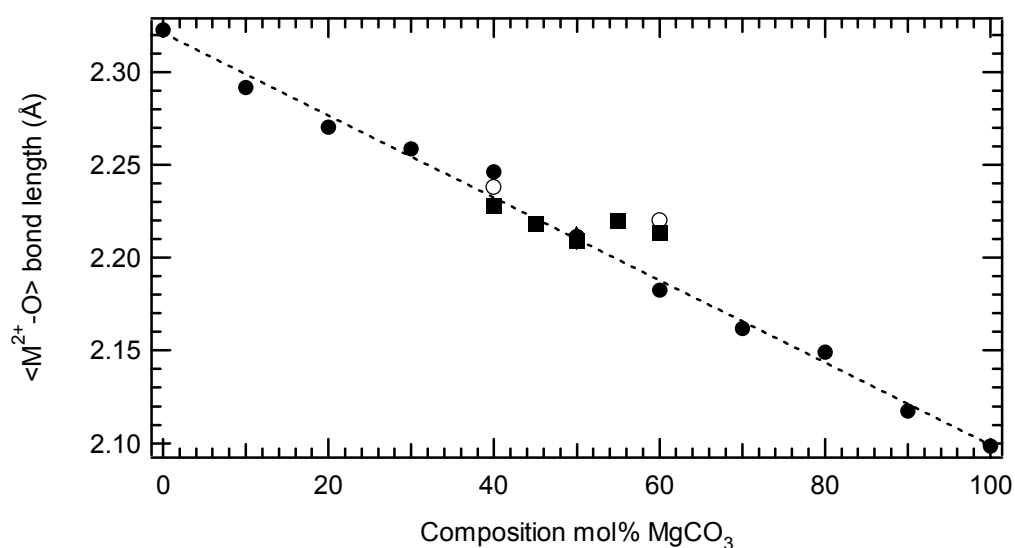


Figure 3.9: Average <M-O> bond lengths versus composition. Symbols: open circle = 600°C, 3hrs, closed circles = 800°C, 1hr, closed square = 600°C, 19hrs, open triangle = 600°C, 86hrs, inverted open triangle = 650°C, 120hrs, closed triangle = 500°C, 96hrs. The dashed line shows the fit through the 800°C series of data, given by $a = 2.3207$, $b = -0.00222$.

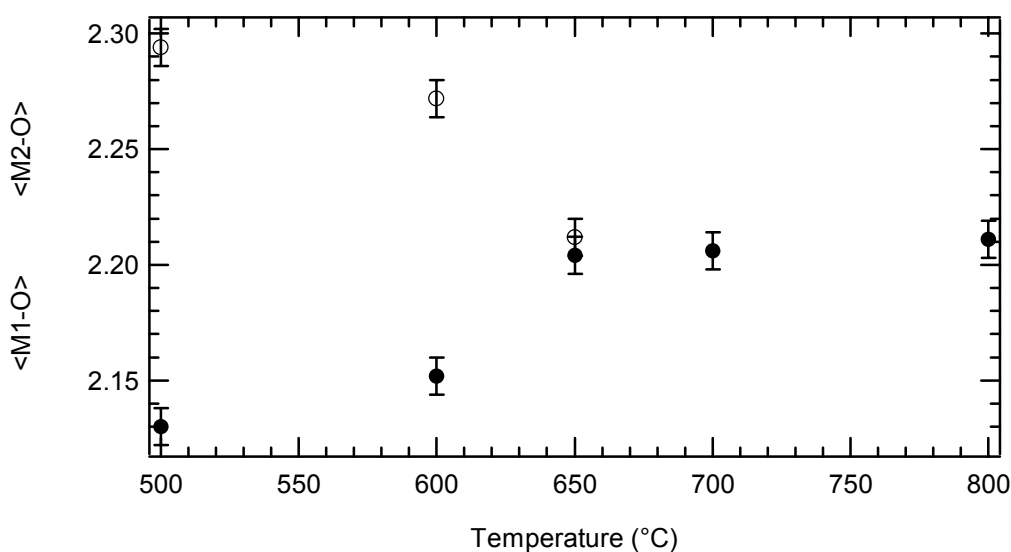


Figure 3.10: $\langle \text{M1-O} \rangle$ and $\langle \text{M2-O} \rangle$ bond lengths versus composition for all samples of composition $\text{Mg}_{0.5}\text{Cd}_{0.5}\text{CO}_3$. Open circles = average bond length for the M2 site, closed circles = average bond length for the M1 site. Note that at 700°C the order-disorder phase transition has taken place, so only one cation site is present in the disordered $R\bar{3}c$ structure.

Carbon-oxygen bond length data are shown as a function of composition in Figure 3.11. The dashed line represents the $\langle \text{C-O} \rangle$ bond length of the CO_3 molecule, which is assumed to be relatively constant ($\sim 1.28 \text{ \AA}$) [Reeder, 1983]. However, Figure 3.11 shows a systematic deviation from this value for cadmium-rich samples, which are not in agreement with data from single-crystal refinements, suggesting that the Rietveld refinements for the powder samples significantly underestimate the $\langle \text{C-O} \rangle$ bond lengths. Oxygen-carbon-oxygen bond angles are shown for ordered samples as a function of composition in Figure 3.12. Note that as the degree of order within a sample increases, so does the deviation of the oxygen-carbon-oxygen bond angle from 120° (solid line), this being a consequence of the carbon atom moving out-of-plane along the z -axis, with respect to the oxygens.

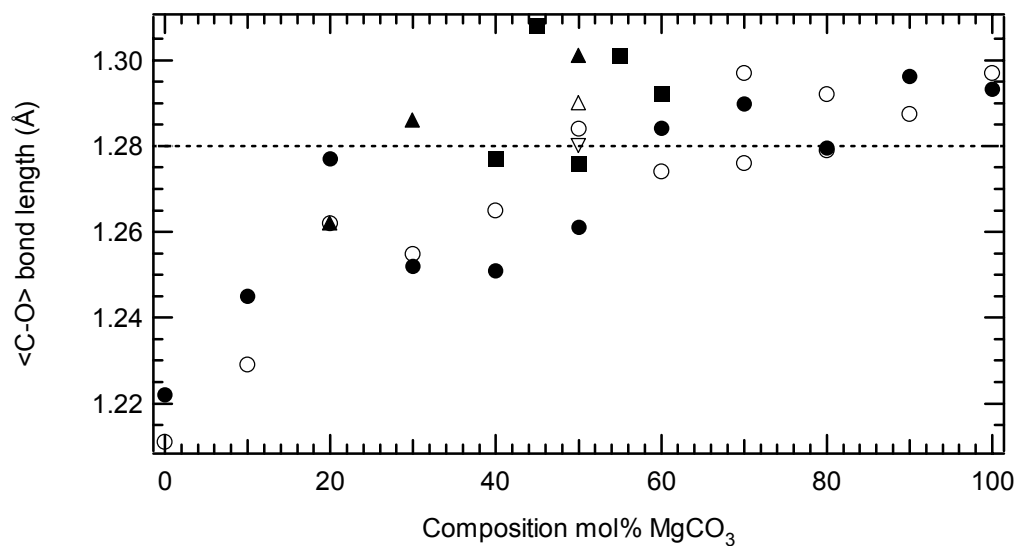


Figure 3.11: Average carbon-oxygen bond length as a function of composition. Symbols as in Figure 3.9. Note the dashed line highlights the expected $\langle\text{C-O}\rangle$ bond length between the two end-members ($\sim 1.28\text{\AA}$) [Reeder, 1983].

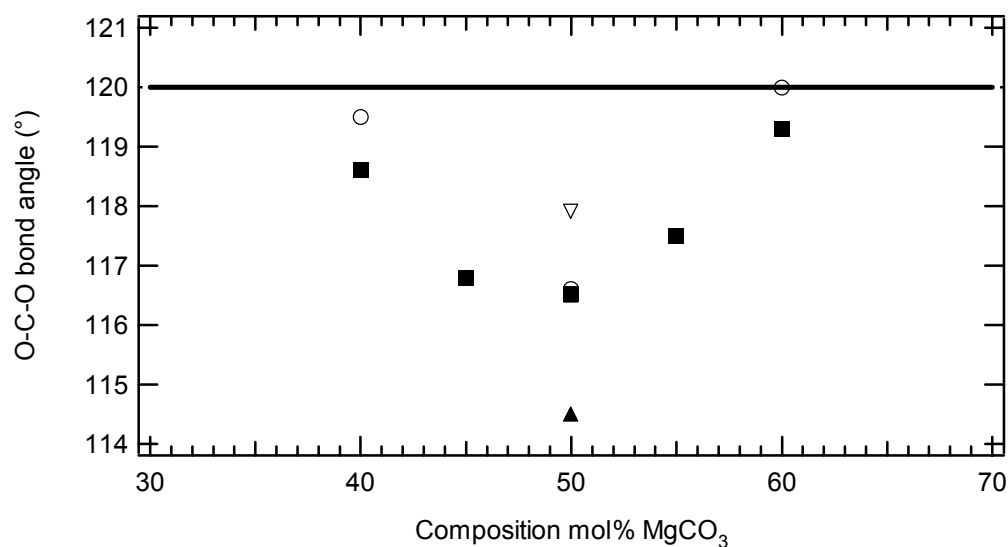


Figure 3.12: Oxygen-carbon-oxygen bond angle as a function of composition. Symbols: open circle = 600°C , 3hrs, closed circles = 800°C , 1hr, closed square = 600°C , 19hrs, open triangle = 600°C , 86hrs, inverted open triangle = 650°C , 120hrs, closed triangle = 500°C , 96hrs.

3.2.4 Site occupancies

Refining the occupancies proved difficult, and it was only possible to refine the occupancies on the specific sites if they were constrained to the nominal compositions. This not only provided quantitative results that could be related to the degree of order within the samples, but also allowed better refinement, especially to peaks in the X-ray powder diffraction patterns due to the $R\bar{3}$ structure. Constraints were placed on the cation sites in such a way that the sum of the magnesium ions on the two sites had to be equal to the mol% magnesium present in the nominal composition, as did the cadmium ions. A second constraint was placed on magnesium and cadmium ions on the same site, which stipulated that they must be equal to one. Table 3.5 presents the results from the refinements for the cation occupancies.

Equation 3.3 shows how cation site occupancies can be used to calculate the order parameter, Q , associated with the $R\bar{3} \rightarrow R\bar{3}c$ phase transition [Boffa Ballaran *et al.*, 1998]. The resulting Q values are reported in Table 3.5. Order parameters have not been calculated for samples of nominal composition $\text{Mg}_{0.7}\text{Cd}_{0.3}\text{CO}_3$ and $\text{Mg}_{0.8}\text{Cd}_{0.2}\text{CO}_3$ from the 600°C series synthesised by Bromiley (2002) as the real composition of these samples can only be estimated.

$$Q = \left[\frac{Cd_{M2} - Cd_{M1}}{\sum Cd} + \frac{Mg_{M1} - Mg_{M2}}{\sum Mg} \right] * 0.5 \quad \text{Equation 3.3}$$

Table 3.5: Magnesium and cadmium occupancies for all samples synthesised in for this study. Standard deviations in parentheses. Note that GSAS Rietveld refinements tend to underestimate errors.

Nominal composition	Mg on the M1 site	Cd on the M1 site	Mg on the M2 site	Cd on the M2 site	Q
600°C Series. Synthesised for 3 hours at 1 GPa					
CdCO ₃	0	1	-	-	-
Mg _{0.1} Cd _{0.9} CO ₃	0.1	0.9	-	-	-
Mg _{0.2} Cd _{0.8} CO ₃	0.2	0.8	-	-	-
Mg _{0.3} Cd _{0.7} CO ₃	0.3	0.7	-	-	-
Mg _{0.4} Cd _{0.6} CO ₃	0.479(5)	0.521(5)	0.321(5)	0.679(5)	0.1603
Mg _{0.5} Cd _{0.5} CO ₃	0.596(7)	0.404(7)	0.404(7)	0.596(7)	0.1928
Mg _{0.6} Cd _{0.4} CO ₃	0.637(5)	0.363(5)	0.563(5)	0.436(5)	0.07605
Mg _{0.7} Cd _{0.3} CO ₃	0.632(4)	0.368(4)	0.568(4)	0.432(4)	-
Mg _{0.7} Cd _{0.3} CO ₃	0.9	0.1	-	-	-
Mg _{0.8} Cd _{0.2} CO ₃	0.653(8)	0.347(8)	0.547(8)	0.453(8)	-
Mg _{0.8} Cd _{0.2} CO ₃	0.9	0.1	-	-	-
Mg _{0.9} Cd _{0.1} CO ₃	0.9	0.1	-	-	-
MgCO ₃	1	0	-	-	-
800°C Series. Synthesised for 1 hour at 1GPa					
CdCO ₃	0	1	-	-	-
Mg _{0.1} Cd _{0.9} CO ₃	0.1	0.9	-	-	-
Mg _{0.2} Cd _{0.8} CO ₃	0.2	0.8	-	-	-
Mg _{0.3} Cd _{0.7} CO ₃	0.3	.07	-	-	-
Mg _{0.4} Cd _{0.6} CO ₃	0.4	.06	-	-	-
Mg _{0.5} Cd _{0.5} CO ₃	0.5	0.5	-	-	-
Mg _{0.6} Cd _{0.4} CO ₃	0.6	0.4	-	-	-
Mg _{0.7} Cd _{0.3} CO ₃	0.7	0.3	-	-	-
Mg _{0.8} Cd _{0.2} CO ₃	0.8	0.2	-	-	-
Mg _{0.9} Cd _{0.1} CO ₃	0.9	0.1	-	-	-

Nominal composition	Mg on the M1 site	Cd on the M1 site	Mg on the M2 site	Cd on the M2 site	Q
MgCO ₃	1	0	-	-	-
Samples synthesised for 19 hours at 600°C and 1GPa					
Mg _{0.4} Cd _{0.6} CO ₃	0.499(9)	0.518(7)	0.318(7)	0.699(9)	0.1884
Mg _{0.45} Cd _{0.55} CO ₃	0.547(4)	0.453(4)	0.353(4)	0.647(4)	0.1954
Mg _{0.5} Cd _{0.5} CO ₃	0.629(3)	0.371(3)	0.371(3)	0.629(3)	0.2578
Mg _{0.55} Cd _{0.45} CO ₃	0.600(4)	0.400(4)	0.500(4)	0.500(4)	0.1004
Mg _{0.6} Cd _{0.4} CO ₃	0.639(4)	0.361(4)	0.561(4)	0.439(4)	0.0819
Sample synthesised for 96 hours at 600°C and 1GPa					
Mg _{0.5} Cd _{0.5} CO ₃	0.630(5)	0.370(5)	0.370(5)	0.630(5)	0.2592
Sample synthesised at 650°C for 120 hours at 1GPa					
Mg _{0.5} Cd _{0.5} CO ₃	0.616(5)	0.384(5)	0.384(5)	0.616(5)	0.2316
Sample synthesised at 500°C for 96 hours at 1GPa					
Mg _{0.2} Cd _{0.8} CO ₃	0.2	0.8	-	-	-
Mg _{0.3} Cd _{0.7} CO ₃	0.3	0.7	-	-	-
Mg _{0.5} Cd _{0.5} CO ₃	0.673(3)	0.327(3)	0.327(3)	0.673(3)	0.3454
Samples synthesised at 700°C for 24 hours at 1GPa					
Mg _{0.4} Cd _{0.6} CO ₃	0.4	0.6	-	-	-
Mg _{0.5} Cd _{0.5} CO ₃	0.5	0.5	-	-	-
Samples disordered from 500°C sample with $R\bar{3}$ symmetry at 600°C					
Mg _{0.5} Cd _{0.5} CO ₃ 20 min.	0.640(6)	0.360(6)	0.360(6)	0.640(6)	0.28
Mg _{0.5} Cd _{0.5} CO ₃ 48 hours	0.593(7)	0.407(7)	0.407(7)	0.593(7)	0.186

Figure 3.13 shows occupancy of magnesium of the M1 site as a function of composition. The linear trend of the 800°C series of data is due to the fact that the site occupancies were constrained to nominal compositions. Ordered samples have two different Mg occupancies, a higher value and a lower value, which relate to the M1 and M2 sites respectively. The distance between corresponding data for the $\text{Mg}_{0.5}\text{Cd}_{0.5}\text{CO}_3$ samples increases with increasing order.

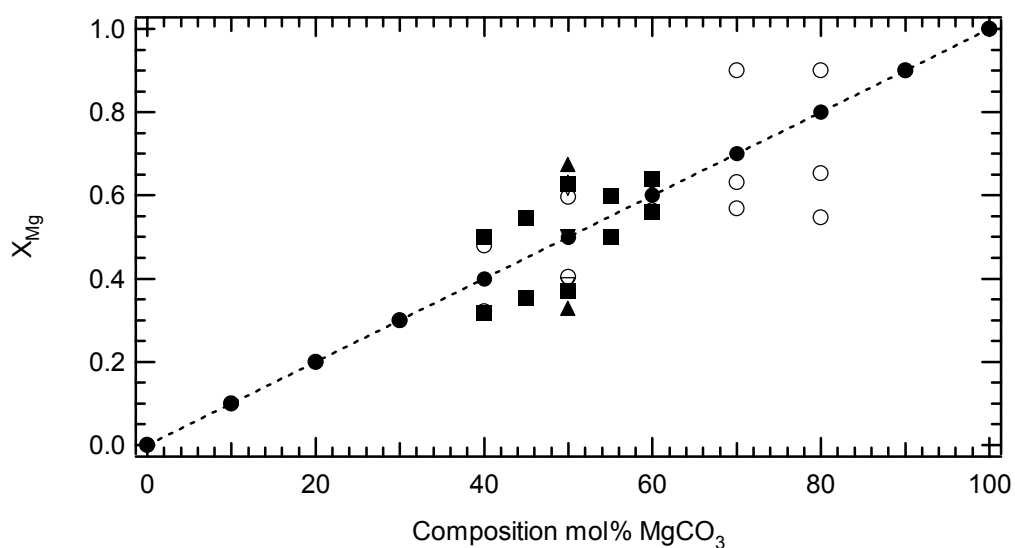


Figure 3.13: Magnesium occupancy on the M1 site as a function of composition. Symbols: open circle = 600°C, 3hrs, closed circles = 800°C, 1hr, closed square = 600°C, 19hrs, open triangle = 600°C, 86hrs, inverted open triangle = 650°C, 120hrs, closed triangle = 500°C, 96hrs. Dashed line shows a linear fit through the 800°C series.

A value proportional to the order parameter may also be derived from the bond lengths of the M1 and M2 sites, as done by Carpenter *et al.* (1990) for omphacites (Equation 3.4).

$$Q_{<M-O>} = \left[\frac{<M2-O> - <M1-O>}{0.5(<M1-O> + <M2-O>)} \right] \quad \text{Equation 3.4}$$

Table 3.6 reports $Q_{<M-O>}$ values for all samples with $R\bar{3}$ symmetry. Despite considerable scatter, $Q_{<M-O>}$ scales linearly with Q (Figure 3.14), confirming that Rietveld structural refinements were good enough to obtain information about the degree of order.

Table 3.6: The order parameter, $Q_{<M-O>}$, as calculated from mean bond distance results, for samples with $R\bar{3}$ symmetry. (Standard deviations in parentheses).

Nominal composition	<M1-O> bond distance (Å)	<M2-O> bond distance (Å)	$Q_{<M-O>}$
600°C Series. Synthesised for 3 hours at 1 GPa			
Mg _{0.4} Cd _{0.6} CO ₃	2.221(13)	2.256(14)	0.0156
Mg _{0.5} Cd _{0.5} CO ₃	2.152(17)	2.27(2)	0.0534
Mg _{0.6} Cd _{0.4} CO ₃	2.203(10)	2.237(11)	0.0153
Samples synthesised for 19 hours at 600°C and 1GPa			
Mg _{0.4} Cd _{0.6} CO ₃	2.219(18)	2.238(19)	0.0085
Mg _{0.45} Cd _{0.55} CO ₃	2.164(13)	2.272(14)	0.0487
Mg _{0.5} Cd _{0.5} CO ₃	2.179(11)	2.240(11)	0.0276
Mg _{0.55} Cd _{0.45} CO ₃	2.203(10)	2.237(11)	0.0279
Mg _{0.6} Cd _{0.4} CO ₃	2.174(11)	2.251 (12)	0.0348

Nominal composition	<M1-O> bond distance (Å)	<M2-O> bond distance (Å)	$Q_{<M-O>}$
Sample synthesised for 96 hours at 600°C and 1GPa			
Mg _{0.5} Cd _{0.5} CO ₃	2.160(7)	2.249(8)	0.04037
Sample synthesised at 650°C for 120 hours at 1GPa			
Mg _{0.5} Cd _{0.5} CO ₃	2.204(15)	2.212(14)	0.0036
Sample synthesised at 500°C for 96 hours at 1GPa			
Mg _{0.5} Cd _{0.5} CO ₃	2.130(7)	2.294(8)	0.0741

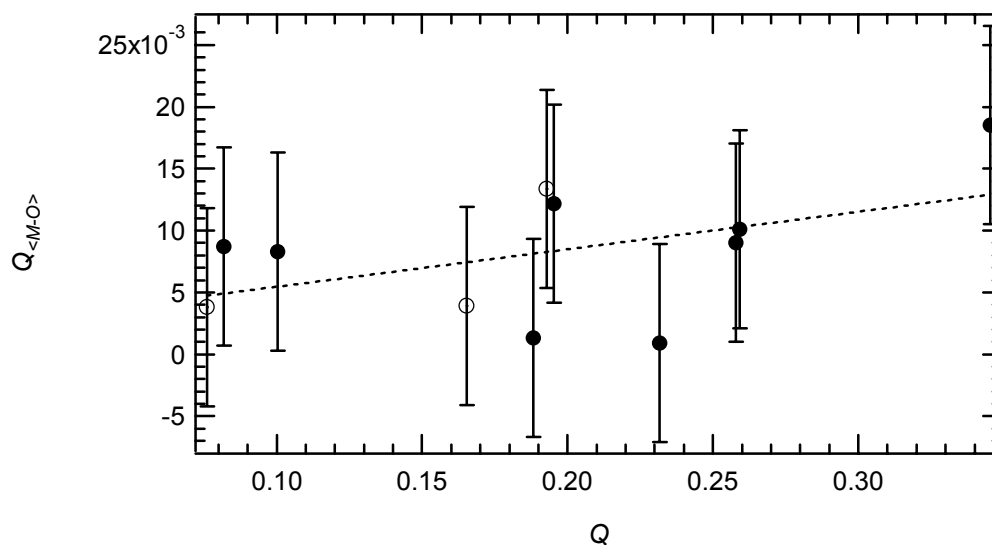


Figure 3.14: $Q_{<M-O>}$ plotted as a function of Q . The open circles are for samples known not to be at equilibrium, closed circles for samples at equilibrium. The dashed line shows a linear fit through all the data points, given by $a = 0.0024242$, $b = 0.030293$.

The error on the $Q_{<M-O>}$ values in Figure 3.14 is much greater than the error for Q , determined from cation occupancies. Therefore the Q values were used to look at the ordering behaviour as a function of both temperature and composition. Figures 3.15 and 3.16 show Q^2 as a function of temperature and composition respectively. The linear trend in Figure 3.15 can be used in order to determine whether the phase transition is thermodynamically discontinuous (first-order), continuous (second-order) or tricritical. The linear behaviour of Q^2 as a function of temperature is indicative of a second-order phase transition. The linear fit through the data gives a critical temperature for the order-disorder phase transition of 719°C. The behaviour of Q^2 as a function of composition, shown in Figure 3.16, may also indicate that the phase transition is second order as a function of composition, although the data for samples synthesised at 600°C for 19 hours show a larger scatter. This may be due to the fact that equilibrium might be achieved at different run durations for different compositions. From Figure 3.16 it appears that the stability field of the ordered cadmium dolomite phase is not symmetric about the $\text{Mg}_{0.5}\text{Cd}_{0.5}\text{CO}_3$ composition.

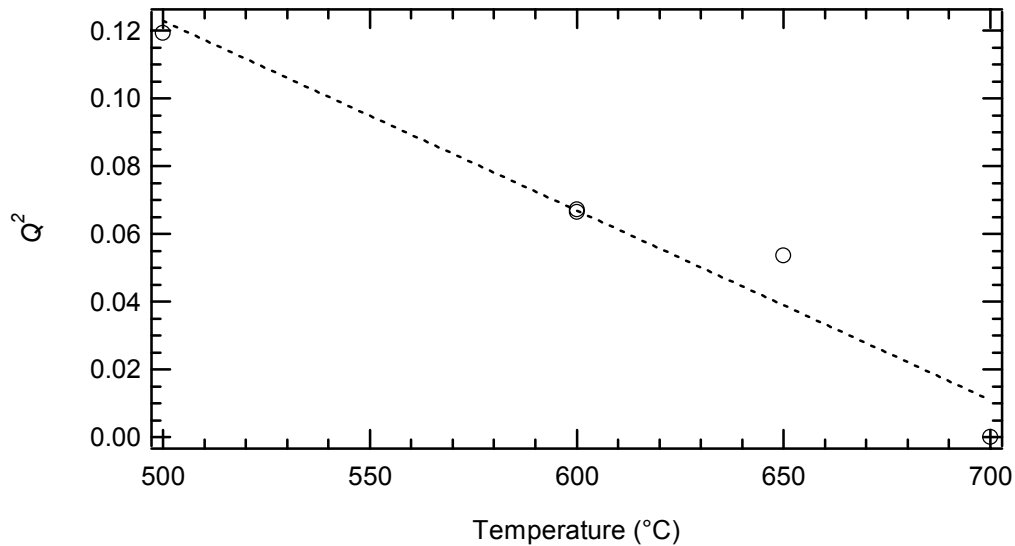


Figure 3.15: Q^2 as a function of temperature for ordered samples at equilibrium. The dashed line shows a linear fit through all the data points given by, $a = 0.40281$, $b = -0.0005598$.

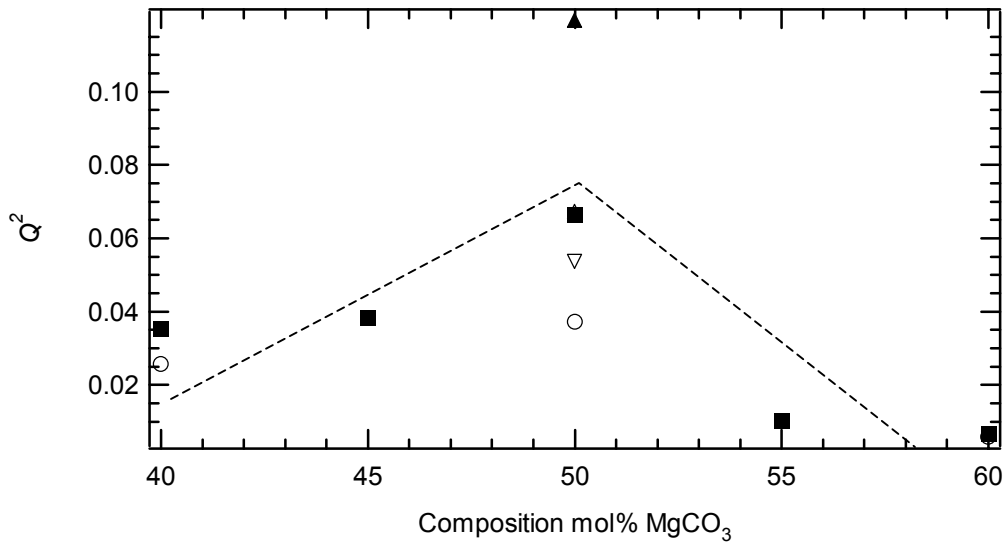


Figure 3.16: Q^2 as a function of composition for all ordered samples. Symbols: open circle = 600°C, 3hrs, closed square = 600°C, 19hrs, open triangle = 600°C, 86hrs, inverted open triangle = 650°C, 120hrs, closed triangle = 500°C, 96hrs. Dashed lines through the series of samples synthesised at 19 hours are a guide to the eye.

3.3 Degree of order from XRD Intensities

In order to ascertain the degree of order directly from the X-ray diffraction patterns, two peaks were used to gain a ratio between a reflection only observed in samples with $R\bar{3}$ symmetry, and a reflection present in samples with both $R\bar{3}$ and $R\bar{3}c$ symmetry. The (101) and the (202) peaks were chosen as they are from the same set of equivalent planes, and hence any anomalies in intensity values due to preferred orientation are avoided. Each of the reflections was fitted with a Gaussian function, so giving values for background, intensity, position and line width. Table 3.7 presents the intensity ratio results from the X-ray powder diffraction patterns for all the samples with $R\bar{3}$ symmetry.

Table 3.7: Intensity ratios for samples with $R\bar{3}$ symmetry, taken from peaks (101):(202) from the X-ray powder diffraction patterns.

Nominal Composition	$I_{(101)}/I_{(202)}$
600°C Series. Synthesised for 3 hours at 1 GPa	
Mg _{0.4} Cd _{0.6} CO ₃	0.087
Mg _{0.5} Cd _{0.5} CO ₃	0.1568
Mg _{0.6} Cd _{0.5} CO ₃	0.0166
Samples synthesised for 19 hours at 600°C and 1GPa	
Mg _{0.4} Cd _{0.6} CO ₃	0.1334
Mg _{0.45} Cd _{0.55} CO ₃	0.1458
Mg _{0.5} Cd _{0.5} CO ₃	0.1601
Mg _{0.55} Cd _{0.45} CO ₃	0.06923
Mg _{0.6} Cd _{0.4} CO ₃	0.0645
Sample synthesised for 96 hours at 600°C and 1GPa	
Mg _{0.5} Cd _{0.5} CO ₃	0.2064
Sample synthesised at 650°C for 120 hours at 1GPa	
Mg _{0.5} Cd _{0.5} CO ₃	0.1277
Sample synthesised at 500°C for 96 hours at 1GPa	
Mg _{0.5} Cd _{0.5} CO ₃	0.307

The results of the intensity ratio as a function of temperature for samples of composition Mg_{0.5}Cd_{0.5}CO₃ are shown in Figure 3.17. Note that the intensity ratio decreases linearly with increase in temperature, as the temperature approaches the phase transition. At 700°C samples show $R\bar{3}c$ symmetry and so the intensity ratio is zero as the (101) reflection is a systematic absence in the $R\bar{3}c$ structure, and hence is no longer present. The linear fit through the data gives a critical temperature, T_c , for the phase transition of 716°C, which is in good agreement with the value calculated from the square of the order parameter, Q , as a function of temperature which was $T_c = 719^\circ\text{C}$.

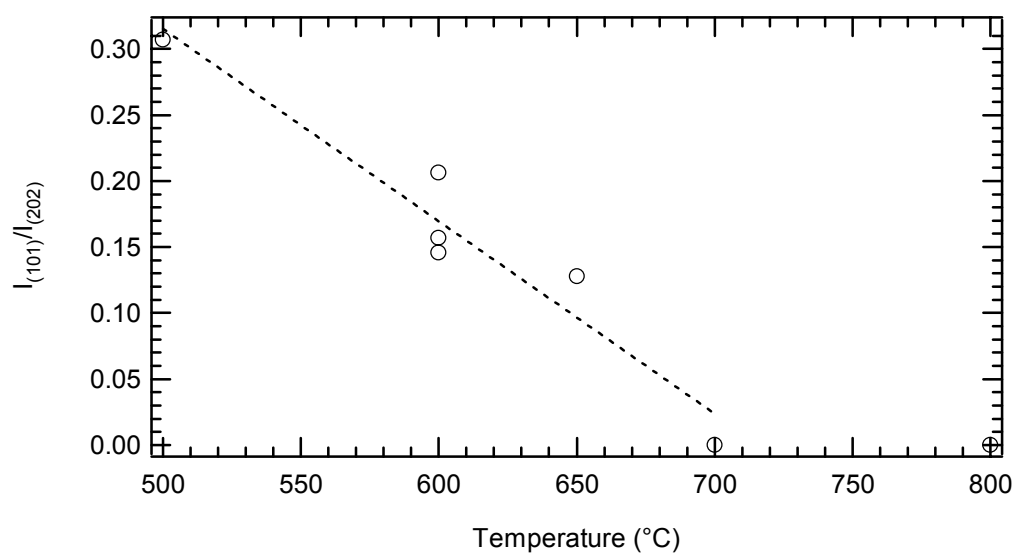


Figure 3.17: Intensity ratio from the (101) and (202) reflections from the X-ray powder diffraction patterns as a function of temperature for samples of composition $\text{Mg}_{0.5}\text{Cd}_{0.5}\text{CO}_3$. The dashed line a linear fit through the ordered samples, up to 700°C, given by, $a = 1.0437$, $b = -0.001457$.

3.4 Order – Disorder Behaviour

The occupancies of the cation sites for samples with $R\bar{3}$ symmetry were also used to determine information regarding the kinetics of the reaction, as well as the time at which equilibrium in the system was reached. Figure 3.18 shows magnesium occupancy on the M1 site for samples of composition $\text{Mg}_{0.5}\text{Cd}_{0.5}\text{CO}_3$ annealed at 600°C , as a function of time. The solid curve represents experiments in which samples were ordered from a completely disordered state. From this curve it is possible to estimate that the ordering reaction reached equilibrium at approximately 10 hours. The dashed curve shows experiments that were partially disordered in order to ascertain the equilibrium value. As no fully ordered sample was synthesised the most ordered sample was used as a starting material. This had been synthesised at 500°C for 96 hours and from Rietveld refinements it showed that the magnesium occupancy on the M1 site = 0.673. Therefore this sample was run at 600°C for durations of 20 minutes and 48 hours.

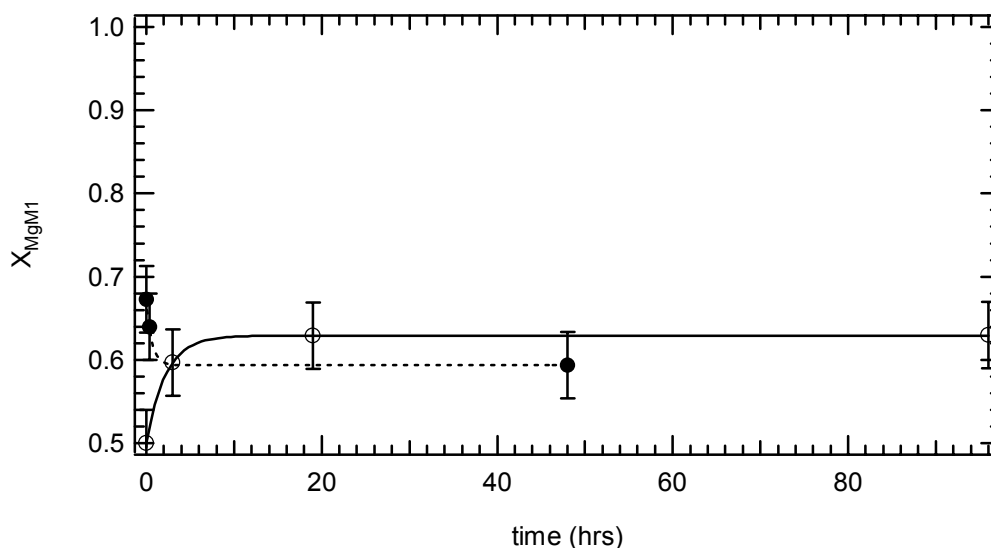


Figure 3.18: Magnesium occupancy on the M1 site as a function of time for samples of composition $\text{Mg}_{0.5}\text{Cd}_{0.5}\text{CO}_3$, synthesised at 600°C . Open circles are from ordering experiments, closed circles from disordering experiments. The solid curve is an exponential fit through the ordering experiments data, given by, $y_0 = 0.62926$, $A = -0.12926$, $B = 0.4565$. The dashed curve is an exponential fit through the disordering experiments data, given by, $y_0 = 0.5934$, $A = 0.0793$, $B = 1.6289$.

The results from the annealing experiments show that the samples with $R\bar{3}$ symmetry synthesised for this study are at equilibrium. The results shown in Figure 3.18 highlight that the same equilibrium value was achieved, within error, for both sets of experiments.

The determination of the equilibrium conditions is also useful as a comparison to previous work, in which it is reported that fully ordered cadmium dolomite samples were synthesised [Goldsmith, 1972; Capobianco *et al.*, 1987]. The order-disorder behaviour investigated in this study, however, suggests that some of the samples synthesised by Goldsmith (1972) and Capobianco *et al.* (1987) may not have been at equilibrium, and may not have been fully ordered.

4. Infra-red Powder Absorption Spectroscopy

Any compositional change as well as cation order gives rise to variations in the vibrational spectrum of a given material, both in terms of band position and linewidth. These changes may be very small, and therefore, in order to quantify them it is essential to collect high-resolution IR spectra.

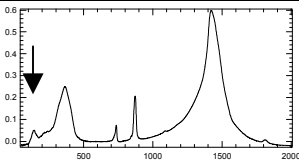
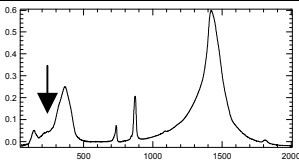
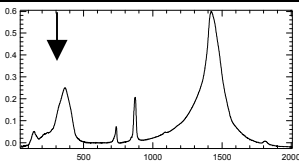
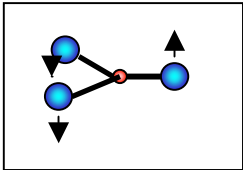
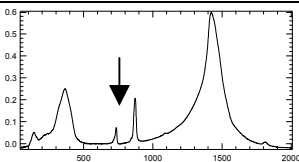
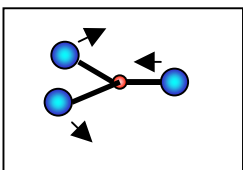
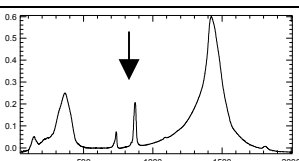
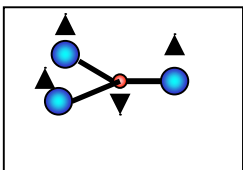
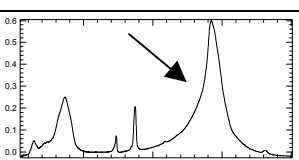
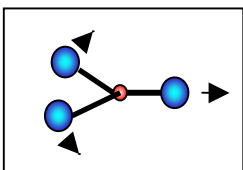
4.1 IR Spectra

Figures 4.1 and 4.2 show stacked and merged spectra for the 600°C (as synthesised by Bromiley, 2002) and 800°C series of samples respectively. From these spectra it may be seen that at higher frequencies the band positions vary continuously as a function of composition, but at low frequencies there are major changes across the solid solution, mainly related to the width of the bands, whereas band positions do not appear to vary as much as a function of composition as those at higher frequencies. The spectra for the ordered series synthesised at 600°C for 19 hours are shown in Figure 4.3, and comparison of the spectra for the composition $\text{Mg}_{0.5}\text{Cd}_{0.5}\text{CO}_3$ synthesised under different conditions are shown in Figure 4.4. Comparison of spectra for ordered and disordered samples of the same composition in Figure 4.4 shows only minor changes at low frequencies.

The phonon bands of carbonate materials can be assigned to vibrations due either to CO_3 groups, or cation – oxygen translations. Magnesite and otavite end-members with $R\bar{3}c$ symmetry have eight IR active modes, whereas ordered dolomite, with $R\bar{3}$ symmetry, has ten IR active modes [White, 1974]. Samples at intermediate compositions with $R\bar{3}c$ symmetry will, of course, have more complex spectra due to the presence of both magnesium and cadmium on the cation sites. Spectra for magnesite and otavite have previously been published by White (1974) and spectra for dolomite have been published by Adler and Kerr (1963) and White (1974). No published spectra were found for cadmium dolomite. The powder absorption IR spectra of the end-members collected for

this study (Figures 4.1 and 4.2) are essentially the same as those reported in the previous studies, although given the higher resolution obtained in this study it is possible that these spectra have more bands present than expected. This can be explained in terms of the powder IR spectra being the sum of the transverse and longitudinal modes, which for carbonates have a large separation [White, 1974]. The band at $\sim 1400\text{cm}^{-1}$ is very broad and the summation of the transverse and longitudinal modes is responsible for this broadening. The aim of this work is, however, to determine the relative changes between the spectra at intermediate compositions and the end-members in order to quantify the effects of cation ordering and substitution, and for this purpose the spectra in Figures 4.1, 4.2, 4.3, and 4.4 are of sufficiently high quality. Table 4.1 is designed to aid the understanding of the origins of the observed bands for samples with $R\bar{3}c$ symmetry. The IR active modes present for dolomite, but not for calcite and magnesite, are due to translational out-of-plane vibrations of the CO_3 groups (ν_5 and ν_{11}) [White, 1974]. As these bands were not observed for the cadmium dolomite IR spectra collected for this study, they are not included in Table 4.1. Understanding the origin of the observed phonon bands becomes of great importance when interpreting the autocorrelation data, as it is then possible to understand how very specific parts of the structure are behaving.

Table 4.1: Band assignment for $R\bar{3}c$ carbonate structures. A fully merged spectrum from a $\text{Mg}_{0.5}\text{Cd}_{0.5}\text{CO}_3$ sample is used for illustrative purposes. Phonon band assignment from Hawthorne (1988).

Wavenumber range (cm^{-1})	Band identified on IR spectra	Bonds Vibrating	Illustration of bonds vibrating
50-200		Translation of cadmium – oxygen bonds	
200-325		Translation of magnesium – oxygen bonds	
325-450		ν_{13+14} : Translation and libration of CO_3 groups	
625-800		ν_4 : Doubly degenerate in-plane bending of CO_3 groups	
800-900		ν_2 : Out-of-plane bending of CO_3 groups	
1000-2000		ν_3 : Doubly degenerate asymmetric stretching of CO_3 groups	

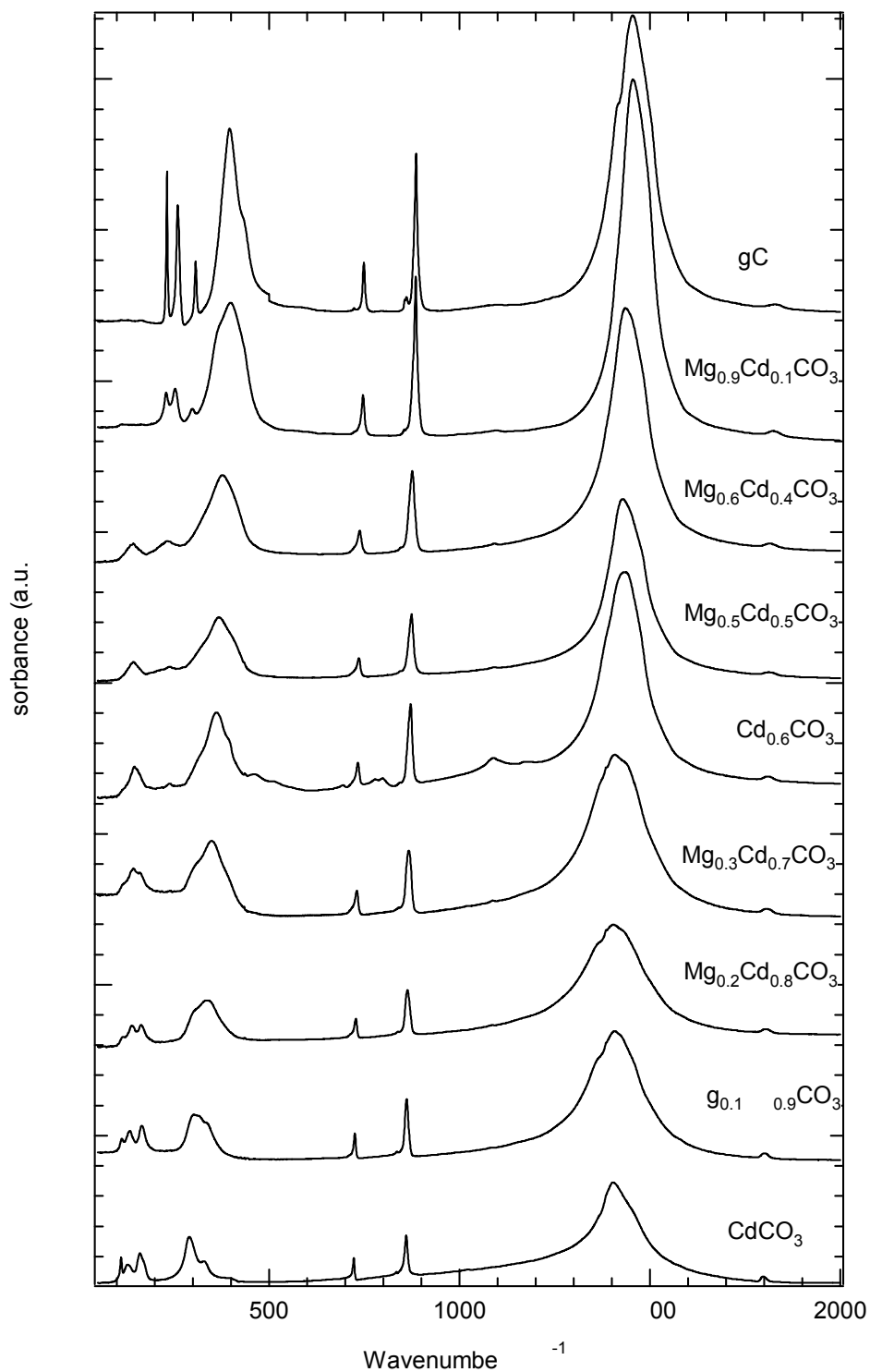


Figure 4.1: Stacked and merged spectra for all samples synthesised at 600°C for 3 hours and 1GPa. Note that in the sample of composition $\text{Mg}_{0.4}\text{Cd}_{0.6}\text{CO}_3$ an overtone is visible at $\sim 1100\text{cm}^{-1}$.

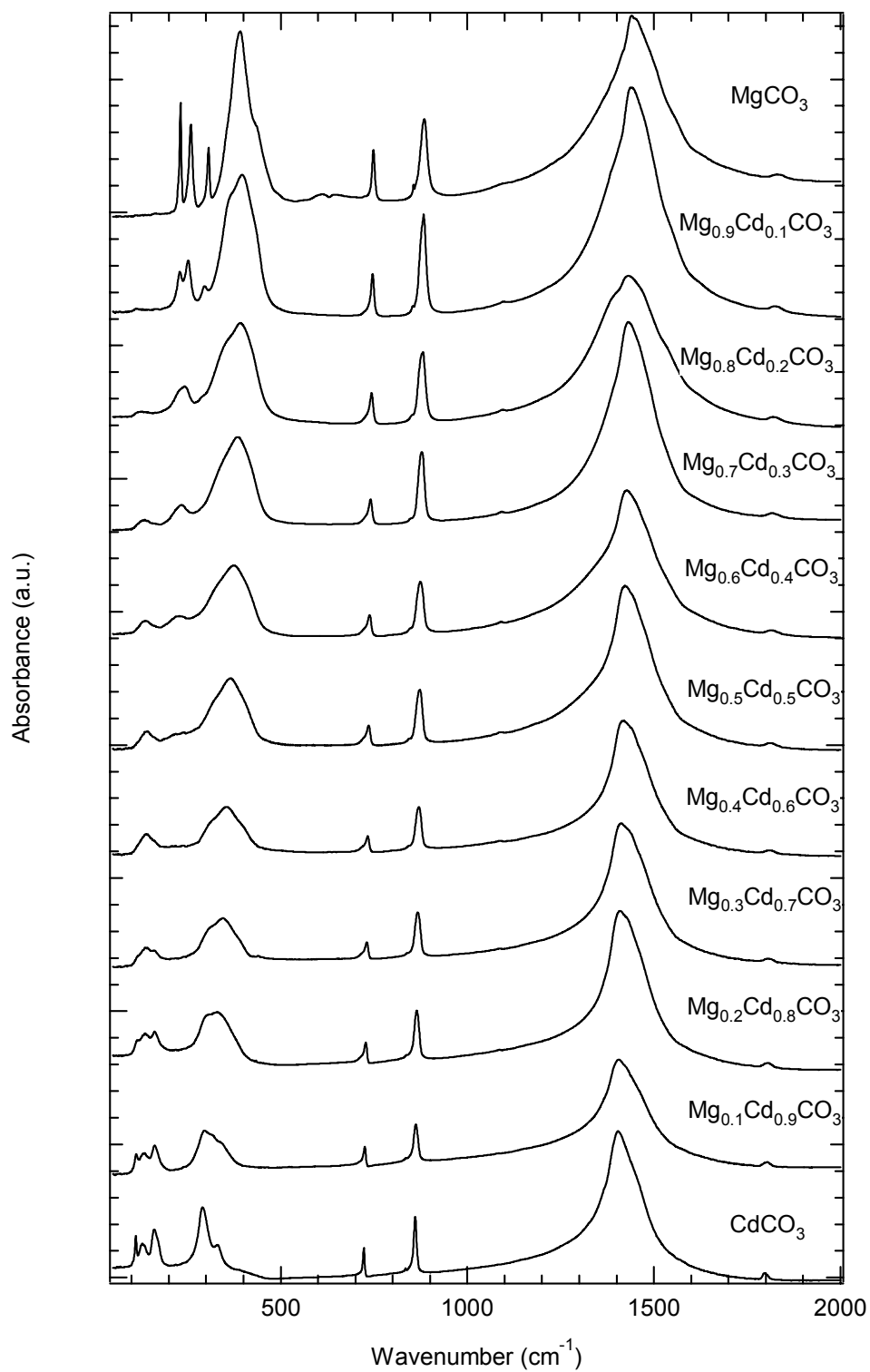


Figure 4.2: Stacked and merged spectra for all samples synthesised at 800°C for 1 hour at 1GPa.

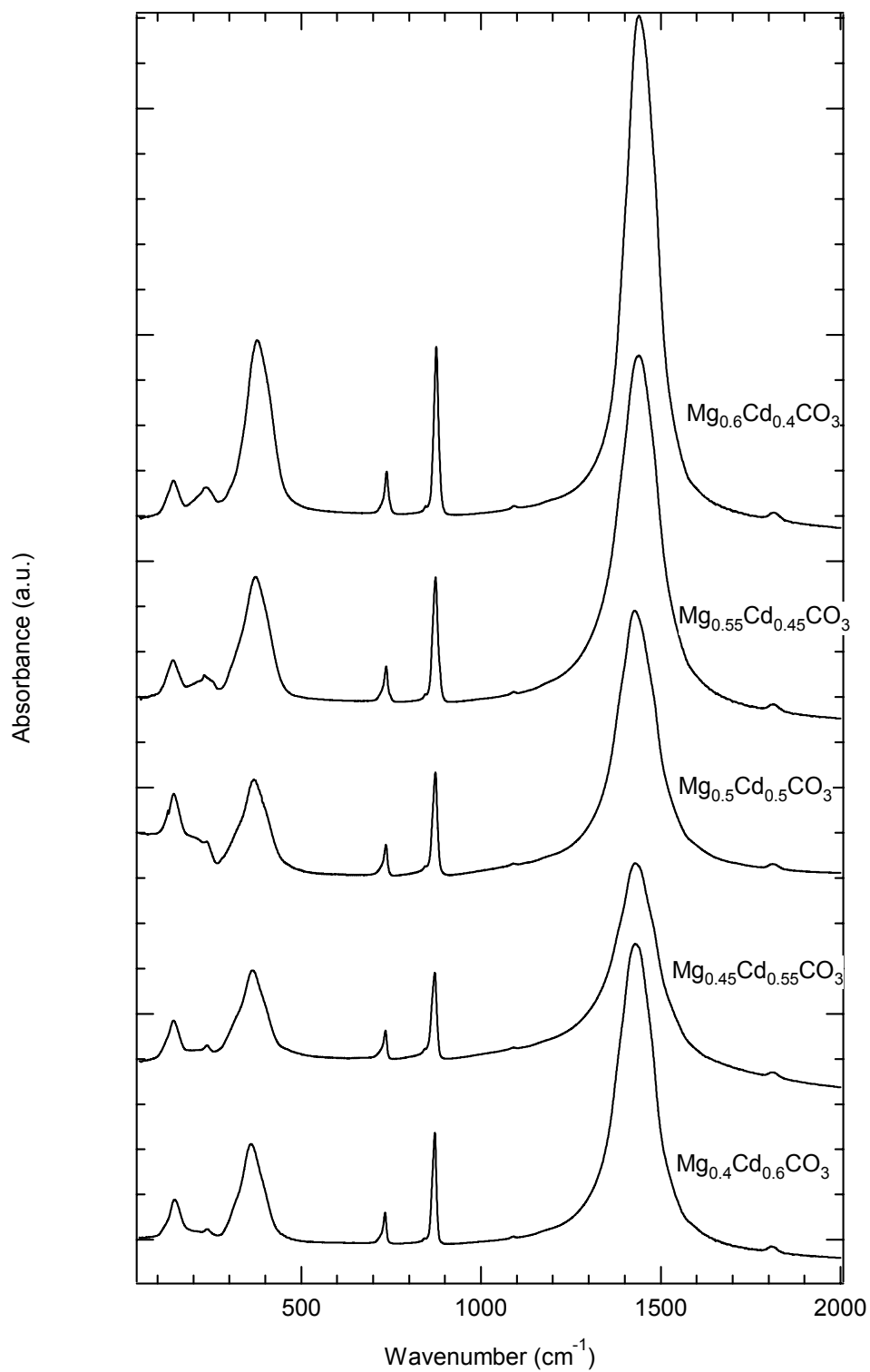


Figure 4.3: Stacked and merged spectra for all ordered samples synthesised at 600°C for 19 hours and 1GPa.

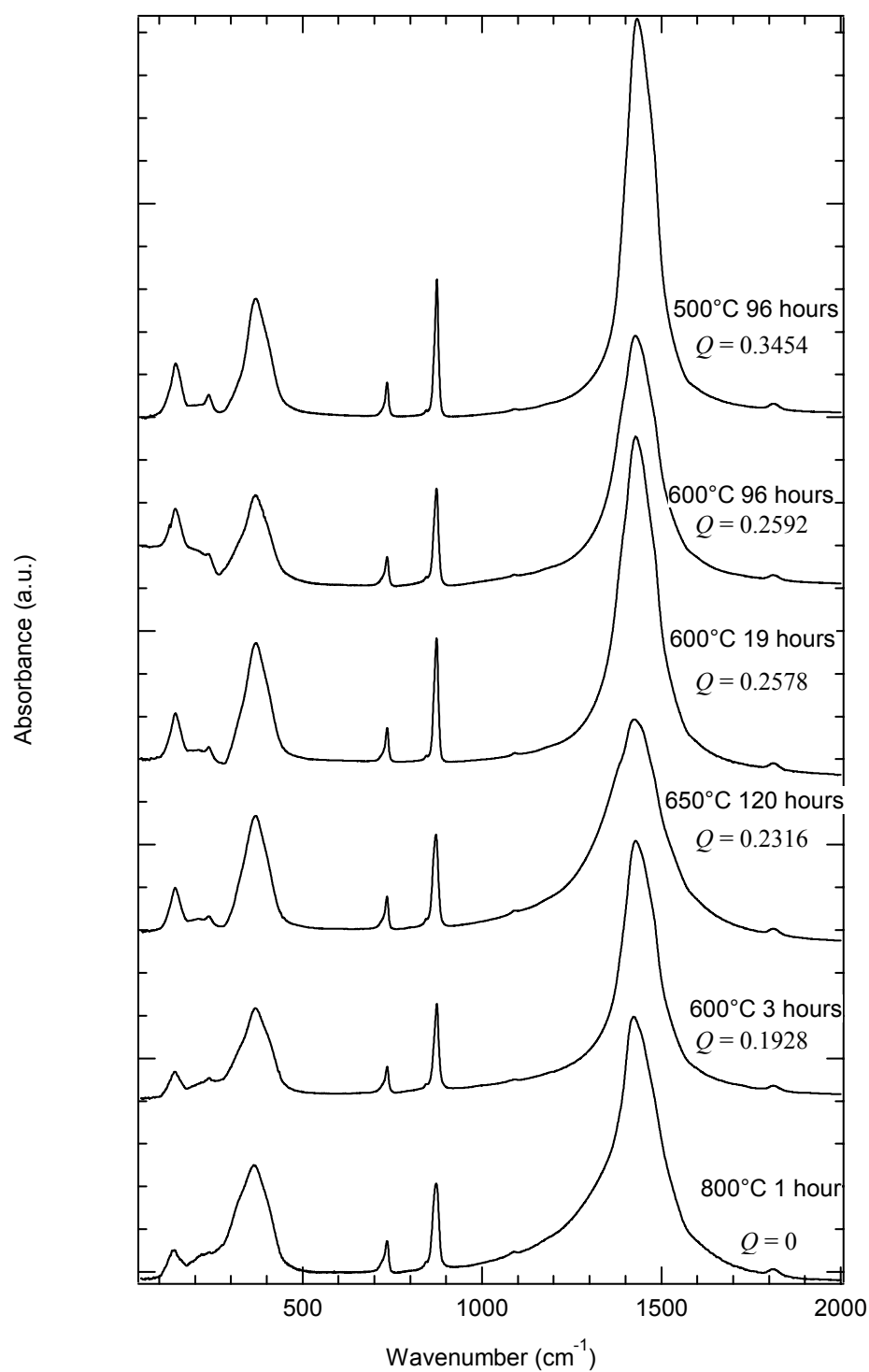


Figure 4.4: Stacked and merged spectra for all synthesised samples of composition $\text{Mg}_{0.5}\text{Cd}_{0.5}\text{CO}_3$ and differing degrees of order. Spectra are stacked to show samples becoming increasingly ordered from bottom to top. Long-range order parameters, Q , are given for each sample.

4.2 The Modal behaviour

Chang and Mitra (1968) observed that two types of behaviour exist in crystals of mixed composition. The first type of behaviour is one-mode behaviour, which was defined by Chang and Mitra as;

“In one class of mixed systems, the “one-mode” behaviour-type, each of the $k \sim 0$ optic mode frequencies (infrared or Raman active) varies continuously and approximately linearly with concentration from the frequency characteristic of one end member to the other end member. Furthermore, the strength of the mode remains approximately constant”

This idea may be thought of as analogous to a series of XRD patterns across a solid solution. The peak shift is continuous across the solid solution with change in composition. The second type of behaviour discussed by Chang and Mitra (1968) is two-mode behaviour and is defined by them as;

“In the other class of mixed crystal systems, the “two-mode” behaviour type, the two phonon frequencies for each of the allowed optic modes of the pure crystal are observed to occur at frequencies close to those of the end members. In addition, the strength of each phonon mode of the mixed crystal is approximately proportional to the mol fraction of the component it represents.”

The behaviour of a solid solution in terms of one- or two-mode can be observed at low frequencies ($50\text{--}350\text{cm}^{-1}$), as this is the region where phonon bands are due to cation translations. Polyethylene IR spectra for the 800°C series are shown in Figure 4.5 to highlight the behaviour of the otavite – magnesite solid solution. It is clearly visible that for samples of intermediate composition both sets of bands relating to the end-members are present (solid arrows). The dashed arrow is shown to illustrate how the vibrational bands of otavite are expected to vary in the case of one-mode behaviour. In order to differentiate between pure two-mode behaviour and a possible mixture of one- and two-

mode behaviour cadmium – oxygen bands, and the magnesium – oxygen bands were considered separately for each spectrum. An example of the Lorentzian peak fitting routine used is illustrated for the end-members in Figure 4.6. For the region $75\text{--}200\text{cm}^{-1}$, due to cadmium-oxygen translations, six Lorentzian profiles were fitted, whereas in the region $200\text{--}350\text{cm}^{-1}$, due to magnesium-oxygen translations, five Lorentzian profiles were used. The number of Lorentzian profiles was chosen in order to obtain the best fit of the end-member spectra and was kept constant for all spectra across the solid solution. The variation of band position with composition for the two regions is shown in Figure 4.7 and Figure 4.8 respectively. The vibrational bands relating to cadmium-oxygen translations can be followed up to a composition of $\text{Mg}_{0.4}\text{Cd}_{0.6}\text{CO}_3$, whereas the absorbance of the magnesium-oxygen translations falls off rapidly with increasing cadmium content and the fitting procedure gives reliable results only to a composition of $\text{Mg}_{0.8}\text{Cd}_{0.2}\text{CO}_3$. Note that the cadmium-oxygen bands (Figure 4.7) remain constant across the solid solution, so displaying two-mode behaviour, whereas the magnesium-oxygen bands (Figure 4.8) show a decrease in wavenumber with addition of cadmium to the magnesite, so showing some degree of one-mode behaviour.

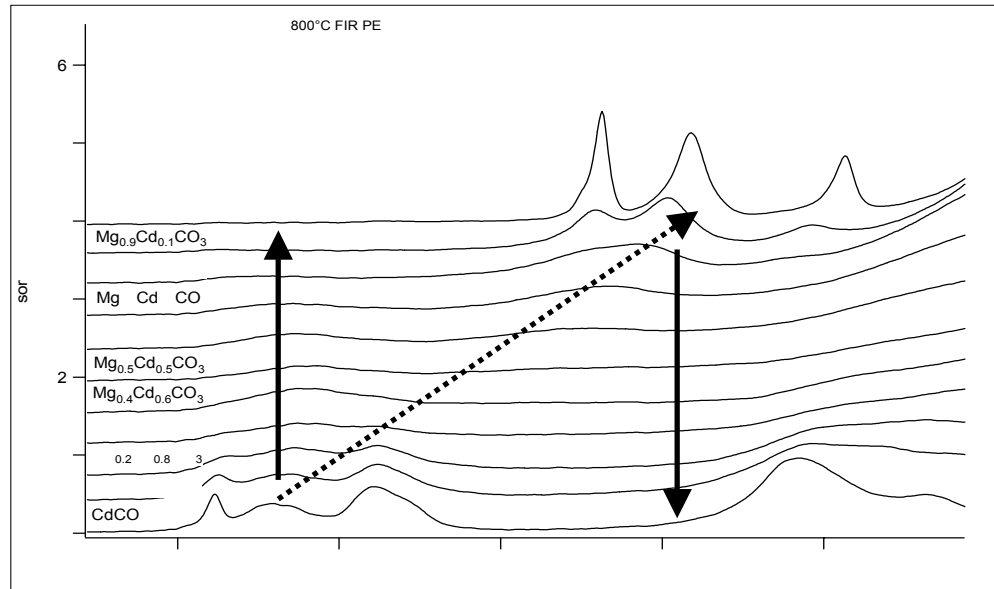


Figure 4.5: The low frequency ($50\text{--}350\text{cm}^{-1}$) region, used to determine the mode of behaviour of the otavite – magnesite system. Analysis was performed in order to ascertain if the system displayed one-mode (dotted arrow), or two-mode (solid arrows) behaviour.

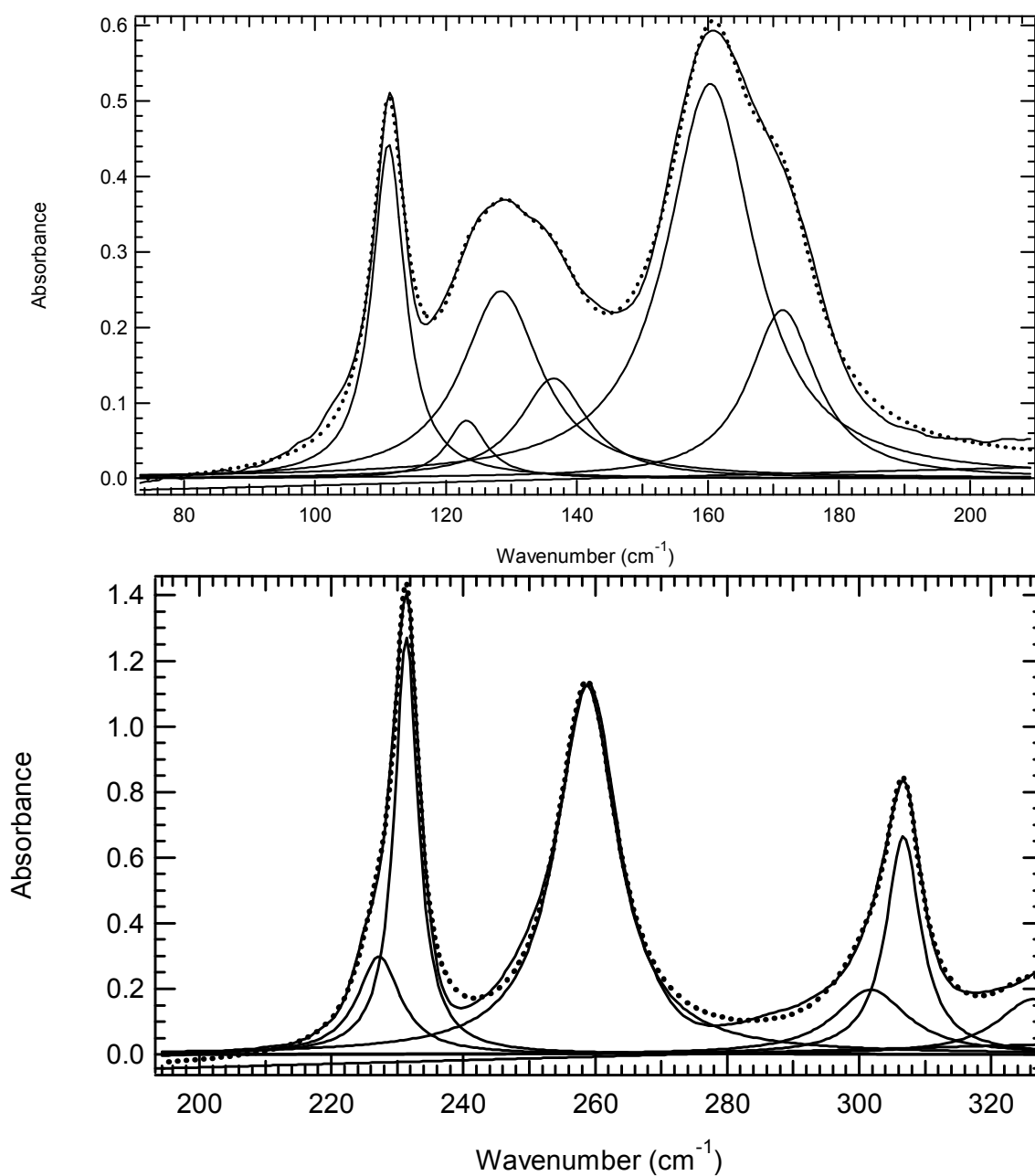


Figure 4.6: a) Lorentzian peak fitting routine for otavite end-member. The dashed line shows the fit output. Six Lorentzian profiles were used for the cadmium-oxygen bands between 75-200cm⁻¹. b) Lorentzian peak fitting routine for magnesite end-member. Dotted line shows fit output. Five Lorentzian profiles were used between 200-350cm⁻¹.

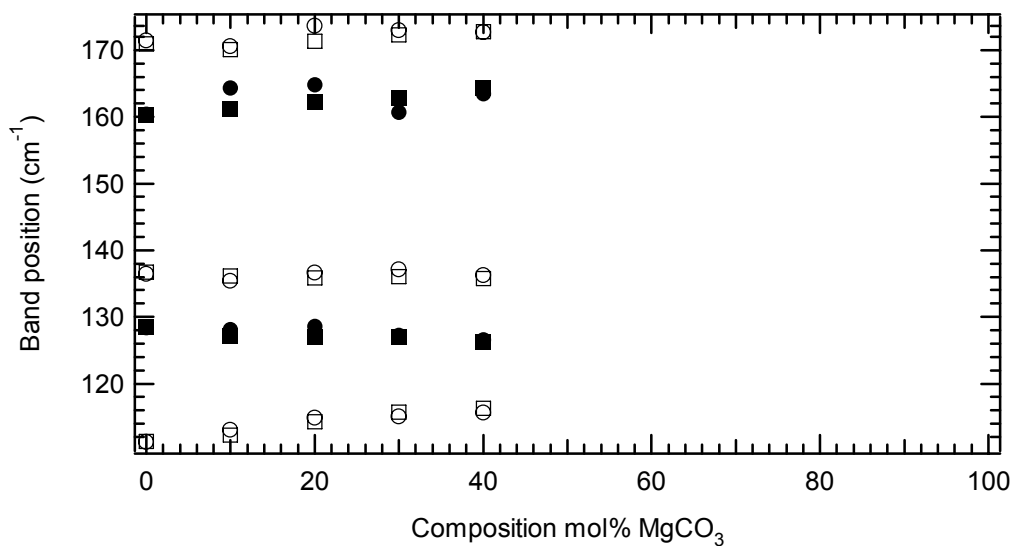


Figure 4.7: Variation of band position for cadmium – oxygen translation bands versus composition for the series of samples synthesised at 600°C, 3hrs (open and closed circles) and 800°C, 1 hour (open and closed squares).

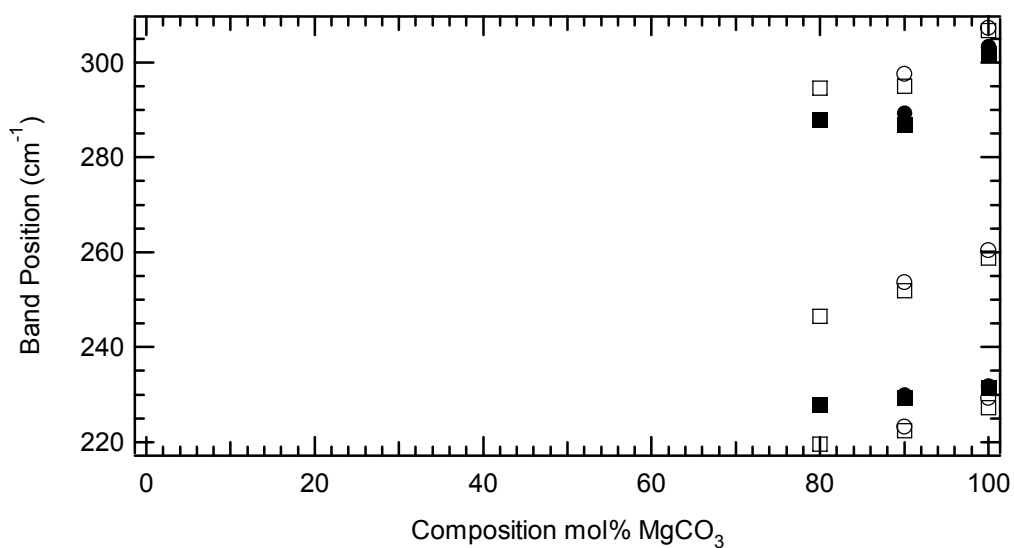


Figure 4.8: Variation of band position for magnesium – oxygen translation bands versus composition for the series of samples synthesised at 600°C, 3hrs (open and closed circles) and 800°C, 1 hour (open and closed squares).

4.3 Carbonate Group Internal Modes

At higher frequencies above 350cm^{-1} only bands relating to different carbonate group vibrations are observed. The “Find Peak” procedure in the Igor Pro 4.09A program was used in order to determine band position. The bands chosen were those between $230\text{--}500\text{cm}^{-1}$, $650\text{--}800\text{cm}^{-1}$, $800\text{--}900\text{cm}^{-1}$ and $1000\text{--}1800\text{cm}^{-1}$. Across all the spectra collected the higher energy bands are very broad, but very well defined, and do not overlap with any other bands, so allowing the bands to be identified with relative ease. In spite of the band broadness, the 800°C series in the highest frequency region shows little scatter, so suggesting an increase in bond strength of the carbonate group with increasing magnesite content. Moreover, this is evidence of the presence of a plateau of band position at the magnesite end-member as cadmium atoms are incorporated into the structure. This plateau is reminiscent of the plateau observed at transition temperatures in solid solutions, and its magnitude, in terms of composition limits, correlates inversely with the magnitude of the strain fields surrounding impurity atoms [Salje *et al.*, 1991; Carpenter, 1992; Hayward and Salje, 1996; Carpenter *et al.*, 1999]. The expectation is that the properties of a pure crystal, such as a phase transition temperature, or in this case, phonon frequency, will remain constant when the second component of a solid solution is added, so long as the microscopic strain fields around the substituting atoms do not overlap. The composition limits are $\sim 10\text{mol}\%$ CdCO_3 , so suggesting that the strain fields associated with cadmium substitution into the magnesite structure are in the order of, or less than two unit cells.

The shift in band position as a function of composition for all the regions given above can be seen in Figures 4.9a, b & c. Figure 4.9a shows band shift in the FIR region. It was possible to resolve two bands in this spectral region, both of which are shown with linear fits through the 800°C series of data. Band positions for samples with $R\bar{3}$ symmetry at intermediate compositions in Figures 4.9a and 4.9b show a linear shift, irrespective of degree of order. The dashed lines in Figure 4.9b show the fit through the 800°C series of data. The non-linear behaviour of band position for the 600°C series in Figure 4.9c can be explained in terms of large separation of the transverse and longitudinal modes observed in carbonate internal modes.

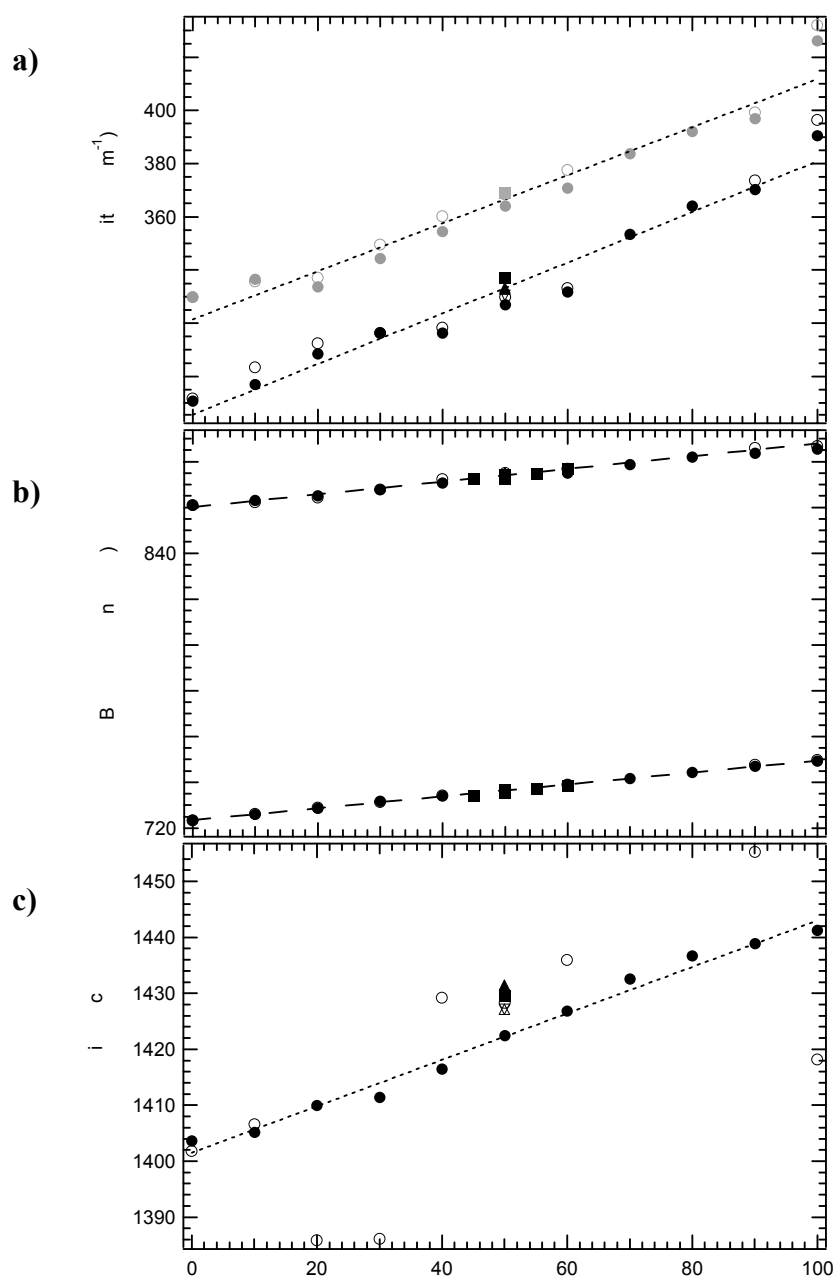


Figure 4.9: a) Band position as a function of composition for the bands in the region 230-550 cm^{-1} . Black symbols are for one band, grey symbols for the second. The dashed lines show linear fits through the two sets of data from the 800°C series, given by $\bar{\nu} = 285.58 + 0.95295\text{mol\% MgCO}_3$ (lower line), and $\bar{\nu} = 321.38 + 0.90336\text{mol\% MgCO}_3$ (upper line). b) Band position as a function of composition for the two bands in the region 650-900 cm^{-1} . The dashed lines show the fit through the 800°C series of data points, as given by, $\bar{\nu} = 723.57 + 0.25847\text{mol\% MgCO}_3$ (lower line) and $\bar{\nu} = 860.38 + 0.25642\text{mol\% MgCO}_3$ (upper line). c) Band position as a function of composition in the region 1000-1800 cm^{-1} . The dashed line show a linear fit through the 800°C series of data, given by, $\bar{\nu} = 1401.6 + 0.4146\text{mol\% MgCO}_3$. Symbols: open circle = 600°C, 3hrs, closed square = 600°C, 19hrs, open triangle = 600°C, 86hrs, inverted open triangle = 650°C, 120hrs, closed triangle = 500°C, 96hrs.

It is of interest to note that in Figure 4.9c at intermediate compositions ($\text{Mg}_{0.4}\text{Cd}_{0.6}\text{CO}_3$ - $\text{Mg}_{0.6}\text{Cd}_{0.4}\text{CO}_3$) the samples within the cadmium dolomite stability field (those with $R\bar{3}$ symmetry) have higher band frequencies than their $R\bar{3}c$ counterparts. The phonon mode operating at this frequency is due to doubly degenerate asymmetric stretching of the carbonate groups. It is therefore suggested that the frequency shift for samples with $R\bar{3}$ symmetry may be attributed to an increase in vibration energy required when the carbonate groups are non-planar (See Tables 3.3 and 3.4 and Figure 3.12). The carbonate groups for samples with $R\bar{3}c$ symmetry are planar, so the corresponding vibrations will have a lower energy. The difference in band position between samples with $R\bar{3}$ and $R\bar{3}c$ symmetry can thus be attributed to the degree of order of the sample.

4.4 Autocorrelation Results

The use of the autocorrelation function as applied to silicate systems was discussed in Section 1.5.1, and the term for the autocorrelation function itself is given in Section 2.4.2. In this section the autocorrelation function has been used to determine the line broadening associated with cation substitution and ordering in the otavite – magnesite solid solution. The homogeneity of a sample on a very small length scale (a few Å) can greatly affect the observed linewidth of the IR spectrum. If a sample is very homogeneous all the atomic vibrations will be in approximately the same environment, so the phonon band will be sharp. Cation substitution and disordering processes result in a decrease in homogeneity of the sample, so the environments within which the atoms are vibrating start to differ, and hence the phonon band becomes correspondingly broader [Boffa Ballaran *et al.*, 1998; Carpenter *et al.*, 1999; Boffa Ballaran *et al.*, 1999; Salje *et al.*, 2000; Carpenter and Boffa Ballaran, 2001; Boffa Ballaran *et al.*, 2001; Tarantino *et al.*, 2002; Tarantino *et al.*, 2003].

An important point to take into account for the interpretation of the autocorrelation data is the lengthscale associated with each spectral region analysed. The lengthscale is a very important consideration as it gives an idea of how large a strain field surrounding substituting cations might be.

An approximation for the length scale is given by,

$$\text{Length scale} \propto 1/\omega$$

where ω is the wavenumber [Salje, 1992]. In order to ascertain an approximation of the length scales for carbonate materials, we consider the phonon band between 1000-2000 cm^{-1} , due to doubly degenerate asymmetric stretching of the CO_3 group (Figures 4.1, 4.2, 4.3 & 4.4). At this wavenumber the length scale must be at least on the order of a C-O bond length, in order that this band is observed. As a first approximation, it may be assumed that at 1000 cm^{-1} a lengthscale of at least 3Å is being sampled. Following on from this assumption, different lengthscales can be related to the proportional wavenumber, as reported in Figure 4.10.

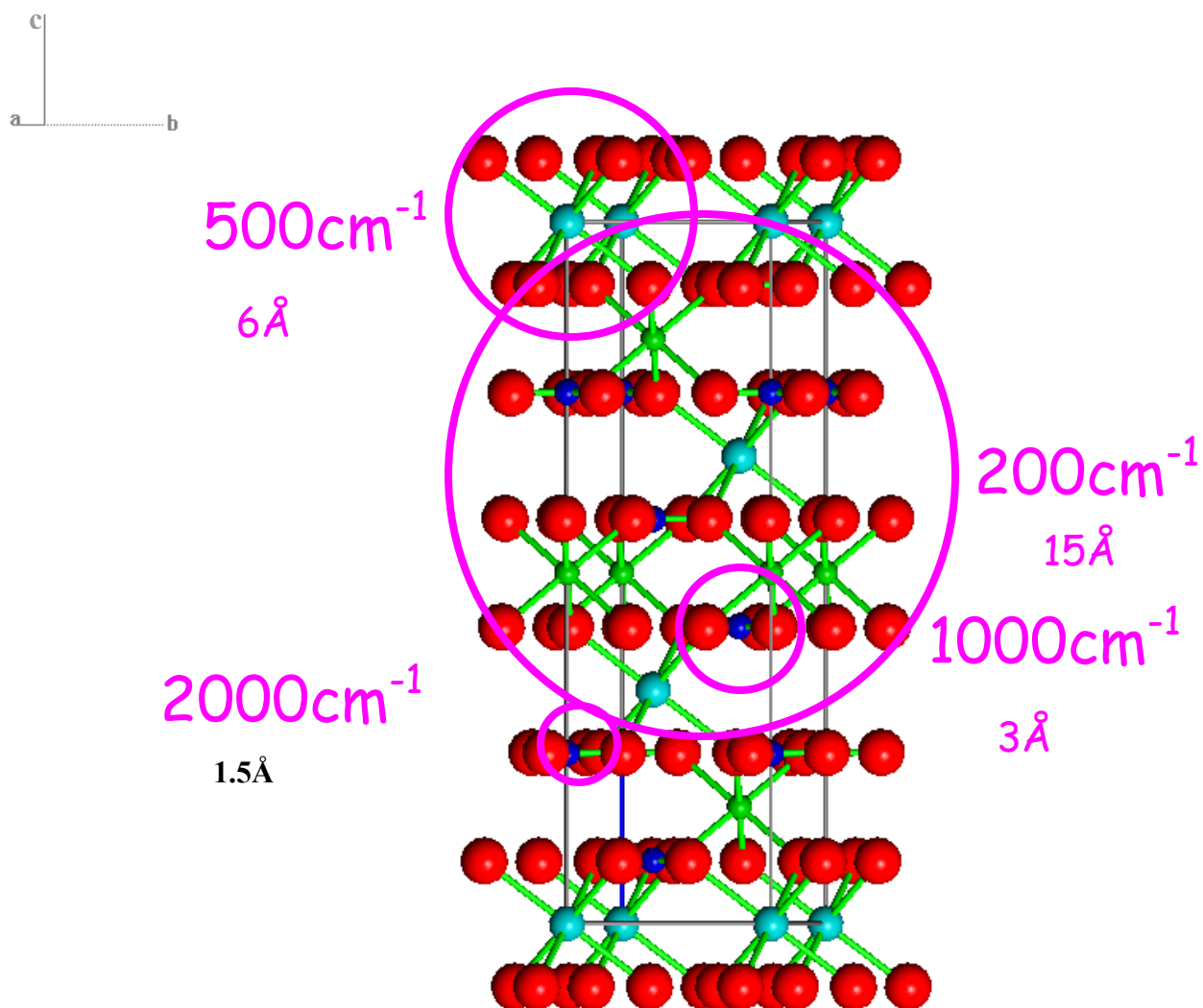


Figure 4.10: Length scales related to wavenumber, illustrated using the ordered $R\bar{3}$ structure from the otavite – magnesite system. Assuming that at 2000cm^{-1} a lengthscale of at least 1.5Å is being sampled, it follows that; $1000\text{cm}^{-1} \sim 3\text{Å}$, $500\text{cm}^{-1} \sim 6\text{Å}$ and $200\text{cm}^{-1} \sim 15\text{Å}$.

The autocorrelation (Δcorr) results for the six regions of the IR spectra investigated (Section 2.4) are presented. The Δcorr results as a function of composition for the cadmium-oxygen bands ($75\text{-}200\text{cm}^{-1}$) and the magnesium – oxygen bands ($200\text{-}350\text{cm}^{-1}$) are shown in Figure 4.11. Given that the absorbance of these phonon signals decreases rapidly at intermediate compositions, the analyses were performed up to 40mol% MgCO_3 for the cadmium-oxygen translation bands, and between 60-100mol% MgCO_3 for the magnesium-oxygen translation bands. Note that the degree of order has no effect on bandwidth, so the degree of heterogeneity within samples of the same composition may be thought of as being alike. The magnesium – oxygen band results in Figure 4.11 (right-hand side axis) are shown in grey and show a larger variation in Δcorr as a function of composition than the Δcorr results from cadmium-oxygen bands. The average linewidths obtained from fitting Lorentzian profiles in this spectral region (Section 4.2) are also reported in Figure 4.11 for comparison. It appears that the increase in Δcorr (i.e. effective linewidth) for samples of intermediate composition is not an artefact of the autocorrelation method.

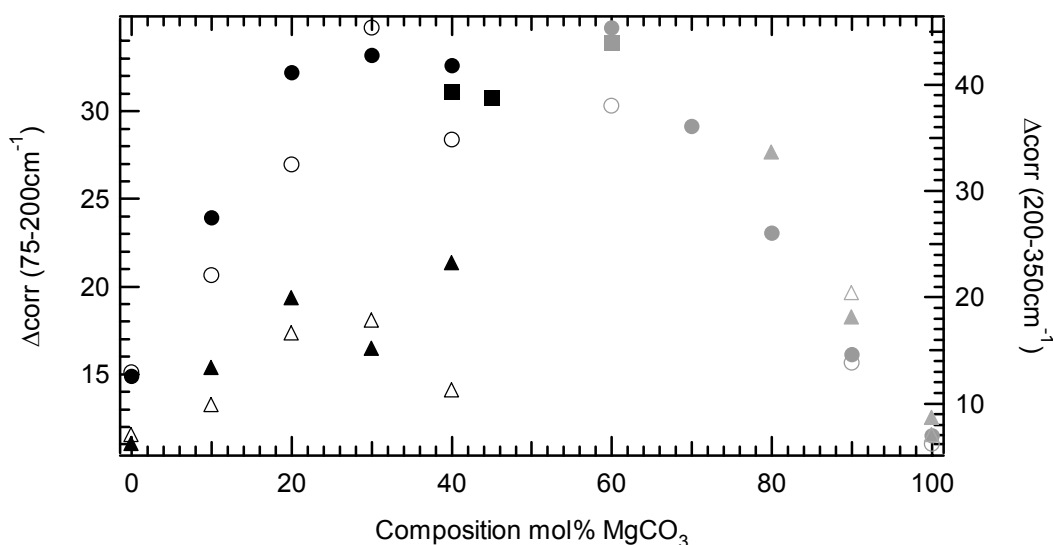


Figure 4.11: Variation of autocorrelation with composition for the region $75\text{-}200\text{cm}^{-1}$ (left-hand axis and black symbols) and $200\text{-}350\text{cm}^{-1}$ (right-hand axis and grey symbols). Vibrations in this region are due to translational motion of cadmium – oxygen bonds (left-hand side) and magnesium – oxygen bonds (right-hand axis). Circles are data from autocorrelation analysis, triangles are average linewidths calculated from a Lorentzian peak fitting routine. Symbols: open circle = 600°C , 3hrs, closed circle = 800°C , 1 hour, closed square = 600°C , 19hrs.

The results shown in Figure 4.12 are for Δcorr as a function of composition in the region $300\text{-}500\text{cm}^{-1}$. Note the positive deviation from linearity at intermediate compositions. Comparisons between samples with differing degrees of order show a very small effect on bandwidth. It is also interesting to note that the 800°C samples close to the $\text{Mg}_{0.5}\text{Cd}_{0.5}\text{CO}_3$ composition have Δcorr values smaller than those corresponding to the polynomial fit through the 800°C data series at magnesium-rich and cadmium-rich compositions. This suggests that some degree of short-range order is present at the length scale sampled in this spectral region.

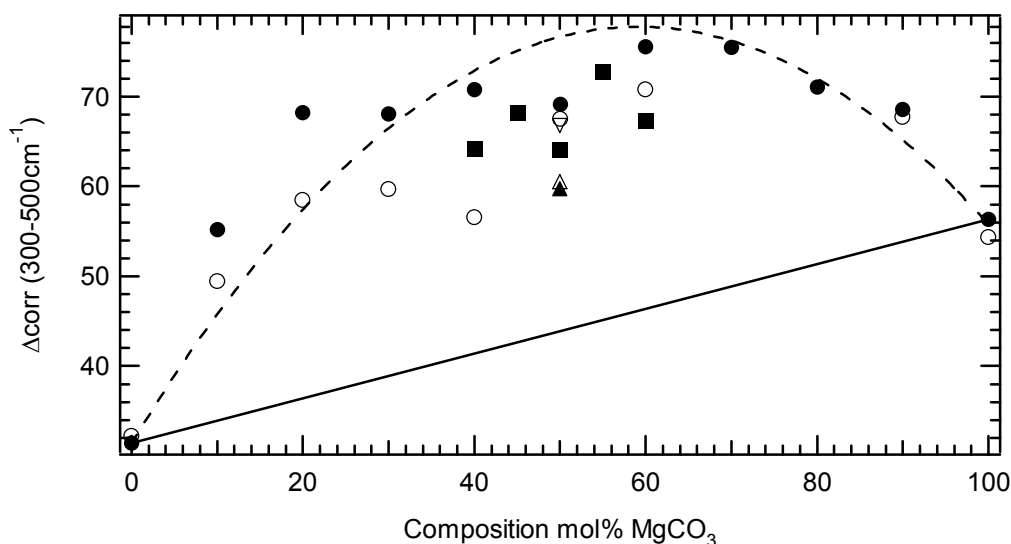


Figure 4.12: Variation of autocorrelation with composition for the region $300\text{-}500\text{cm}^{-1}$. Vibrations in this region are due to translation (ν_{13}) and libration (ν_{14}) of the carbonate (CO_3) group. Symbols: open circle = 600°C , 3hrs, closed square = 600°C , 19hrs, open triangle = 600°C , 86hrs, inverted open triangle = 650°C , 120hrs, closed triangle = 500°C , 96hrs.

In the MIR region Δcorr results for three regions were determined. Δcorr as a function of composition for the region $700\text{-}800\text{cm}^{-1}$ are shown in Figure 4.13. The trend is similar to that reported in Figure 4.12, although a more asymmetric positive deviation from linearity is observed. Again, no effect of degree of order is observed. Results of Δcorr as a function of composition for the region $800\text{-}900\text{cm}^{-1}$ are shown in Figure 4.14.

Note that in this region at composition $\text{Mg}_{0.5}\text{Cd}_{0.5}\text{CO}_3$ a significant decrease in bandwidth is observed as a function of degree of order. The phonon mode in this region is due to out-of-plane bending of the carbonate group and can be related to the non-planar carbonate group, as discussed in Section 3.2.3. The difference in Δ_{corr} values for ordered samples with respect to the disordered sample is defined as $\delta\Delta_{\text{corr}}$, and can be used to measure the local order parameter, q . The magnesite sample and sample of composition $\text{Mg}_{0.9}\text{Cd}_{0.1}\text{CO}_3$ synthesised at 600°C have much smaller Δ_{corr} values than samples of the same composition synthesised at 800°C . It is likely that this result is due to the better resolution of the small shoulder at around 825cm^{-1} , which in the IR spectra of the 600°C samples appears as a well-defined band (Figure 4.1). The 800°C series trend shows steep increase in Δ_{corr} as magnesium is substituted into the otavite structure, whereas a plateau is reached at the magnesite rich end. This suggests that the microscopic strain fields around the magnesium atoms in the otavite structure are much larger than those surrounding the cadmium atoms in the magnesite structure. Δ_{corr} as a function of composition for the region $1000\text{--}2000\text{cm}^{-1}$ are shown in Figure 4.15. The dashed line shows a linear fit through the 800°C series of data.

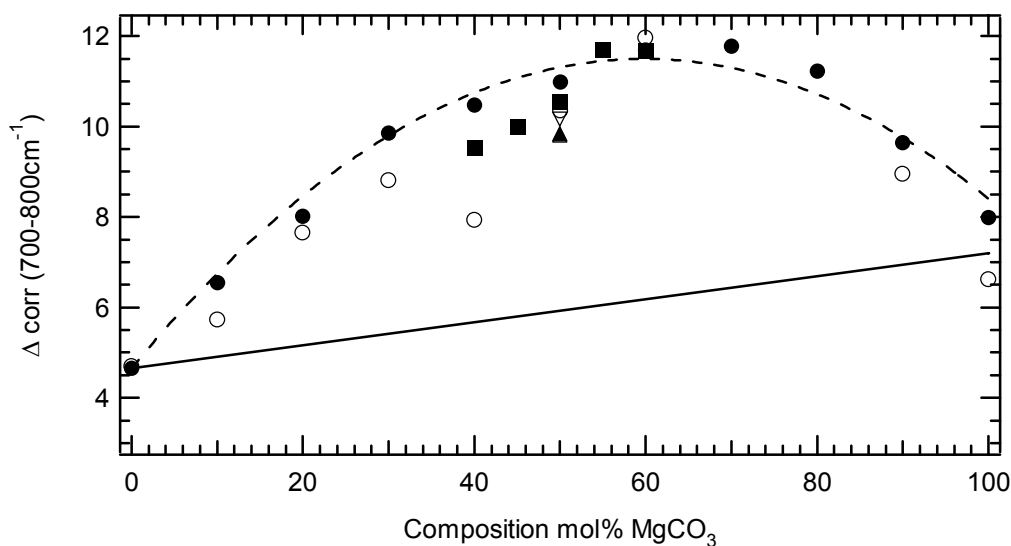


Figure 4.13: Variation of autocorrelation with composition for the region $625\text{--}800\text{cm}^{-1}$. Vibrations in this region are due to doubly degenerate in-plane bending (ν_4) of the carbonate (CO_3) group. Symbols as in Figure 4.12.

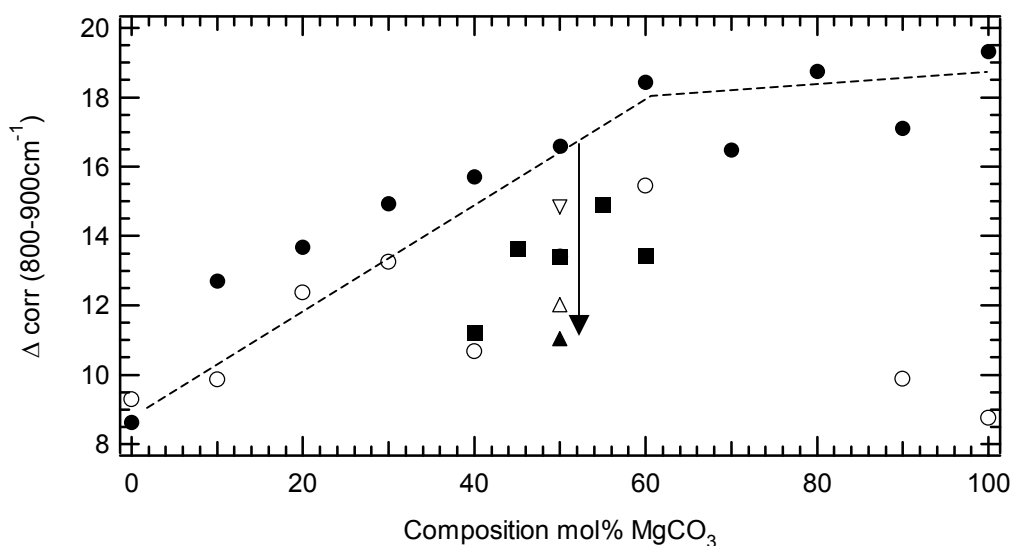


Figure 4.14: Variation of autocorrelation with composition for the region $800\text{-}900\text{cm}^{-1}$. Vibrations in this region are due to out-of-plane bending (ν_2) of the carbonate (CO_3) group. Symbols: open circle = 600°C , 3hrs, closed square = 600°C , 19hrs, open triangle = 600°C , 86hrs, inverted open triangle = 650°C , 120hrs, closed triangle = 500°C , 96hrs. The dashed lines are a guide to the eye for the 800°C series.

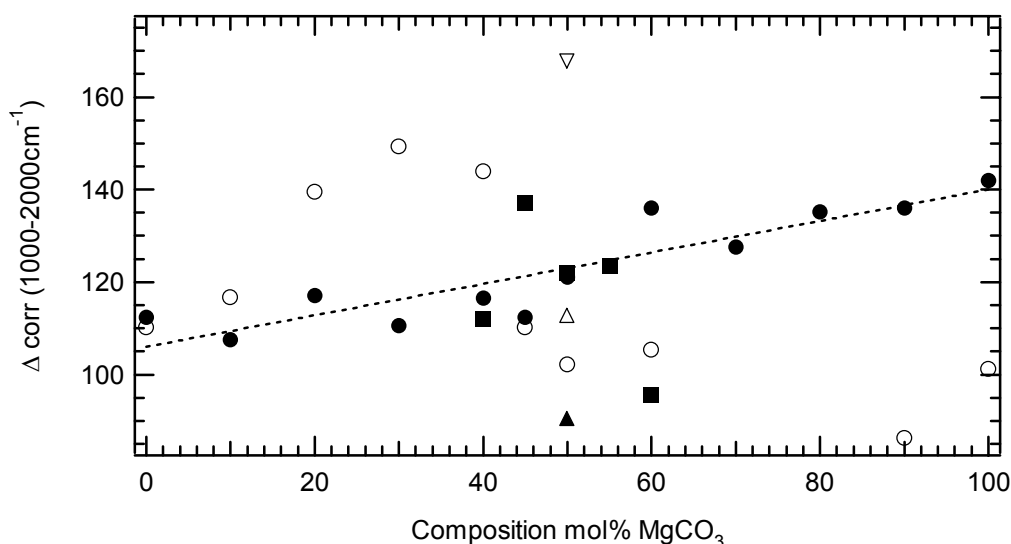


Figure 4.15: Variation of autocorrelation with composition for the region $1000\text{-}2000\text{cm}^{-1}$. Vibrations in this region are due to doubly degenerate asymmetric stretching (ν_3) of the carbonate (CO_3) group. Symbols: open circle = 600°C , 3hrs, closed square = 600°C , 19hrs, open triangle = 600°C , 86hrs, inverted open triangle = 650°C , 120hrs, closed triangle = 500°C , 96hrs. The dashed line shows a linear fit through the 800°C series of data, given by $a = 105.99$, $b = 0.34005$.

The carbonate group asymmetric stretching mode appears to be affected slightly by the different degrees of order at a composition of $\text{Mg}_{0.5}\text{Cd}_{0.5}\text{CO}_3$. Note that the sample synthesised at 650°C has a very large Δcorr value. This may suggest the presence of short-range order in this sample, with a consequent increase of heterogeneities surrounding the carbonate groups. The deviation from the linear trend shown by cadmium-rich samples from the 600°C series is tentatively interpreted as a result of short-range order. Following this interpretation, it may be concluded that the 800°C series is highly homogeneous, at least in terms of sampling of the carbonate group.

It is also interesting to note that in Figures 4.11, 4.12 and 4.14 in particular, a large difference in behaviour of the two end-members is observed. It can be seen in Figure 4.11 that substituting magnesium into the otavite end-member has a huge effect on the bandwidth. In Figure 4.10 the minimum length scale associated with each region of the powder absorption IR spectra was shown. If this is now considered, then the length scale under consideration in Figure 4.11 is approximately 30\AA . If the number of magnesium atoms per unit cell is considered for 10mol% MgCO_3 in the otavite end-member, it is found that there are 0.6 magnesium atoms per unit cell, or approximately one magnesium atom every other unit cell. The c -axis of the otavite end-member is $\sim 16\text{\AA}$, so at this frequency two unit cells are being sampled, and hence the strain field associated with the addition of 10mol% MgCO_3 to the otavite end-member must be in the region of 30\AA (two unit cells) so that the strain is seen at this frequency. In contrast, if Figures 4.12 and 4.14 are considered, the reverse is true for the magnesite end-member. Substituting cadmium into the magnesite end-member has very little effect on the structure, until a composition of $\text{Mg}_{0.6}\text{Cd}_{0.4}\text{CO}_3$ is reached. If 40mol% CdCO_3 is substituted into magnesite, then only when there are an average of 2.4 cadmium atoms every six sites does a difference start to be observed. These phenomena are observed in four regions of the spectra, so giving rise to the asymmetry in the autocorrelation results in Figures 4.11, 4.12, 4.13 and 4.14.

5: Discussion and conclusions

Results from this study have given an insight into the macroscopic and microscopic behaviour of the otavite – magnesite system. The main areas of interest for the discussion are the phase stability with respect to previously published data, comparison between the mixing and ordering behaviour obtained at two different lengthscales, namely X-ray powder diffraction and infrared powder absorption spectroscopy, how the response of the carbonate structure to cation substitution and ordering compares to silicate systems displaying order-disorder phase transitions, a comparison between the otavite - magnesite system with the “parent” calcite – magnesite system and the comparison of lattice parameters, inter-atomic distances, bond angles and atomic positions with those measured in previous studies.

5.1 Phase Stability in the Otavite – Magnesite System

The work discussed in Section 1.3 by Goldsmith (1972), Capobianco *et al.* (1987) and Burton and Van de Walle (2003) has been instrumental in aiding the progress of this study. The comparison of the Goldsmith (1972), Capobianco *et al.* (1987) and Burton and Van de Walle (2003) studies with results from this study are shown in Figure 5.1. Although this study was not concerned primarily with mapping the phase diagram of the magnesite – otavite system, the comparison illustrated in Figure 5.1 can help to better constrain the phase boundaries of the solid solution. Goldsmith (1972) observed a miscibility gap in the cadmium-rich half at temperatures of ~650°C. The models used by Capobianco *et al.* (1987) and Burton and Van de Walle (2003) also predict this miscibility gap, although the compositional range and temperatures over which the two studies claim the miscibility gap to be stable differ significantly. It may be noted that the study by Burton and Van de Walle (2003) shows a very narrow miscibility gap in the cadmium-rich half of the phase diagram, which is stable to ~600°C. The sample of composition $\text{Mg}_{0.3}\text{Cd}_{0.7}\text{CO}_3$ synthesised at 500°C for this study (Figure A5.29) shows

very broad diffraction peaks with respect to the sample synthesised under the same conditions of composition $\text{Mg}_{0.2}\text{Cd}_{0.8}\text{CO}_3$. It is therefore suggested that the significant increase in linewidth between these two samples indicates the presence of a miscibility gap in the cadmium-rich half of the system. It is possible that the sample of composition $\text{Mg}_{0.3}\text{Cd}_{0.7}\text{CO}_3$ synthesised at 500°C lies on the solvus between the complete, disordered solid solution and the miscibility gap, and hence some degree of exsolution may be present in the sample, so causing an increase in linewidth. The very narrow miscibility gap predicted by Burton and Van de Walle (2003) (Figure 5.1) may suggest that the two phases present in the miscibility gap are, in fact, too compositionally similar to accurately refine two distinct phases.

The main discrepancy between the experimental work done for this study and the results from Goldsmith (1972), Capobianco *et al.* (1987) and Burton and Van de Walle (2003) is the compositional range over which the cadmium dolomite phase is stable. Goldsmith (1972) and Capobianco *et al.* (1987) show a very narrow stability field for cadmium dolomite between compositions $\text{Mg}_{0.45}\text{Cd}_{0.55}\text{CO}_3$ and $\text{Mg}_{0.55}\text{Cd}_{0.45}\text{CO}_3$ at 600°C . The study by Burton and Van de Walle (2003) shows good agreement with this study in the cadmium-rich part of the phase diagram, with the phase boundary at a composition of $\text{Mg}_{0.4}\text{Cd}_{0.6}\text{CO}_3$, but in the magnesium-rich half of the phase diagram the phase boundary is very close to the $\text{Mg}_{0.5}\text{Cd}_{0.5}\text{CO}_3$ composition. Although the experimental results from this study show a larger stability field for the cadmium dolomite ($\text{Mg}_{0.4}\text{Cd}_{0.6}\text{CO}_3$ - $\text{Mg}_{0.6}\text{Cd}_{0.4}\text{CO}_3$) at 600°C , it is interesting to note that the degree of order drops off more rapidly in the magnesium rich region, as opposed to the cadmium rich region (Figure 3.16), so indicating asymmetry in the cadmium dolomite phase field, as predicted in the phase diagrams mapped out in the previous studies [Goldsmith, 1972; Capobianco *et al.*, 1987, Burton, 1987; Burton and Van de Walle, 2003]. The observed asymmetry in the cadmium dolomite phase field is not only observed for the M site occupancies, and hence the order parameter, Q , values (Figure 3.16), but also for the oxygen-carbon-oxygen bond angles (Figure 3.12). It was noted in Section 3.2.3 that there was a correlation between the degree of order of the samples with the oxygen-carbon-oxygen bond angle. As the degree of order increases, so the bond angle decreases, as the carbon of the carbonate group moves out of plane with respect to

the oxygens. Figure 3.12 shows the oxygen-carbon-oxygen bond angle as a function of composition, and the asymmetry is clearly visible. Another discrepancy is the transition temperature for the cadmium dolomite of the order-disorder process. Goldsmith (1972) and Capobianco *et al.* (1987) both reported that the ordered cadmium dolomite was stable up to $\sim 850^{\circ}\text{C}$. However, the experimental results in this study are consistent with a transition temperature of $\sim 700^{\circ}\text{C}$ (Figures 3.15 & 3.17). Burton and Van de Walle (2003) note that the modelling technique used to acquire the phase diagram in Figures 1.7 and 5.1 does tend to overestimate transition temperatures. They also note that this is especially problematic when vibrational effects are ignored, as in the model used to derive the phase diagram for their study in 2003. Taking these observations into account, it can be concluded that the results from Burton and Van de Walle (2003) show very good agreement with the experimental results from this study.

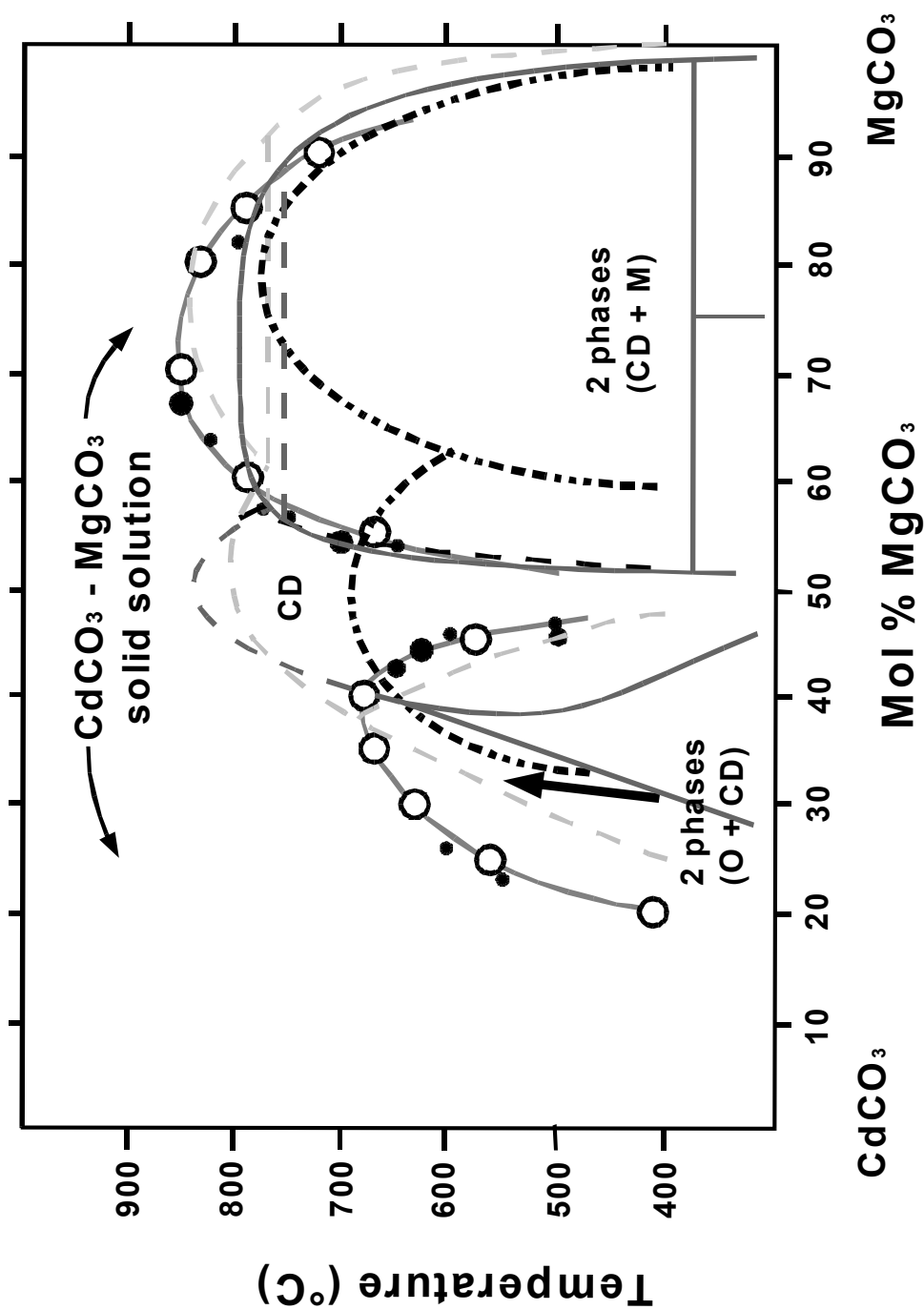


Figure 5.1: Phase diagram for the otavite – magnesite solid solution. Solid grey lines are from the experimental work of Goldsmith (1972), dashed light grey lines are from model from Capobianco *et al.* (1987), dark grey solid lines are from experimental results from this study. These boundaries from experimental work from this study.

5.2 Variation of Unit-Cell Lattice Parameters, Atomic Positions and Inter-atomic Distances

5.2.1 Variation of Unit-Cell Lattice Parameters

The results in Section 3.2.1 show the variation of unit-cell parameters as a function of composition and synthesis temperature across the otavite – magnesite solid solution (Figures 3.6a-c). A positive deviation from linearity was observed in the plot of the c -axis as a function of composition (Figure 3.6b), which can be related to spontaneous strain associated with the order-disorder phase transition. Goldsmith and Heard (1960) observed the same phenomenon in dolomites with differing degrees of order. They noted that as the dolomite became increasingly disordered, so the length of the c -axis increased, although they did not quantify the degree to which this occurred, or relate it to the degree of order of the dolomite.

The data obtained from this study is compared with single crystal data from Oh *et al.* (1973) and Markgraf and Reeder (1985) for magnesite, and with X-ray powder diffraction data from Graf (1961) for cadmium dolomite and Borodin *et al.* (1979) for otavite (Table 5.1). Note that the comparison with the data from Graf (1961) is done with samples from this study synthesised at like conditions with those synthesised by Graf (1961).

Table 5.1: Comparison of unit-cell lattice parameters for magnesite [Oh *et al.*, 1973; Markgraf and Reeder, 1985], cadmium dolomite [Graf, 1961] and otavite [Borodin *et al.*, 1979]. Standard deviations in parentheses.

Study	a (Å)	c (Å)
Magnesite		
Oh <i>et al.</i> (1973)	4.637(1)	15.023(3)
Markgraf and Reeder (1985)	4.635(2)	15.019(3)
This study (600°C series)	4.6338(5)	15.0197(2)
This study (800°C series)	4.6337(2)	15.0196(9)
Cadmium Dolomite		
Graf (1961) - $R\bar{3}$	4.7770(9)	15.641(3)
This study - $R\bar{3}$ (600°C series)	4.7791(7)	15.6888(4)
Graf (1961) - $R\bar{3}c$	4.7746(9)	15.678(3)
This study - $R\bar{3}c$ (800°C series)	4.7785(8)	15.697(4)
Otavite		
Borodin <i>et al.</i> (1979)	4.923(3)	16.287(6)
This study (600°C series)	4.92043(5)	16.2964(2)
This study (800°C series)	4.9204(4)	16.2957(3)

The results from previous studies for magnesite [Oh *et al.*, 1973; Markgraf and Reeder, 1985], cadmium dolomite [Graf, 1961] and otavite [Borodin *et al.*, 1979] shown in Table 5.1 show good agreement with results obtained in this study. It is of interest to note that the lattice parameters published by Graf (1961) for both ordered and disordered cadmium dolomite show that the sample with $R\bar{3}$ symmetry has a shorter c -axis than the

sample with $R\bar{3}c$ symmetry, which is consistent with the results of this study, as well as observations made by Goldsmith and Heard (1960) for dolomite.

5.2.2 Variation of Atomic Positions

Results in Section 3.2.2. show the effect of temperature and composition across the magnesite – otavite solid solution. Table 5.2 presents a comparison of previously published data for magnesite [Oh *et al.*, 1973; Markgraf and Reeder, 1985] and otavite [Borodin *et al.*, 1979] as compared to data from this study. No data are available for cadmium dolomite as none of the previous experimental studies published unit-cell, atomic position or inter-atomic distances data for the system. Graf (1961) published a table of estimated atomic positions for cadmium dolomite, which were used to calculate X-ray powder diffraction intensities for the system, but the estimations were based on the fact that the carbon-oxygen bond length was constant across the solid solution, whereas it is suggested in this study that carbon-oxygen bond lengths depend slightly on the degree of order.

Table 5.2: Comparison of atomic position parameters for magnesite [Oh *et al.*, 1973; Markgraf and Reeder, 1985], cadmium dolomite [Graf, 1961] and otavite [Borodin *et al.*, 1979; Bromiley, 2002]. Standard deviations in parentheses.

Study	Position of Oxygen			Position of carbon on the z-axis
	x	y	z	
Magnesite				
Oh <i>et al.</i> (1973)	0.2767(2)	0	0.25	0.25
Markgraf and Reeder (1985)	0.2778(2)	0	0.25	0.25
This study (600°C series)	0.2798(8)	0	0.25	0.25
This study (800°C series)	0.2790(3)	0	0.25	0.25

Study	Position of Oxygen			Position of carbon on the z-axis
	<i>x</i>	<i>y</i>	<i>z</i>	
Cadmium Dolomite				
Graf (1961)	0.2399	-0.0364	0.244	0.2435
This study (600°C series)	0.266(2)	0.006(4)	0.254(2)	0.238(2)
Otavite				
Borodin <i>et al.</i> (1979)	0.2621(7)	0	0.25	0.25
Bromiley (2002) transmission	0.2637(7)	0	0.25	0.25
Bromiley (2002) reflection	0.227(1)	0	0.25	0.25
This study (600°C series)	0.246(1)	0	0.25	0.25
This study (800°C series)	0.2486(9)	0	0.25	0.25

Comparison of the atomic position parameters for the three studies for the magnesite end-member shows good agreement. However, comparison of the otavite end-member with the previous studies shows some discrepancy. The two values obtained from this study are significantly lower than the value published by Borodin *et al.* (1979). Bromiley (2002) used X-ray powder diffraction in reflection mode to characterise the otavite sample. Bromiley suggested that the large difference between the value obtained and that of Borodin *et al.* (1979) could be due to preferential orientation. The sample was re-run in a Stoe STADI-P diffractometer operating in transmission mode and showed much better agreement with the Borodin *et al.* (1979) study. Improvement in the Rietveld

Refinements in this study (namely with the addition of a parameter to take preferential orientation into consideration) show that there is a significant improvement for the atomic position parameters for the otavite end-member values. The study by Borodin *et al.* (1979) was carried out on a single crystal of otavite, and so results for positional parameters and inter-atomic distances should be considered more accurate than the Rietfeld Refinements carried out on powder samples for this study.

5.2.3 Variation of Inter-atomic Distances

The results presented in Section 3.2.3 show the variation of cation-oxygen bond lengths, carbon-oxygen bond lengths and oxygen-carbon-oxygen bond angle as a function of both composition and temperature. The average bond lengths for magnesium/cadmium ions and oxygen ions are useful for gaining an insight into the effect of cation substitution and ordering on the structure. Comparison with results from previously published work for magnesite [Oh *et al.*, 1973; Markgraf and Reeder, 1985] and otavite [Borodin *et al.*, 1979; Bromiley, 2002] are presented in Table 5.3. No data for inter-atomic distances has been published for cadmium dolomite.

Table 5.3 Comparison of inter-atomic distances for magnesite [Oh *et al.*, 1973; Markgraf and Reeder, 1985] and otavite [Borodin *et al.*, 1979; Bromiley, 2002]. Standard deviations in parentheses.

Study	<M-O> bond length (Å)	<C-O> bond length (Å)
Magnesite		
Oh <i>et al.</i> (1973)	2.105(1)	1.283(1)
Markgraf and Reeder (1985)	2.1018(4)	1.288(1)
This study (600°C series)	2.096(3)	1.297(4)
This study (800°C series)	2.098(8)	1.2932(17)
Otavite		
Borodin <i>et al.</i> (1979)	2.288(2)	1.291(1)
Bromiley (2002) reflection	2.38(3)	1.116(5)
Bromiley (2002) transmission	2.28(2)	1.298(4)
Study	<M-O> bond length (Å)	<C-O> bond length (Å)
This study (600°C series)	2.328(3)	1.211(5)
This study (800°C series)	2.322(3)	1.222(5)

The values obtained for magnesite from this study show reasonable agreement with previously published data [Oh *et al.*, 1973; Markgraf and Reeder, 1985], although the Rietveld refinements from the X-ray powder diffraction study tend to underestimate the magnesium-oxygen bond length, and overestimate the carbon-oxygen bond length. The poor agreement shown for the otavite end-member between different results is, as expected, due to difference in atomic position (Section 5.2.2).

5.3 The Order Parameter and the Order-Disorder Phase Transition

The degree of order for samples with $R\bar{3}$ symmetry, which lie in the cadmium dolomite stability field at intermediate compositions, were ascertained from cation site occupancies in Section 3.2.4. The maximum degree of order obtained was ~34%, for the sample synthesised at 500°C. In previous studies [Goldsmith, 1972; Capobianco *et al.*, 1987], the degree of order was calculated for samples with $R\bar{3}$ symmetry from a sample of ordered cadmium dolomite, which was assumed to be fully ordered. Goldsmith (1972) determined the degree of order from a powder camera film, comparing the intensity of the lines by eye. The exact degree of order was therefore not determined quantitatively and the assumption was made that the sample with the most intense reflections due to ordering was completely ordered. Capobianco *et al.* (1987) also used a powder camera. Again, the degree of order was ascertained by comparison of the intensity of different peaks. This was done by obtaining the average areas from three scans for given peaks. The intensity ratios were then compared in order to ascertain the degree of order. The assumption was therefore made that the sample with the highest degree of order was a fully ordered sample.

To my knowledge, the results presented in this study are the first assessing the “real” degree of order from synthesised samples. Furthermore, it would appear that a fully ordered cadmium dolomite has not been synthesised to date. In fact, runs performed by Goldsmith (1972) were at 10kbar and run durations varied between 0.5-4 hours, significantly shorter than the equilibrium run time established for this study (Figure 3.18). Capobianco *et al.* (1987) synthesised samples initially in hydrothermal apparatus at 1kbar for 4 days. Bromiley (2002) attempted to use this method of synthesis but noted that not only did samples show limited ordering, but the long run duration at such low pressure allowed for dissociation of the carbonate materials and run products contained significant amounts of brucite or monteponite, even when a CO₂ source was added to the capsule. Samples synthesised by Capobianco *et al.* (1987) were then further annealed at temperatures in the range 600-850°C to look at the effect of temperature on ordering. The annealing experiments ranged in duration between 1.5-3 hours, with only one experiment

being run for 168 hours. Results obtained in this study suggest that the shorter experiments might not have been at equilibrium.

5.3.1 The Phase Transition

As already discussed at the end of Section 5.1, the temperature and type of order-disorder phase transition in cadmium dolomite has been determined experimentally by Goldsmith (1972) and Capobianco *et al.* (1987), and using modelling techniques by Burton (1987), Capobianco *et al.* (1987) and Burton and Van de Walle (2003). The temperature at which the cadmium dolomite, having $R\bar{3}$ symmetry, undergoes a disordering phase transformation to the calcite-like structure, having $R\bar{3}c$ symmetry, differs greatly between studies. Results from this study show that samples synthesised at 600°C have some degree of order, at 650°C the degree of order has decreased and at 700°C the disordering process appears to be complete, with samples synthesised at 700°C and a composition of $\text{Mg}_{0.5}\text{Cd}_{0.5}\text{CO}_3$ being refined for the $R\bar{3}c$ structure. Critical temperatures, T_c , for the $R\bar{3} \rightarrow R\bar{3}c$ phase transition for all the studies mentioned above are summarised in Table 5.5. Note that the temperatures given are only approximate.

Table 5.5 Approximate critical temperatures, T_c , for the $R\bar{3} \rightarrow R\bar{3}c$ phase transition in the magnesite – otavite system for samples of composition $Mg_{0.5}Cd_{0.5}CO_3$.

Study	T_c
Goldsmith (1972) Experimental	825°C
Burton (1987) Tetrahedron Approximation in the Cluster Variation Method	800°C
Capobianco <i>et al.</i> (1987) Experimental	850°C
Capobianco <i>et al.</i> (1987) Tetrahedron Approximation in the Cluster Variation Method	800°C
Capobianco <i>et al.</i> (1987) Point Approximation Model 1	950°C
Capobianco <i>et al.</i> (1987) Point Approximation Model 2	975°C
Burton and Van de Walle (2002) Planewave pseudopotential calculations, based on first-principles calculations.	820°C
This study	718°C

Although it may be possible to explain the discrepancies between T_c obtained using modelling techniques with the experimental data presented for this study, due to the fact that modelling techniques tend to overestimate transition temperatures, it is not clear at present, why there are discrepancies between experimental results.

The consistency of the data from this study is particularly visible in Figure 5.2 where the square of the order parameter, Q , as a function of the intensity ratios, obtained from the X-ray powder diffraction patterns, are compared for samples of composition $Mg_{0.5}Cd_{0.5}CO_3$. Despite different values of T_c between studies, the results obtained from this study are consistent with an $R\bar{3} \rightarrow R\bar{3}c$ phase transition that is second order in character (Figure 5.3), in accordance with previous work.

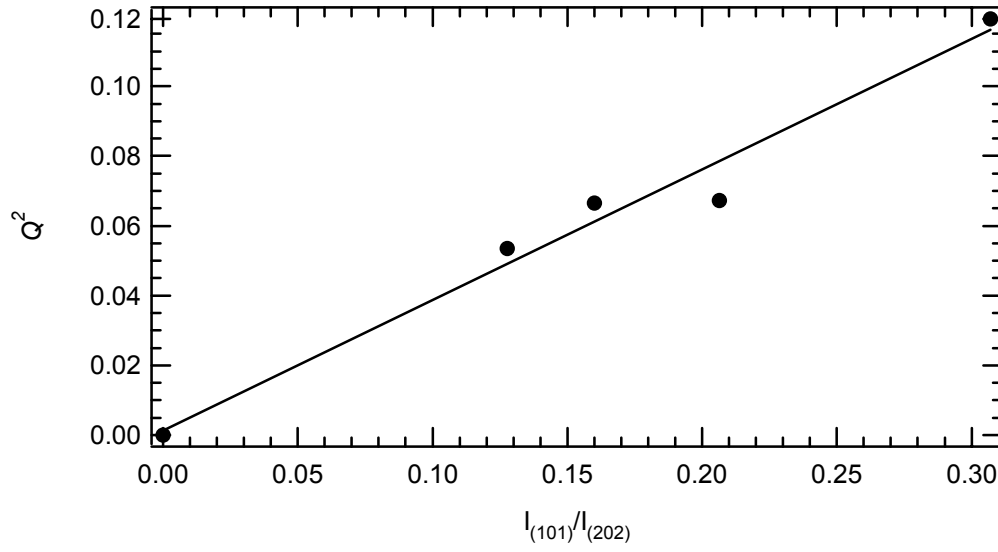


Figure 5.2: The order parameter, Q , as a function of intensity ratio for samples of composition $\text{Mg}_{0.5}\text{Cd}_{0.5}\text{CO}_3$, which are at equilibrium. The solid line is a linear fit through the intensity ratio data, given by, $a = 0$, $b = 0.37411$.

5.4 Macroscopic versus Microscopic Behaviour

As discussed in Section 4.4, the autocorrelation analysis in the spectral region $800\text{-}900\text{cm}^{-1}$, due to out-of-plane bending of the carbonate group, shows a clear effect of order at intermediate compositions. This can be related to results obtained from Rietveld refinements of the X-ray powder diffraction patterns. In the lower symmetry $R\bar{3}$ phase the carbon atom is free to move in the z direction, which in turn allows a reduction in the oxygen-carbon-oxygen bond angle (constrained by symmetry to 120° in samples with $R\bar{3}c$ symmetry), so resulting in a non-planar carbonate group and an oxygen-carbon-oxygen bond angle that changes as a function of degree of order (Figure 5.3). Beran and Zemann (1977) observed the same phenomenon for dolomite and Zemann (1981) noted that for some carbonates the deviation could be as much as 11° . Given the decrease in Δcorr values with increasing degree of order in the spectral region $800\text{-}900\text{cm}^{-1}$, it appears that the environments surrounding the carbonate groups become more homogeneous, in other words, the carbonate groups “see” the same environment with increasing order.

The local order parameter, q , as defined in Section 4.4, can be compared with the long-range order-parameter, Q , calculated from cation site occupancies (Table 3.5). Figure 5.4 shows the order-parameter, Q , as a function of the local order parameter, q .

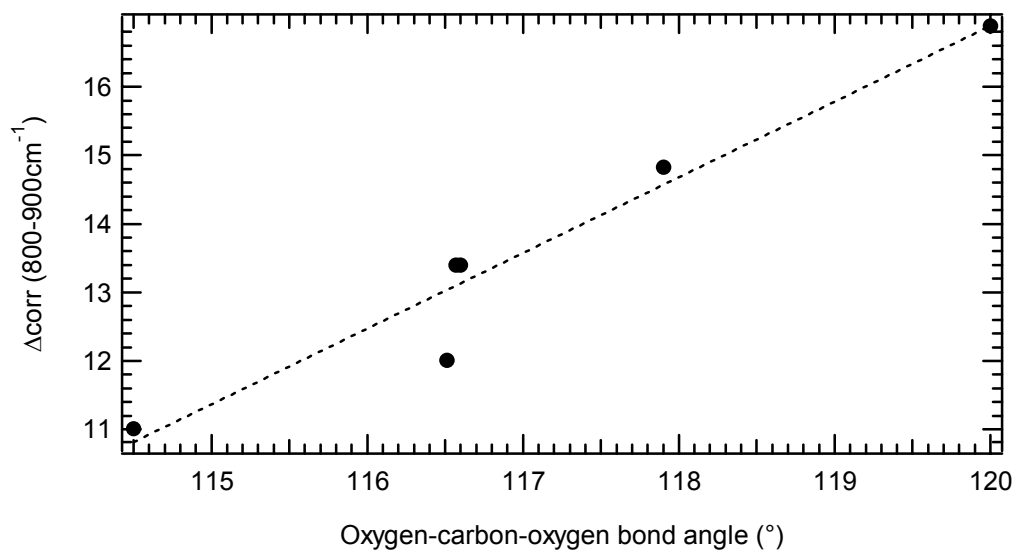


Figure 5.3: $\Delta_{\text{corr}} (800-900\text{cm}^{-1})$ as a function of oxygen-carbon-oxygen bond angle for samples of composition $\text{Mg}_{0.5}\text{Cd}_{0.5}\text{CO}_3$. The dashed line shows a linear fit through the data.

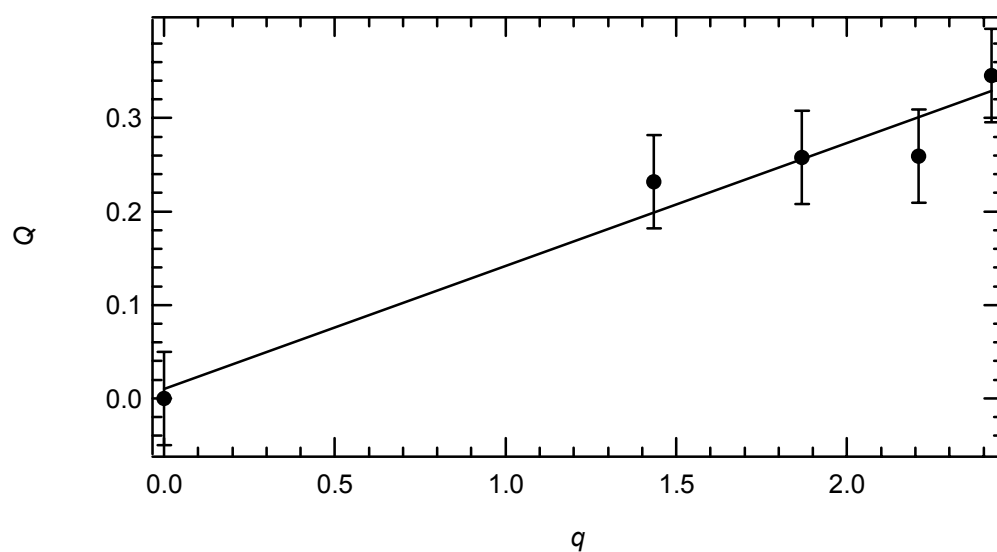


Figure 5.4: The order-parameter, Q , as a function of the local order parameter, q , calculated from the Δ_{corr} results in the spectral region $800-900\text{cm}^{-1}$. The dashed line shows a linear fit through the data, given by $a = 0$, $b = 0.066504$.

The scatter of data in Figure 5.4 is mainly due to the uncertainties from the cation site occupancies determined from Rietveld refinements. It appears, however, that the ordering process is the same at both length scales sampled using X-ray diffraction and IR spectroscopy. The calculation of the local order parameter is based on the assumption that at 800°C samples are completely disordered, also on a local scale. This is consistent with the Δcorr results presented in Figure 4.15, where the 800°C series follow a linear trend as a function of composition, suggesting that the carbonate groups are in a homogeneous environment. In order to ascertain the presence of short-range order, the intensity ratios calculated from reflections of X-ray powder diffraction patterns are compared directly with the Δcorr values for ordered samples in the spectral region 800-900 cm^{-1} (Figure 5.5). The results can be interpreted in two different ways hence two linear fits shown in Figure 5.5. The solid line is a linear fit through all the data points, and implies that the $R\bar{3} \rightarrow R\bar{3}c$ phase transition follows the same mechanism on both macroscopic and local scales, as seen in Figure 5.4. The dashed line shows a linear fit through the 500°C sample and the 600°C samples synthesised for different run durations. The difference between the Δcorr value at the intercept value for the dashed line with $I_{(101)}/I_{(202)}$ equal to zero and the Δcorr value for the sample synthesised at 800°C, can be interpreted as the degree of short-range order present in samples of intermediate composition.

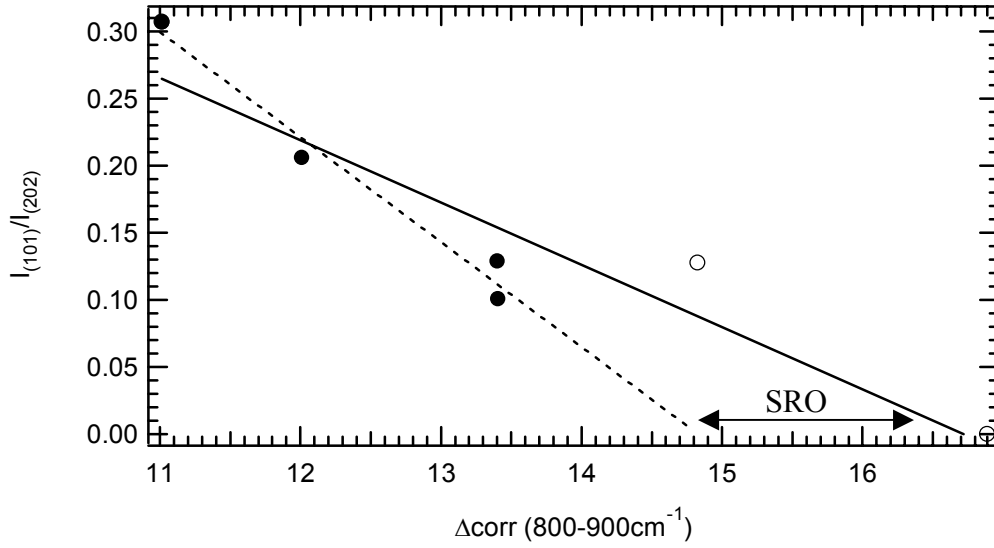


Figure 5.5: Intensity ratio as a function of Δcorr for the spectral region $800\text{-}900\text{cm}^{-1}$. The dashed line shows a linear fit through samples synthesised at 500 and 600°C (closed circles), with $R\bar{3}$ symmetry, given by, $a = 0.55065$, $b = -0.031529$. The solid black line shows a linear fit through all the data (open and closed circles), given by, $a = 1.1594$, $b = -0.078166$. The difference between the Δcorr values for the two linear fits, when the intensity ratio is zero can be interpreted as being due to short-range order. SRO = short-range order.

It has previously been shown that the widths of IR bands scale with the square of the order parameter, Q [Boffa Ballaran and Carpenter, 2003]. From Landau theory it is also known that the excess enthalpy due to a phase transition can be represented by a series expansion (of the form $\Delta H = AQ^2 + BQ^4 + CQ^6 + \dots$). Therefore, unless high values of Q are considered, it may be approximated by $\Delta H \propto Q^2$. Therefore, it is expected that a correlation exists between Δcorr values from IR spectra and ΔH values obtained from calorimetry, due to their mutual dependence on Q^2 . Capobianco *et al.* (1987) published enthalpies of disordering (ΔH_{dis}) obtained from solution calorimetric data. These enthalpies were calculated with respect to their most ordered sample. In order to compare Δcorr results with ΔH_{dis} , the difference was calculated between the Δcorr values for samples of composition $\text{Mg}_{0.5}\text{Cd}_{0.5}\text{CO}_3$ with different degrees of order, with that of the

most ordered sample (synthesised at 500°C for 96 hours) from the spectral region 800-900 cm^{-1} . This parameter, denoted $\Delta\text{corr}^{\text{dis}}$, and the enthalpy of mixing data from Capobianco *et al.* (1987) are shown in Figure 5.6. The linear correlation between ΔH_{dis} and $\Delta\text{corr}^{\text{dis}}$ is as expected for a phase transition where $\Delta H \propto Q^2$.

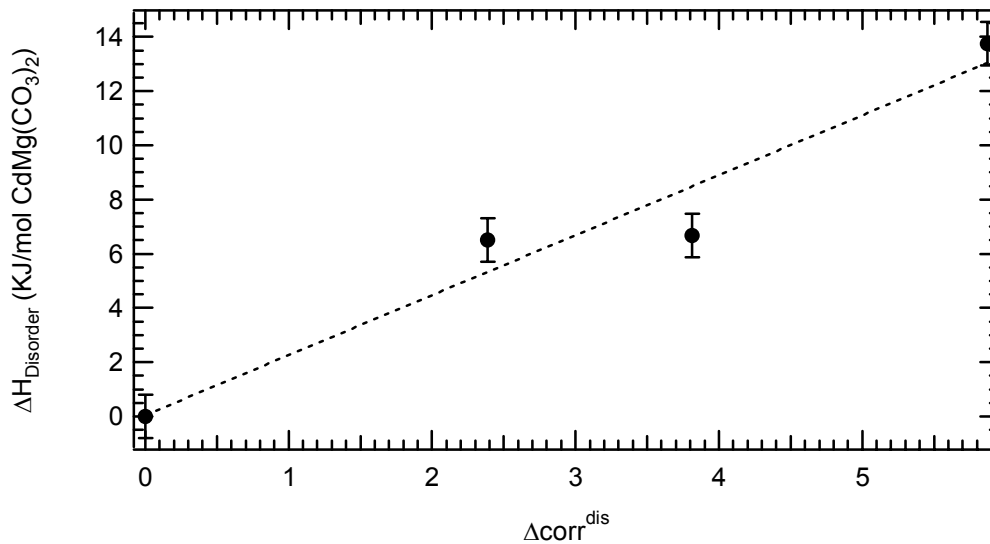


Figure 5.6: The enthalpy of disordering (ΔH_{dis}) from Capobianco *et al.* (1987) as a function of $\Delta\text{corr}^{\text{dis}}$. The dashed line shows a linear fit through the data, given by, $a = 0.060329$, $b = 2.2114$. Error bars taken from Capobianco *et al.* (1987).

Although the Δcorr values for the highest frequency region (1000-2000 cm^{-1}) (Figure 4.15) only show a very small effect of ordering, band positions in this spectral region show a shift, not only as a function of composition, but also as a function of order (Figure 4.9c). It is clearly visible that samples with $R\bar{3}$ symmetry have a higher phonon mode frequency than those with $R\bar{3}c$ symmetry. As discussed in Section 4.3, the phonon mode in the spectral region 1000-2000 cm^{-1} is due to doubly degenerate asymmetric stretching of the carbonate group. It is suggested that as the carbonate group becomes non-planar, due to the carbon moving out of plane with respect to the oxygens (Table 3.3 and Figure 3.12), the energy required for asymmetric stretching of the carbonate group increases, so causing a shift of the vibrational band to higher frequencies.

5.5 Comparison of Mixing and Ordering Behaviour of Carbonates and Silicates

The difference between the autocorrelation results obtained from this study with those of previous autocorrelation studies on silicate systems is of great interest as it gives information relating to the local strain associated with cation substitution and order-disorder phase transitions in different mineral structures.

The autocorrelation results presented in Section 4.4 show different behaviour depending on the frequency range analysed. The same was found for the jadeite-diopside system [Boffa Ballaran *et al.*, 1998] (Section 1.5.1. and Figure 1.8). Substitution of cations in the pyroxene structure is accommodated by a rigid unit type mechanism, which involves out-of-plane tilting of relatively unmodified tetrahedra. The pattern of strain heterogeneity developed within the tetrahedral chains may, therefore, be different from the pattern of distortions shown by larger units in the structure. At the tetrahedral length scale it appears that substitution of calcium and magnesium into the jadeite structure involves different local structural changes from substitution of sodium and aluminium into the diopside structure, but the tetrahedral response depends, only slightly, on the degree of order. In the case of carbonate materials, the carbonate groups also behave like rigid units. The major difference with respect to the pyroxenes, however, is that carbonates are very sensitive to the local (on the order of a few Å) degree of order.

At the lowest frequencies exactly the opposite occurs. Although the pattern of local heterogeneities due to cation substitution is similar for both systems, such heterogeneities seem to be reduced by cation ordering in omphacites, whereas no effect of order is visible on the line broadening of IR spectra of carbonates. It appears, therefore, that at the length scale of a few unit cells the carbonate structure is more elastic with respect to the omphacite structure in accommodating cations of different sizes. Another major difference at low frequencies is seen by the modal behaviour of the two systems. The magnesite – otavite solid solution shows two-mode- behaviour in contrast to the jadeite – diopside solid solution, which shows one-mode behaviour [Boffa Ballaran *et al.*, 1998]. This difference is most likely due to the large difference in atomic weight

between magnesium and cadmium with respect to the difference between calcium and sodium.

5.6 The Magnesite – Otavite System as an Analogue to the Magnesite – Dolomite -Calcite System

The magnesite – otavite system was investigated as a possible low temperature analogue to the geologically important magnesite – dolomite – calcite system. As discussed in Section 1.2, synthesis of $R\bar{3}c$ symmetry dolomite is difficult as a slow quench rate means that reversion to $R\bar{3}$ symmetry dolomite occurs. Even a small degree of reversion to $R\bar{3}$ symmetry on quench could have a very large effect on X-ray and IR results. The magnesite – otavite system allows synthesis of a continuous solid solution at temperatures of 800°C, so eliminating the problems of quench rate associated with the magnesite – calcite system. Comparison of the phase diagram for magnesite – calcite (Figure 1.1) with those mapped out by Goldsmith (1972), Capobianco *et al.* (1987) and Burton and Van de Walle (2003) (Figure 5.1) shows that the two systems exhibit the same topology but, as expected, the $R\bar{3} \rightarrow R\bar{3}c$ phase transition occurs at significantly lower temperatures in the magnesite – otavite system. As discussed in Section 5.1, the main aim of this study was not to map the phase diagram of magnesite – otavite solid solution, so no work was done to constrain phase boundaries. However, work carried out for this study produced tentative phase boundaries, which are shown in Figure 5.1. The data from this study is compared with the phase diagram for the magnesite – calcite solid solution in Figure 5.9. The dashed grey lines show possible phase boundaries as determined from the results of this study. The black arrow shows the equivalent conditions of synthesis for the 800°C series in the magnesite – calcite solid solution. It shows that for a continuous solid solution in the magnesite – calcite solid solution samples, analogous to those synthesised in this study, would have to be synthesised at 1450°C. The grey arrow shows the equivalent conditions of synthesis for 600°C series of samples (900°C for the magnesite – calcite solid solution).

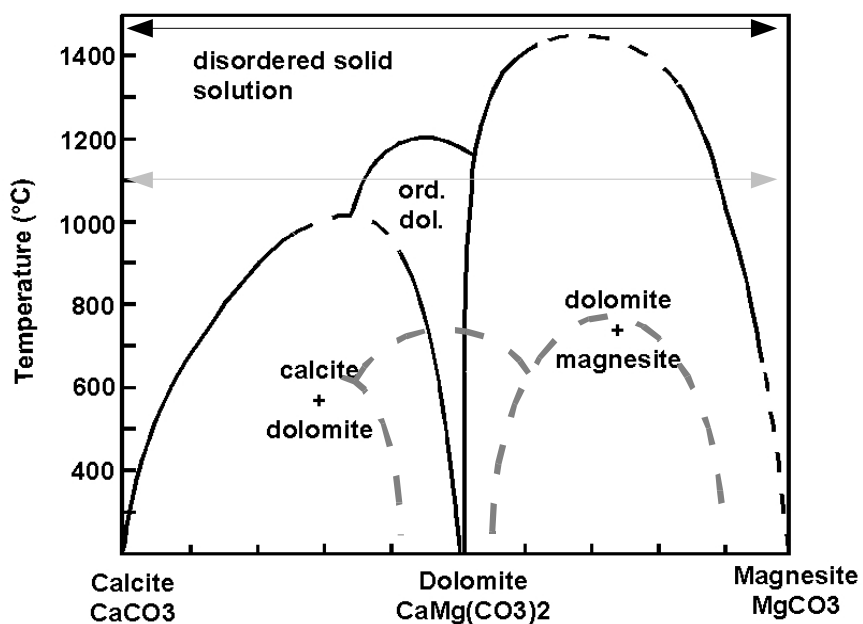


Figure 5.9: Phase diagram for the magnesite – dolomite – calcite solid solution compared with that of the magnesite – cadmium dolomite – otavite solid solution. Black lines are phase boundaries for the magnesite - calcite system. Grey dashed lines are tentative phase boundaries determined from the experimental results of this study. The black arrow shows the equivalent temperature for synthesis for the 800°C series from this study, the grey arrow shows the same, but for the 600°C series.

The results presented in the previous chapters are consistent with an asymmetric dolomite stability field about the $\text{Mg}_{0.5}\text{Ca}_{0.5}\text{CO}_3$ composition, as reported in Figure 5.9, and with a second order $R\bar{3} \rightarrow R\bar{3}c$ phase transformation.

Given the larger difference in atomic size between calcium and magnesium as opposed to cadmium and magnesium, it may be expected that the pattern of local heterogeneities obtained from low frequency IR spectra would show a larger deviation from linearity than shown by the magnesite – otavite system. However, due to the smaller difference in atomic weight between magnesium and calcium, than magnesium and cadmium, it may be that the magnesite – calcite solid solution shows one-mode behaviour at low frequencies, compared to the two-mode behaviour shown by the magnesite – otavite solid solution.

The autocorrelation results obtained from this study suggest that the $R\bar{3}c \rightarrow R\bar{3}$ phase transition is not driven by a strain reduction mechanism, but is controlled by another mechanism, which has not been established during this study.

References

Adler, H.H. and Kerr, P.F. (1963) **Infrared spectra, symmetry and structural relations of some carbonate minerals**, *American Mineralogist*, vol. 48, pp839-853.

Althoff, P.L. (1977) **Structural refinements of dolomite and a magnesian calcite and implications for dolomite formation in the marine environment**, *American Mineralogist*, vol. 62, pp772-783,

Bebout, G.E. (1995) **The impact of subduction-zone metamorphism on mantle-ocean chemical cycling**, *Chemical Geology*, vol. 126, pp191-218.

Beran, A. and Zemmann, J. (1977) **Refinement and comparison of the crystal structures of a dolomite and of an Fe-rich ankerite**, *Tschermaks Mineralogische und Petrographische Mitteilungen*, vol. 24, pp279-286.

Boffa Ballara, T., Carpenter, M.A., Chiara Domeneghetti, M. and Tazzoli, V. (1998) **Structural mechanisms of solid solution and cation ordering in augite-jadeite pyroxenes: I. A macroscopic perspective**, *American Mineralogist*, vol.83, pp419-433.

Boffa Ballaran, T., Carpenter, M.A., Domeneghetti, M.C., Salje, E.K.H. and Tazzoli, V. (1998) **Structural mechanisms of solid solution and cation ordering in augite-jadeite pyroxenes: II. A microscopic perspective**, *American Mineralogist*, vol. 83, pp434-443.

Boffa Ballaran, T. Carpenter, M.A., Geiger, C.A. and Koziol, A.M. (1999) **Local structural heterogeneity in garnet solid solutions**, *Physics and Chemistry of Minerals*, vol. 26, pp554-569.

Boffa Ballaran, T., Carpenter, M.A. and Ross, N.L. (2001) **Infrared powder-absorption spectroscopy of Ca-free P2₁/c clinopyroxenes**, *Mineralogical Magazine*, vol. 65(3), pp339-350.

Boffa Ballaran, T., Carpenter, M.A. and Domeneghetti, M-C. (2001) **Phase transition and mixing behaviour of the cummingtonite-grunerite solid solution**, *Physics and Chemistry of Minerals*, vol. 28, pp87-101.

Boffa Ballaran, T. and Carpenter, M.A. (2003) **Line broadening and enthalpy: some empirical calibrations fo solid solution behaviour from IR spectra**, *Phase Transitions*, vol. 76, pp137-154.

Borodin, V.L., Lyntin, V.I., Ilyukhin, V.V. and Belov, N.V. (1979) **Isomorphous calcite – otavite series**, *Soviet Physics*, vol. 24, pp226-227.

- Boyd, F.R. and England, J.L. (1960) **Apparatus for phase-equilibria measurements at pressures up to 50 kilobars and temperatures up to 1750°C**, *Journal of Geophysical Research*, vol. 65, pp741-748.
- Bradley, W.F., Burst, J.F. and Graf, D.I. (1953) **Crystal chemistry and differential thermal effects of dolomite**, *American Mineralogist*, vol. 38, pp207.
- Bratkovsky, A.M., Marais, S.C., Heine, V. and Saljie, E.K.H. (1984) **The theory of fluctuations and texture embryos in structural phase transitions mediated by strain**, *Journal of Physics: Condensed Matter*, vol. 6, pp3679-3696.
- Bromiley, F.A. (2002) **Mixing behaviour in the Magnesite – Otavite solid solution** Mphil. Thesis, UMIST.
- Burton, B. and Kikuchi, R. (1984) **Thermodynamic analysis of the system $\text{CaCO}_3\text{-MgCO}_3$ in the tetrahedron approximation of the cluster variation method**, *American Mineralogist*, vol. 69, pp165-175.
- Burton, B. (1987) **Theoretical analysis of cation ordering in the binary rhombohedral carbonate systems**, *American Mineralogist*, vol. 72, pp329-336.
- Burton, B. and Van de Walle, A. (2003) **First-principles-based calculations of the $\text{CaCO}_3\text{-MgCO}_3$ and $\text{CdCO}_3\text{-MgCO}_3$ subsolidus phase diagrams**, *Physics and Chemistry of Minerals*, vol. 30, pp88-97.
- Byrnes, A.P. and Wyllie, P.J. (1981) **Subsolidus and melting relations for the join $\text{CaCO}_3\text{ – MgCO}_3$ at 10kbar**, *Geochimica et Cosmochimica Acta*, vol. 45, pp321-328.
- Capobianco, C., Burton, B.P., Davidson, P.M. and Navrotsky, A. (1987) **Structural and calorimetric studies of order-disorder in $\text{CdMg}(\text{CO}_3)_2$** , *Journal of Solid State Chemistry*, vol. 71, pp214-223.
- Carpenter, M.A., Domeneghetti, M-C and Tazzoli, V. (1990) **Application of Landau theory to cation ordering in omphacite. I: Equilibrium behaviour**, *European Journal of Mineralogy*, vol. 2, pp7-18.
- Carpenter, M.A. (1992) **Equilibrium thermodynamics of Al/Si ordering in anorthite**, *Physics and Chemistry of Minerals*, vol. 19, pp1-24.
- Carpenter, M.A. and Saljie, E.K.H. (1998) **Elastic anomalies in minerals due to structural phase transitions**, *European Journal of Mineralogy*, vol. 10, pp693-812.
- Carpenter, M.A., Saljie, E.K.H. and Graeme-Barber, A. (1998) **Spontaneous strain as a determinant of thermodynamic properties for phase transitions in minerals**, *European Journal of Mineralogy*, vol. 10, pp621-691.

Carpenter, M.A., Boffa-Ballaran, T and Atkinson, A.J. (1999) **Microscopic strain, local structural heterogeneity and the energetics of silicate solid solutions**, *Phase Transitions*, vol. 69, pp95-109.

Carpenter, M.A. and Boffa-Ballaran (2001) **The influence of elastic strain heterogeneities in silicate solid solutions**, *EMU Notes in Mineralogy*, vol.3 chapter 7, pp155-178.

Chai, L. and Navrotsky, A. (1993) **Thermochemistry of carbonate-pyroxene equilibria**, *Contributions to Mineralogy and Petrology*, vol. 114, pp139-147.

Chang, I.F. and Mitra, S.S. (1968) **Application of a modified random-element-isodisplacement model to long-wavelength optic phonons of mixed crystals**, *Physical Review*, vol. 172 no.3, pp924-933.

Dove, M.T. and Powell, B.M. (1989) **Neutron diffraction study of the tricritical orientational order/disorder phase transition in calcite at 1260K**, *Physics and Chemistry of Minerals*, vol. 16, pp503-507.

Dove, M.T. (1997) **Theory of displacive phase transitions in minerals**, *American Mineralogist*, vol. 82, pp213-244.

Dove, M.T. (2001) **Computer simulations of solid solutions**. In Geiger, C.A. (ed.): *Solid solutions in silicate and oxide systems /EMU Notes Mineralogy*, vol. 3. Budapest: Eötvös University Press, 225-250.

Edmond, J.M. and Huh, Y. (2003) **Non-steady state carbonate recycling and implications for the evolution of atmospheric P_{CO_2}** , *Earth and Planetary Science Letters*, vol. 216, pp125-139.

Farmer, V.C. (1974) **The infrared spectra of minerals**, *Mineralogical Society*.

Frost, D.J. and Wood, B.J. (1997) **Experimental measurements of the properties of the H_2O - CO_2 mixtures at high pressures and temperatures**, *Geochimica et Cosmochimica Acta*, vol. 61 no. 16, pp3301-3309.

Goldsmith, J.R. and Heard, H.C. (1961) **Subsolidus phase relations in the system $CaCO_3$ - $MgCO_3$** , *Journal of Geology*, vol. 69, pp45-74.

Goldsmith, J.R. and Newton, R.C. (1969) **P-T-X relations in the system $CaCO_3$ - $MgCO_3$ at high temperatures and pressures**, *American Journal of Science*, vol. 267-A, pp160-190.

Goldsmith, J.R. (1972) **Cadmium dolomite and the system $CdCO_3$ - $MgCO_3$** , *Journal of Geology*, vol. 80, pp617-626.

- Graf, D.L. and Goldsmith, J.R. (1955) **Dolomite-magnesian calcite relations at elevated temperatures and CO₂ pressures**, *Geochimica et Cosmochimica Acta*, vol. 7, pp109-128.
- Graf, D.L. (1961) **Crystallographic tables for the rhombohedral carbonates**, *American Mineralogist*, vol. 46, pp1283-1316.
- Harker, R.I. and Tuttle, O.F. (1955) **Studies in the system CaO-MgO-CO₂ , part 2, Limits of the solid solution along the binary join CaCO₃-MgCO₃**, *American Journal of Science*, vol. 253, pp274-282.
- Hawthorne, F.C. (1988) **Reviews in Mineralogy: Spectroscopic methods in mineralogy and geology**, *Mineralogical Society of America* , vol.18.
- Hayward, S. and Salje, E.K.H. (1996) **Displacive phase transition in anorthoclase: The “plateau effect” and the effect of T1-T2 ordering on the transition temperature**, *American Mineralogist*, vol. 81, pp1332-1336.
- Haywood, H.M., Eyre, J.M. and Scholes, H. (2001) **Carbon dioxide sequestration as stable carbonate minerals – environmental barriers**, *Environmental Geology*, vol. 41, pp11-16.
- Hofmeister, A.M. and Chopelas, A. (1991) **Vibrational spectroscopy of end-member silicate garnets**, *Physics and Chemistry of Minerals*, vol. 17, pp503-526.
- Hofmeister, A.M., Fagan, T.J., Campbell, K.M. and Schaal, R.B. (1996) **Single-crystal IR spectroscopy of pyrope-almandine garnets with minor amounts of Mn and Ca**, *American Mineralogist*, vol. 81, pp418-428.
- Holl, C.M., Smyth, J.R., Laustsen, H.M.S., Jacobsen, S.D. and Downs, R.T. (2000) **Compression of witherite to 8GPa and the crystal structure of BaCO₃II**, *Physics and Chemistry of Minerals*, vol. 27, pp467-473.
- Irving, A.J. and Wyllie, P.J. (1975) **Subsolidus and melting relationships for calcite, amngesite and the join CaCO₃ – MgCO₃ to 36kb**, *Geochimica et Cosmochimica Acta*, vol. 39, pp 35-53.
- Isshiki, M., Irifune, T., Hirose, K., Ono, S., Ohishi, Y., Watanuki, T., Nishibori, E., Takata, M. and Sakata, M. (2004) **Stability of magnesite and its high-pressure form in the lowermost mantle**, *Nature*, vol. 427, pp60-63
- Jendrzewski, N., Trull, T.W., Pineau, F. and Javoy, M. (1997) **Carbon solubility in Mid-Ocean Ridge basaltic melt at low pressures (250-1950 bar)**, *Chemical Geology*, vol. 138, pp81-92.

Keppeler, H., Wiedenbeck, M. And Shcheka, S.S. (2003) **Carbon solubility in olivine and the mode of carbon storage in the Earth's mantle**, *Nature*, vol. 424, pp 414-416.

Kerrick, D.M. and Connolly, J.A.D. (2001) **Metamorphic devolatilization of subducted oceanic metabasalts: implications for seismicity, arc magmatism and volatile recycling**, *Earth and Planetary Science Letters*, vol. 189, pp19-29.

Koziol, A.M. and Newton, R.C. (1998) **Experimental determination of the reaction: Magnesite + enstatite = forsterite + CO₂ in the ranges 6-25 kbar and 700-1100°C**, *American Mineralogist*, vol. 83, pp213-219.

Lackner, K.S., Butt, D.P. and Wendt, C.H. (1998) **The need for carbon dioxide disposal: a treat and an opportunity**, *Appeared in the Proceedings of the 23rd International Conference on Coal Utilization and Fuel Systems, Clearwater Florida, March 1998*, pp5695-82.

Lackner, K.S., Grimes, P. and Ziok, H-J. (1999) **Carbon dioxide extraction from air: Is it an option?**, *Proceedings of the 24th Annual Technical Conference on Coal Utilization and Fuel Systems, March 8-11 1999, Clearwater Florida*.

Larson, A. and Van Dreele, R.B. (1994) **GSAS General Structure Analysis System**. Los Alamos National Laboratory, New Mexico, USA.

Malcherek, T., Kroll, H., Schleiter, M. And Salje, E.K.H. (1995) **The kinetics of the monoclinic to monoclinic phase transition in BaAl₂Ge₂O₈ feldspar**, *Phase Transitions*, vol. 55, pp199-215.

Markgraf, S.A. and Reeder, R.J. (1985) **High-temperature structure refinements of calcite and magnesite**, *American Mineralogist*, vol. 70, pp.590-600.

Molina, J.F. and Poli, S. (2000) **Carbonate stability and fluid composition in subducted oceanic crust: an experimental study on H₂O-CO₂ – bearing basalts**, *Earth and Planetary Science Letters*, vol. 176, pp295-310.

Newton, R.C. and Wood, B.J. (1980) **Volume behaviour of silicate solid solutions**, *American Mineralogist*, vol. 65, pp733-745.

O'Connor, W.K., Dahlin, D.C., Nilsen, D.N., Rush, G.E., Walters, R.P. and Turner, P.C. (2000) **Carbon dioxide sequestration by direct mineral carbonation: Results from recent studies and current status**, *Albany Research Center, Office of Fossil Energy, US DOE*.

Oh, K.D., Morikawa, H., Iwai, S. and Aoki, H. (1973) **The crystal structure of magnesite**, *American Mineralogist*, vol. 58, pp.1029-1033.

Paquette, J. and Reeder, R.J. (1990) **Single-crystal X-ray structure refinements of two biogenic magnesian calcite crystals**, *American Mineralogist*, vol. 75, pp1151-1158.

Putnis, A (1992) **Introduction to Mineral Sciences**, *Cambridge University Press*, Cambridge, pp275-300.

Reeder, R.J. and Wenk, H.R. (1983) **Structure refinements of some thermally disordered dolomites**, *American Mineralogist*, vol. 68, pp769-776.

Reeder, R.J. (1983) **Crystal Chemistry of the Rhombohedral Carbonates**, *Reviews in Mineralogy : Carbonates: Mineralogy and Chemistry*, *Mineralogical Society of America*, vol. 11, pp1-47.

Reeder, R.J. and Markgraf, S.A. (1986) **High-temperature crystal chemistry of dolomite**, *American Mineralogist*, vol. 71, pp795-804.

Reeder, R.J., Redfern, S.A.T. and Salje, E.K.H. (1988) **Spontaneous strain at the structural phase transition in NaNO_3** , *Physics and Chemistry of Minerals*, vol. 15, pp605-611.

Ross, N.L. and Reeder, R.J. (1992) **High-pressure structural study of dolomite and ankerite**, *American Mineralogist*, vol. 77, pp 412-421.

Salje, E.K.H. (1992) **Hard mode spectroscopy: Experimental studies of structural phase transitions**, *Phase Transitions*, vol. 37, pp83-110.

Salje, E.K.H. and Bismayer, U. (1997) **Hard mode spectroscopy: the concept and applications**, *Phase Transitions*, vol. 63, pp1-75.

Salje, E.K.H., Carpenter, M.A., Malcherek, T. and Boffa-Ballaran, T. (2000) **Autocorrelation analysis of infrared spectra from minerals**, *European Journal of Mineralogy*, vol. 12, pp503-519.

Santillán, J., Williams, Q. and Knittle, E. (2003) **Dolomite II: a high-pressure polymorph of $\text{CaMg}(\text{CO}_3)_2$** , *Geophysical Research Letters*, vol.30 no. 2, pp26-1 – 26-4.

Santillán, J. and Williams, Q. (2004) **A high-pressure infrared and X-ray study of FeCO_3 and MnCO_3 : comparison with $\text{CaMg}(\text{CO}_3)_2$ – dolomite**, *Physics of the Earth and Planetary Interiors*, in press.

Smyth, J.R. and Ahrens, T.J. (1997) **The crystal structure of calcite III**, *Geophysical Research Letter*, Vol.24 No. 13, pp1595-1598.

Steinfink, H. and Sans, F.J. (1959) **Refinement of the crystal structure of dolomite**, *American Mineralogist*, vol. 44, pp 679-682.

Sterner, S.M. and Bodnar, R.J. (1991) **Synthetic fluid inclusions. X: experimental determination of P-V-T-X properties in the CO₂-H₂O system to 6KB and 700°C**, *American Journal of Science*, vol. 291, pp1-54.

Tarantino, S.C., Boffa Ballaran, T., Carpenter, M.A., Domeneghetti, M-C. and Tazzoli, V. **Mixing properties of the enstatite-ferrosilite solid solution: II. A microscopic perspective**, *European Journal of Mineralogy*, vol. 14(3), pp537-547.

Tarantino, S.C., Carpenter, M.A. and Domeneghetti, M-C. (2003) **Strain and local heterogeneity in the forsterite-fayalite solid solution**, *Physics and Chemistry of Minerals*, vol. 30, pp495-502.

Toby, B.H. (2001) **EXPGUI, a graphical user interface for GSAS**, *Journal of Applied Crystallography*, vol. 34, pp210-213.

Walter, K. (2001) **A solution for carbon dioxide overload**, <http://www.llnl.gov/str/Johnson.html>

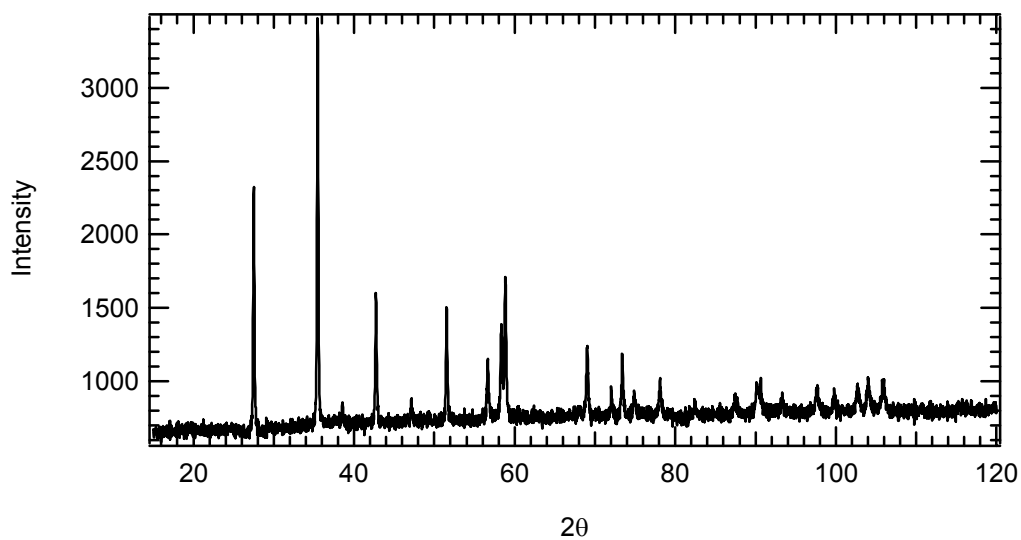
Watson, E.B., Wark, D.A., Price, J.D. and Van Orman, J.A. (2002) **Mapping the thermal structure of solid-media pressure assemblies**, *Contributions to Mineralogy and Petrology*, vol. 142, pp640-652.

White, W.B. (1974) **The carbonate minerals**. Chapter 12 in Farmer, V.C., *The infrared spectra of minerals*, Mineralogical Society. Monograph 4, pp227-284.

Wood, B.J., Holland, T.J.B., Newton, R.C. and Kleppa, O.J. (1980) **Thermochemistry of jadeite-diopside pyroxenes**, *Geochimica et Cosmochimica Acta*, Vol. 44(9), pp1363-1371.

Zemann, J. (1981) **Zur Stereochemie der Karbonate**, *Fortschritt der Mineralogie*, vol. 59, pp95-116.

Appendix 1: X-ray Diffraction Patterns and IR Spectra for Starting Materials



A1.1: X-ray powder diffraction pattern for otavite (CdCO_3) starting material.

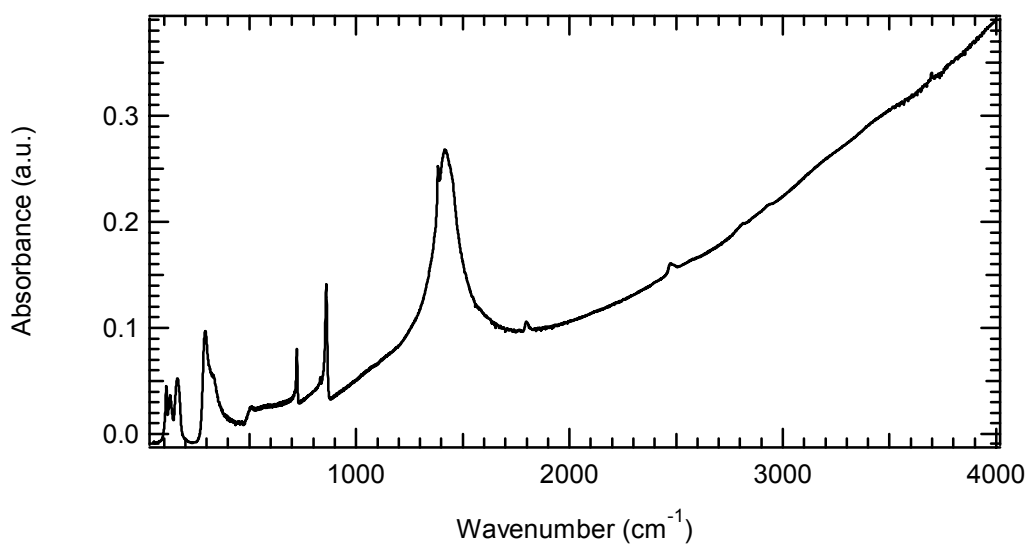
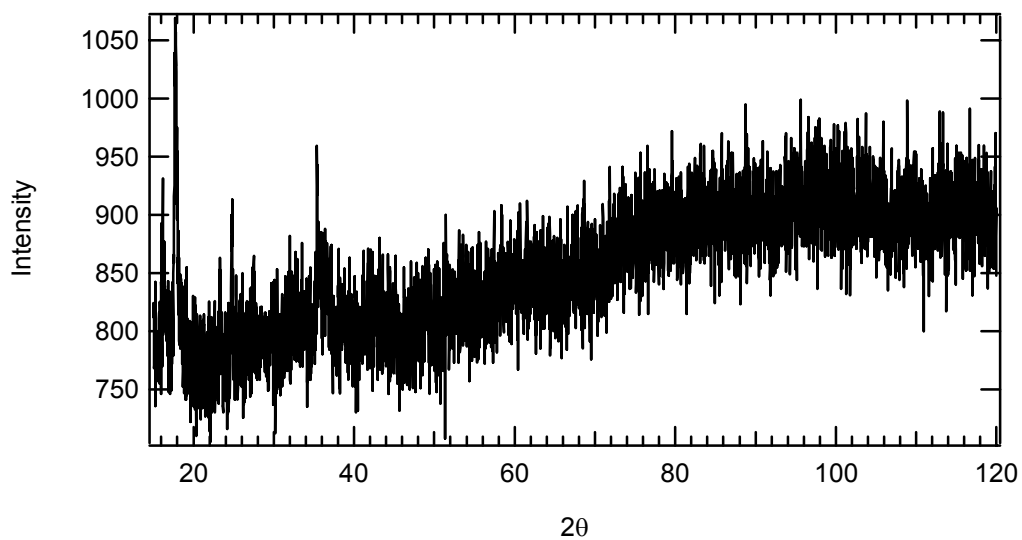
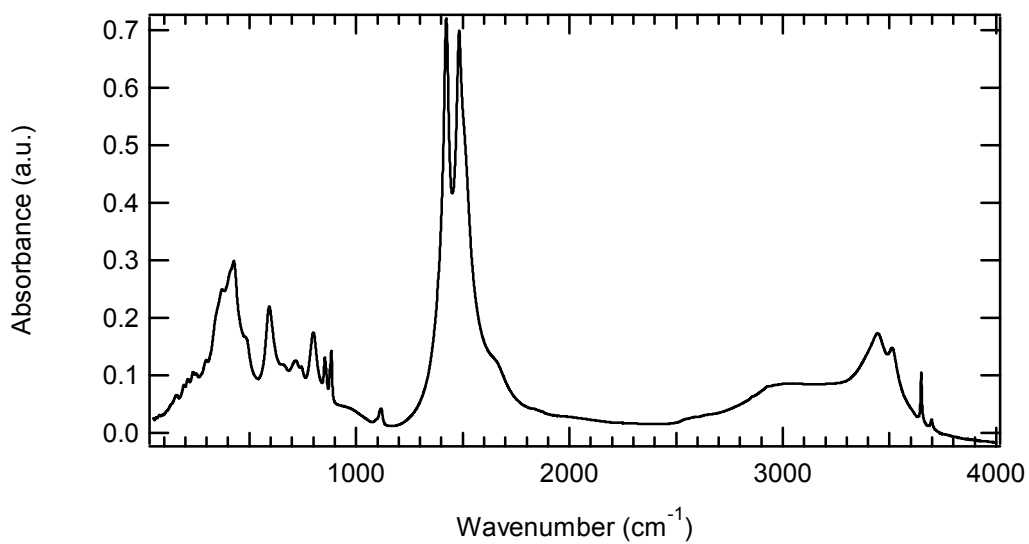


Figure A1.2: Merged powder absorption IR spectrum for otavite (CdCO_3) starting material.



A1.3: X-ray powder diffraction pattern for magnesite (MgCO_3) starting material.



A1.4: Merged powder absorption IR spectrum for magnesite (MgCO_3) starting material.

Note that the high background is due to the poor crystallinity of the starting powders.

Appendix 2: Experiments Performed

SAMPLE	T(°C)	P(kbar)	t(hrs)	Appearance and Comments	XRD
MgCO ₃ (H)	300	1	48	White powder	Mgco3300
MgCO ₃ (H)	600	1	48	White powder	
MgCO ₃ OH + Ag ₂ (H)	600	1	48	White powder	Mgco3ohag600
50(1) (H)	600	1	24	White powder	50(1)
50(2) (H)	850	1	24	Grey/brown	50(2)
50(3) (H)	600	1	72	White powder	50(3)
90(1) 90:10 Cd:Mg (H)	600	1	24	White powder	
90(2) (H)	600	1	24	White with CdO crystals (500µm)	
CdCO ₃ (1) (H)	600	1	24	Black powder	CdCO ₃
90(4) (PC)	600	10	3	White powder	90(4)
90(5) (PC)	600	10	4	Grey powder	90(5)
90(6) (PC)	600	10	3	White powder	90(6)
50(4) (PC)	600	10	3	White powder	50(4)
50(5) (PC)	900	10	3	-	-
50(6) (PC)	900	10	3	-	-
50(7) (PC)	900	10	1	Brown powder	50(7) looks amorphous
50(8) (PC)	900	10	1	Brown powder	
50(9) (PC)	800	10	1	-	-
50(10) (PC)	800	10	1	Grey powder	50(10)
0(1) Mg (PC)	600	10	1	White powder	0(1)
0(2) (PC)	800	10	1	White powder	0(2)
0(3) (PC)	850	10	0.5	White powder	0(3)
0(4) (PC)	850	10	0.5	White powder	0(4)
30(1) (PC) 30:70 Cd:Mg	850	10	1	-	-
30(2) (PC)	600	10	1	Grey powder	30(2)
30(3) (PC)	600	10	3	White powder	30(3)
0(5) (PC)	600	10	3	White powder	0(5)
100(1) (PC)	600	10	3	Grey powder	100(1)
10(1) (PC)	600	10	3	White powder	10(1)
20(1) (PC)	600	10	3	Grey powder	Two_one
40(1) (PC)	600	10	3	Grey powder	Fort_one

SAMPLE	T(°C)	P(kbar)	T(hrs)	Appearance and Comments	XRD
60(1) (PC)	600	10	3	Grey powder	Six_one
70(2) (PC)	600	10	3	White powder	Sev_one
80(1) (PC)	600	10	3	White powder	Eight_on
50h(1) (PC)	900	10	3	Brown powder	50h(1)
40h(1) (PC)	600 - 850	10	3 – 0.6	Brown powder	
40h(2) (PC)	850	20	2	White powder	For_twoh
40h(3) (PC)	850	20	2	White powder	Forh_3
60h(1) (PC)	850	20	2	White powder	Sixh_1
Mg70h (PC)	850	20	3	Grey powder	Mg70h
Mg70h2 (PC)	900	20	3	White powder	Mg70h2
Mg70h3 (PC)	900	20	3	Grey powder	Mg70h3
Mg40h1 (PC)	900	20	3	-	-
Mg40h2 (PC)	900	20	3	Grey powder	Mg40h2
Mg40h3 (PC)	850	20	2		
Mg60h1 (PC)	850	20	2		
Mg70h1 (PC)	850	20	2	Failed	
Mg70h2 (PC)	850	20	2	Failed	
Mg70h3 (PC)	900	20	2	Bad peak shape-redo	Mg70h3
Mg40h1 (PC)	900	20	3	Failed	
Mg40h2 (PC)	900	20	3	Failed	
Mg10h1 (PC)	800	10	1.5	Failed	
Mg90h1 (PC)	800	10	1	Good	Mg90h1
Mg80h1 (PC)	800	10	1	Failed	
Mg60h1 (PC)	800	10	1	Good	Mg60h1
Mg70h4 (PC)	800	10	1	Good	Mg70h4
Mg40h3 (PC)	800	10	1	Good	Mg40h3
Mg30h1 (PC)	800	10	1	Failed – loss of CO ₂	
Mg20h1 (PC)	800	10	1	Good	Mg20h1
Mg90h2 (PC)	800	10	1	Good	Mg90h2
Mg100h1 (PC)	800	10	1	Good	Mg100h1
Mg90h3 (PC)	800	10	1	Good	Mg90h3
Mg100h2 (PC)	800	10	1	Failed-loss of CO ₂	
Mg80h2 (PC)	800	10	1	Good	Mg80h2
Mg100h3 (PC)	800	10	1	Good	Mg100h3
Mg0h1 (PC)	800	10	1	Good	Mg0h1
Mg2011 (PC)	500	10	3	Failed – loss of CO ₂	

SAMPLE	T(°C)	P(kbar)	T(hrs)	Appearance and Comments	XRD
Mg50l1 (PC)	500	10	6	Good	Mg50l1
Mg5071 (PC)	700	10	2	Good but disordered	Mg5071
Mg506N (PC)	600	10	19.5	Good	Mg50N
Mg407 (PC)	700	10	3	Good	Mg407
Mg30l1 (PC)	500	10	48	No gas	Mg30l1
Mg20l1 (PC)	500	10	72	Good	Mg20l1
Mg50l2 (PC)	500	10	72	Failed	
Mg50l3 (PC)	500	10	96	Good	Mg50l3
Mg50h4 (PC)	650	10	120	Good	Mg50h4
Mg5072 (PC)	700	10	24	Good	Mg5072
Mg50(11) (PC)	600	10	96	Good	Mg50l1
Mg40lo (PC)	600	10	19	Good	Mg40lo
Mg60lo (PC)	600	10	19	Good	Mg60lo
Mg55(1) (PC)	600	10	19	? Black powder but gas + ordered	Mg55l
Mg45(1) (PC)	600	10	19	Good, although small amount of gas	Mg45
Mg50sc (PC)	600	10	72	Added lots of silver oxalate as a fluid phase for crystals to grow into, but not successful	Mg50sc
Mg50sc2 (PC)	1000 - 600	10	2 - 72	No silver oxalate. Tried to melt sample then quench. Obvious loss of CO ₂ on opening. Larger crystallites then previously.	Mg50sc2 Mg50sc2a Mg50sc2t
Mg80h3 (PC)	800	10	1	Good, white powder	Mg80h3

SAMPLE	T(°C)	P(kbar)	T(hrs)	Appearance and Comments	XRD
Mg2086 (PC)	800-600	10	1-3	Good	Mg2086
Mg50dis1	-	-	-	Exploded on weld	-
Mg50dis2	-	-	-	Exploded on weld	-
Mg50dis3 (PC)	600	10	0.3	Good. Material from Mg50l3, to disorder	Mg50dis3
Mg50dis4 (PC)	600	10	48	Good. Material from Mg50l3, then Mg50dis3.	Mg50dis4

Appendix 3: IR Powder Absorption Spectra to Establish Optimum Grinding Time

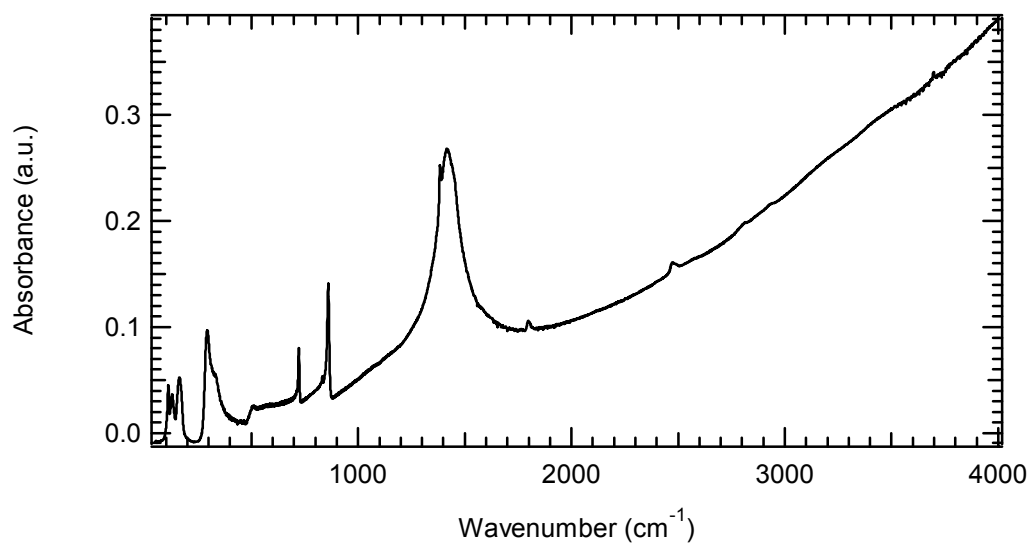


Figure A3.1: Merged powder absorption IR spectrum for otavite (CdCO_3). Hand ground under acetone for 5 minutes.

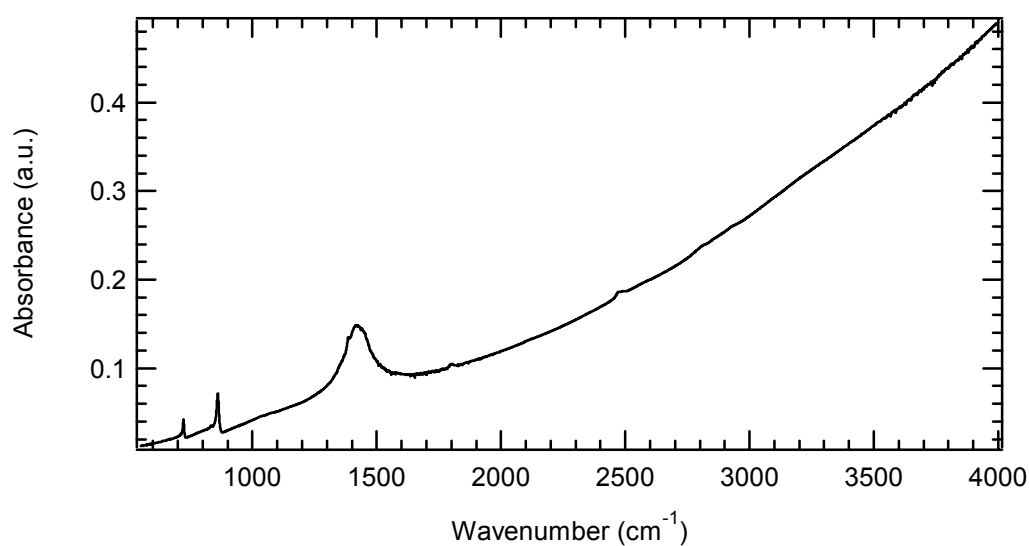


Figure A3.2: Merged powder absorption IR spectrum for otavite (CdCO_3). Hand ground under acetone for 10 minutes.

Appendix 4: X-ray Diffraction Pattern and IR Spectrum for Brucite

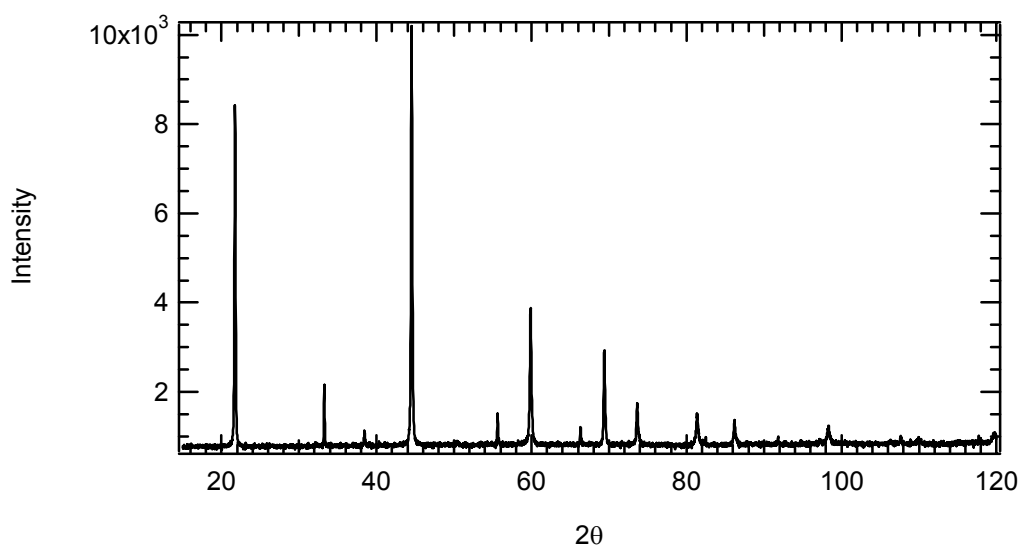


Figure A4.1: X-ray powder diffraction pattern for Brucite $[\text{Mg}(\text{OH})_2]$.

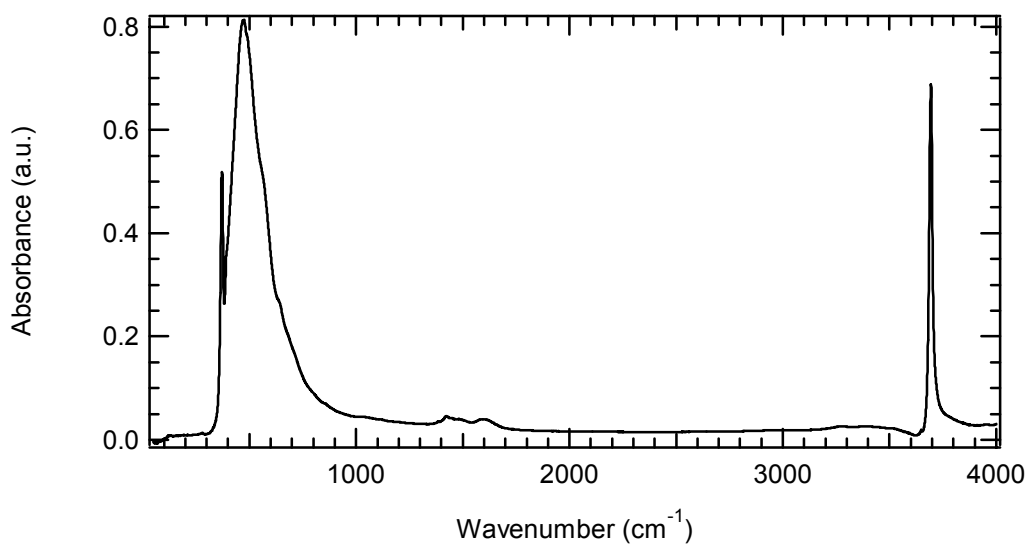


Figure A4.2: Merged powder absorption IR spectrum for brucite $[\text{Mg}(\text{OH})_2]$.

Appendix 5: Rietveld Refinement Patterns

Samples synthesised at 600°C, 1GPa, 3 hours:

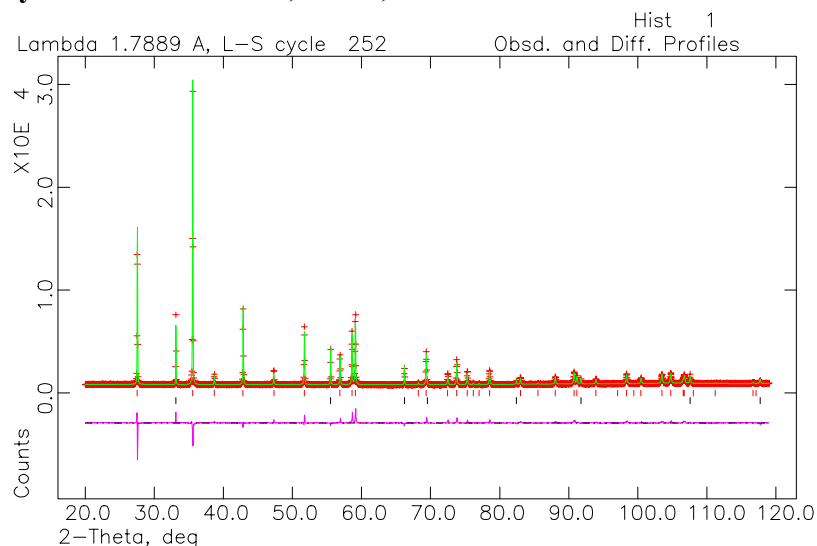


Figure A5.1: Rietveld refinement of the diffraction pattern for $\text{Mg}_{0.1}\text{Cd}_{0.9}\text{CO}_3$ with Si standard. Purple line shows the difference between the calculated and observed intensities. $R^2 = 0.0559$, $\Gamma = 0.1123 \times 10^2$.

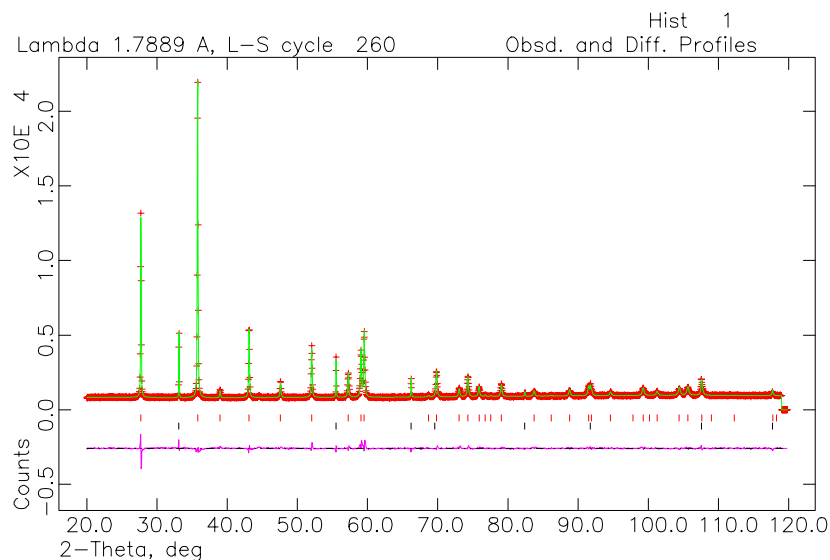


Figure A5.2: Rietveld refinement of the diffraction pattern for $\text{Mg}_{0.2}\text{Cd}_{0.8}\text{CO}_3$ with Si standard. Purple line shows the difference between the calculated and observed intensities. $R^2 = 0.0424$, $\Gamma = 0.2203 \times 10^2$.

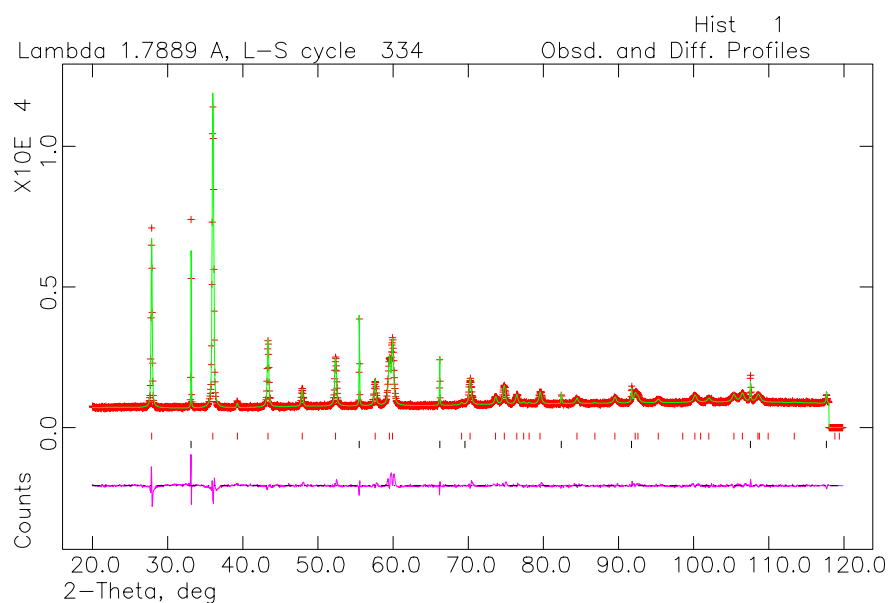


Figure A5.3: Rietveld refinement of the diffraction pattern for $\text{Mg}_{0.3}\text{Cd}_{0.7}\text{CO}_3$ with Si standard. Purple line shows the difference between the calculated and observed intensities. $R^2 = 0.0479$, $\Gamma = 0.3642 \times 10^2$

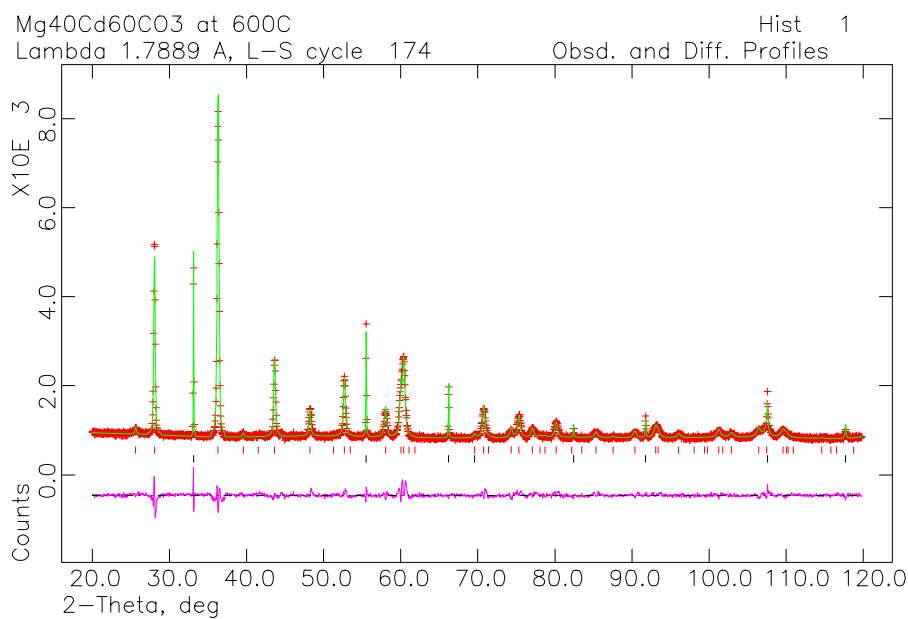


Figure A5.4: Rietveld refinement of the diffraction pattern for $\text{Mg}_{0.4}\text{Cd}_{0.6}\text{CO}_3$ with Si standard. Purple line shows the difference between the calculated and observed intensities. $R^2 = 0.0408$, $\Gamma = 0.4043 \times 10^2$

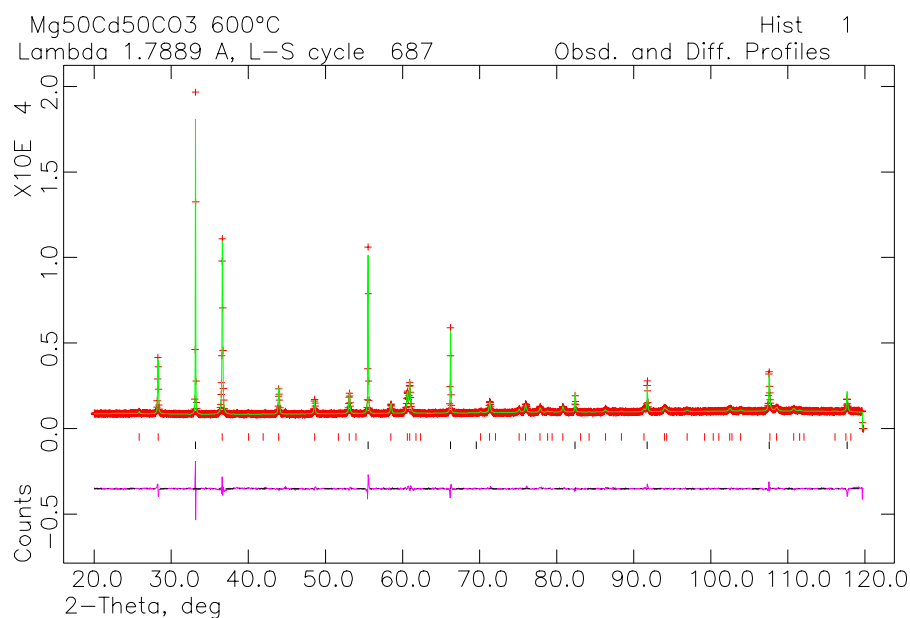


Figure A5.5: Rietveld refinement of the diffraction pattern for $\text{Mg}_{0.5}\text{Cd}_{0.5}\text{CO}_3$ with Si standard. Purple line shows the difference between the calculated and observed intensities. $R^2 = 0.0427$, $\Gamma = 0.2437 \cdot 10^2$

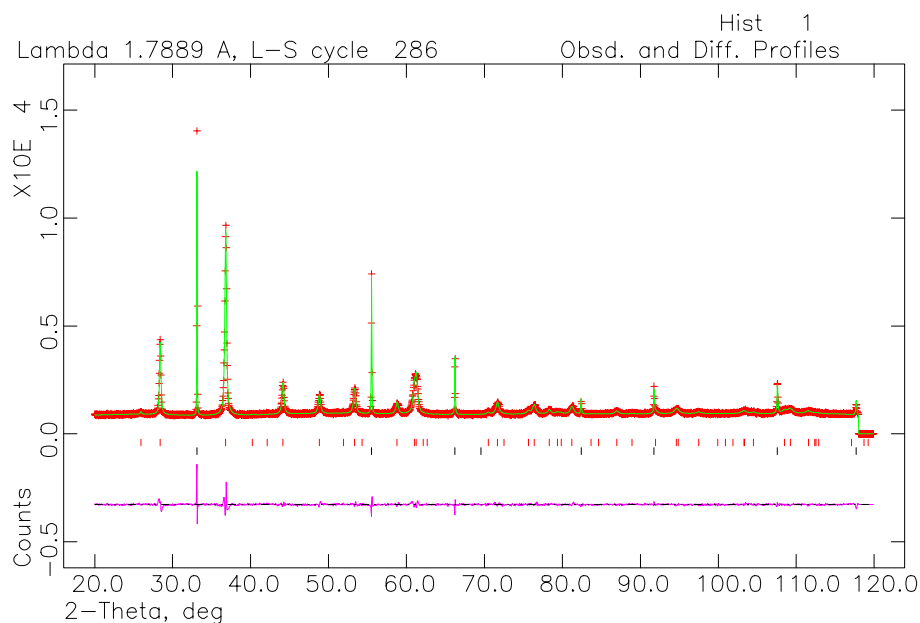


Figure A5.6: Rietveld refinement of the diffraction pattern for $\text{Mg}_{0.6}\text{Cd}_{0.4}\text{CO}_3$ with Si standard. Purple line shows the difference between the calculated and observed intensities. $R^2 = 0.0398$, $\Gamma = 0.5837 \cdot 10^2$

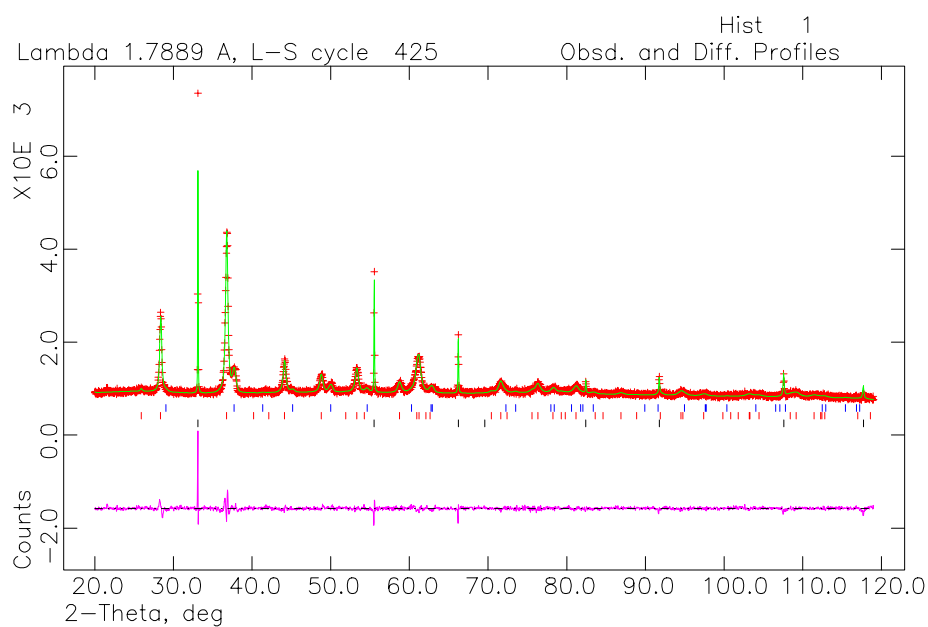


Figure A5.7: Rietveld refinement of the diffraction pattern for $\text{Mg}_{0.7}\text{Cd}_{0.3}\text{CO}_3$ with Si standard. Purple line shows the difference between the calculated and observed intensities. $R^2 = 0.0357$, $\Gamma = 0.8802 \times 10^2$ and 0.5442×10^2

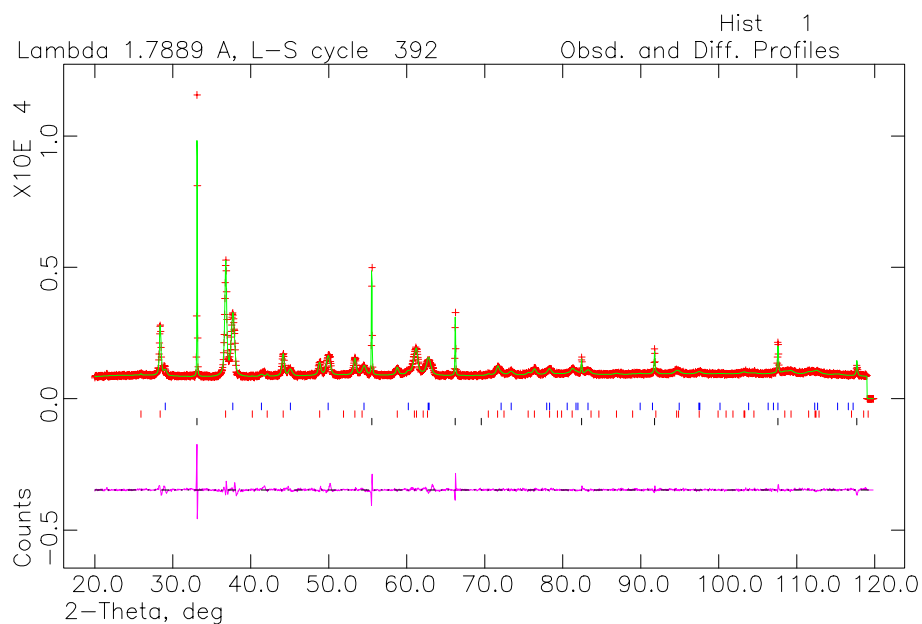


Figure A5.8: Rietveld refinement of the diffraction pattern for $\text{Mg}_{0.8}\text{Cd}_{0.2}\text{CO}_3$ with Si standard. Purple line shows the difference between the calculated and observed intensities. $R^2 = 0.0444$, $\Gamma = 0.6903 \times 10^2$ and 0.6381×10^2

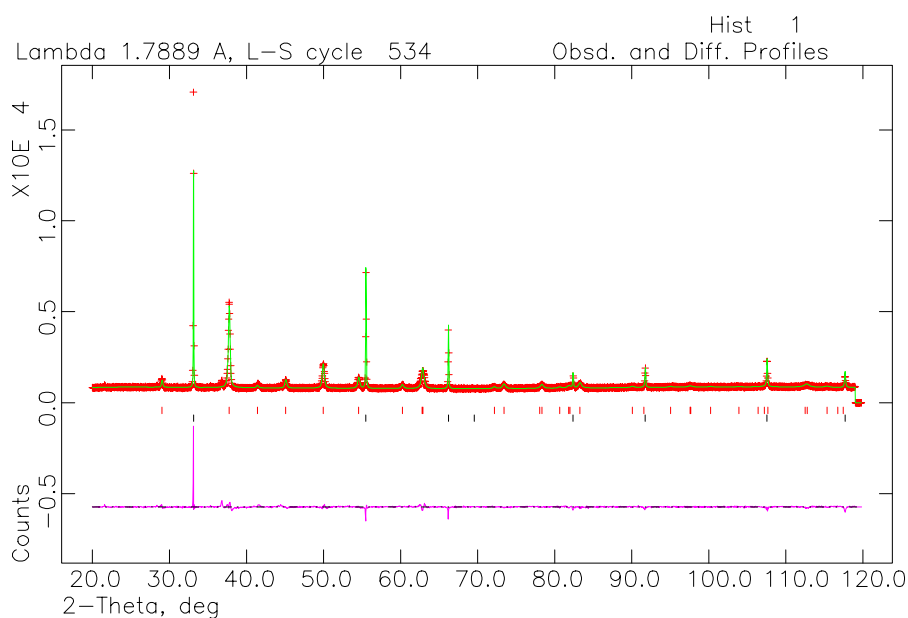


Figure A5.9: Rietveld refinement of the diffraction pattern for $\text{Mg}_{0.9}\text{Cd}_{0.1}\text{CO}_3$ with Si standard. Purple line shows the difference between the calculated and observed intensities. $R^2 = 0.0507$, $\Gamma = 0.4799 \cdot 10^2$

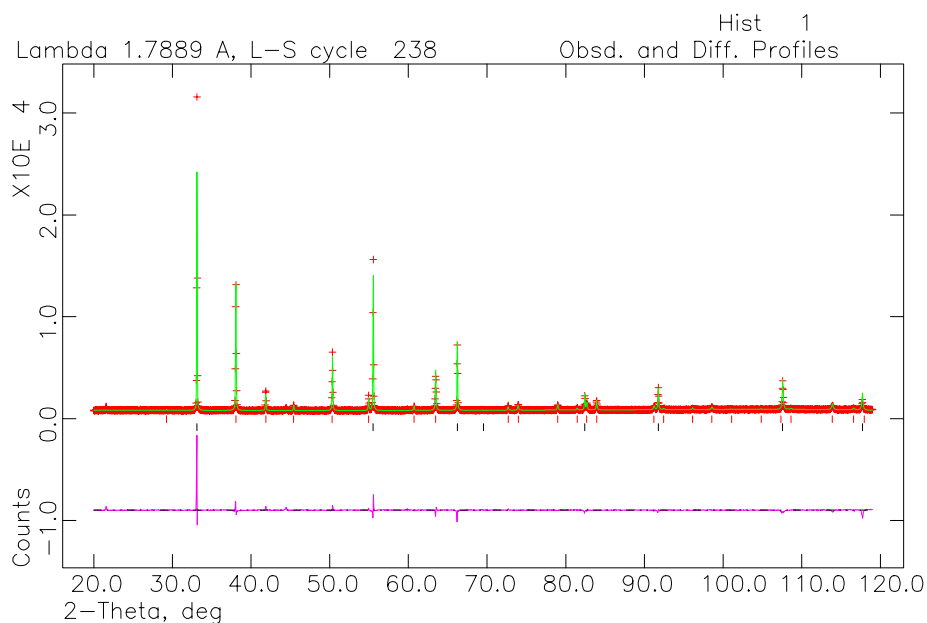


Figure A5.10: Rietveld refinement of the diffraction pattern for MgCO_3 with Si standard. Purple line shows the difference between the calculated and observed intensities. $R^2 = 0.0625$, $\Gamma = 0.1221 \cdot 10^2$

Sample synthesised at 800°C, 1GPa, 1 hour.

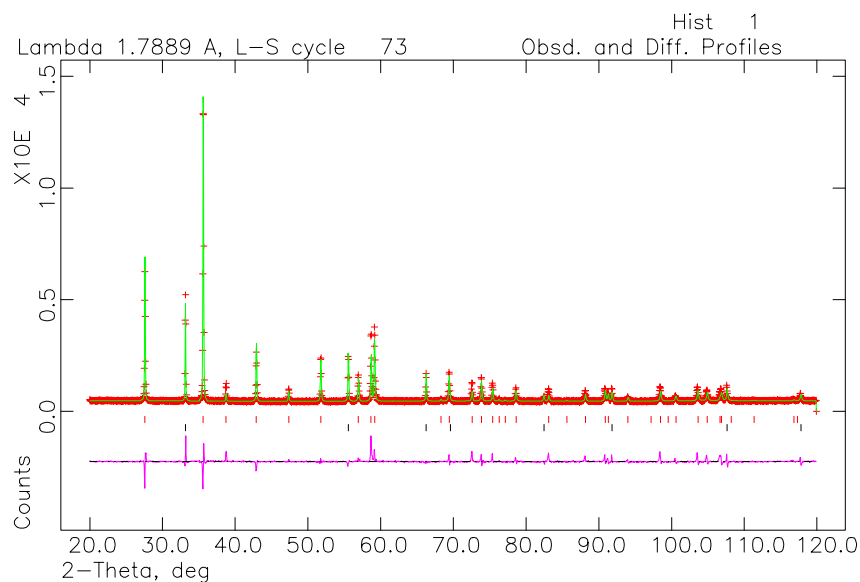


Figure A5.11: Rietveld refinement of the diffraction pattern for $\text{Mg}_{0.1}\text{Cd}_{0.9}\text{CO}_3$ with Si standard. Purple line shows the difference between the calculated and observed intensities. $R^2 = 0.0943$, $\Gamma = 0.1314 \times 10^2$

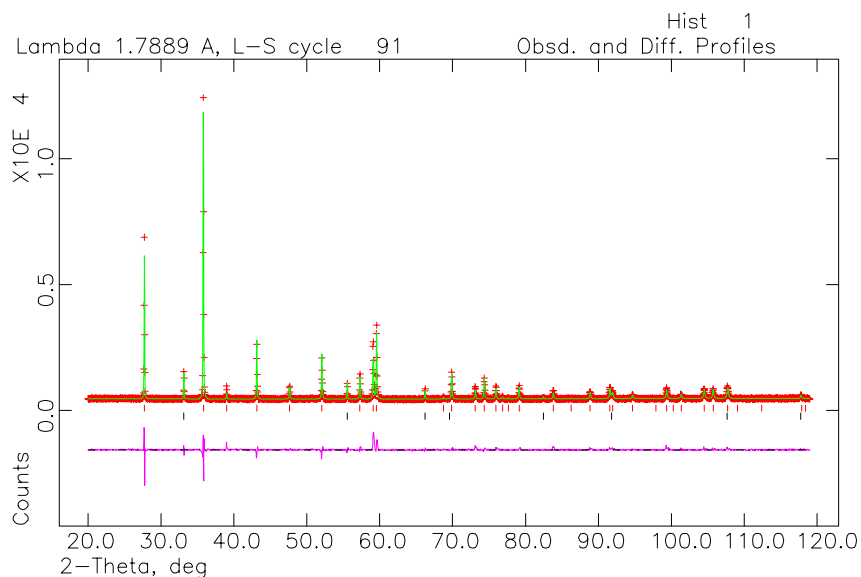


Figure A5.12: Rietveld refinement of the diffraction pattern for $\text{Mg}_{0.2}\text{Cd}_{0.8}\text{CO}_3$ with Si standard. Purple line shows the difference between the calculated and observed intensities. $R^2 = 0.0661$, $\Gamma = 0.1123 \times 10^2$

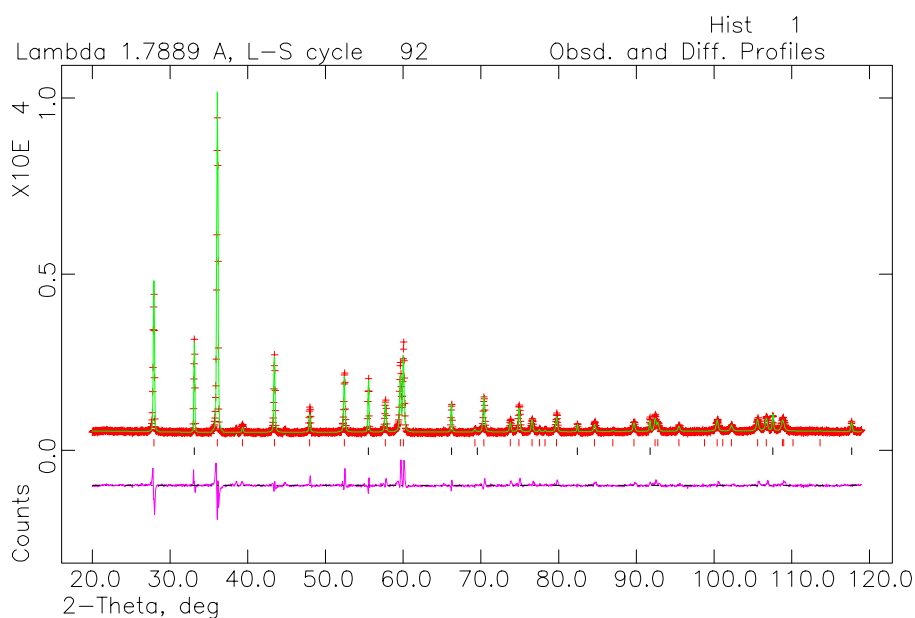


Figure A5.13: Rietveld refinement of the diffraction pattern for $\text{Mg}_{0.3}\text{Cd}_{0.7}\text{CO}_3$ with Si standard. Purple line shows the difference between the calculated and observed intensities. $R^2 = 0.0787$, $\Gamma = 0.1680 \times 10^2$

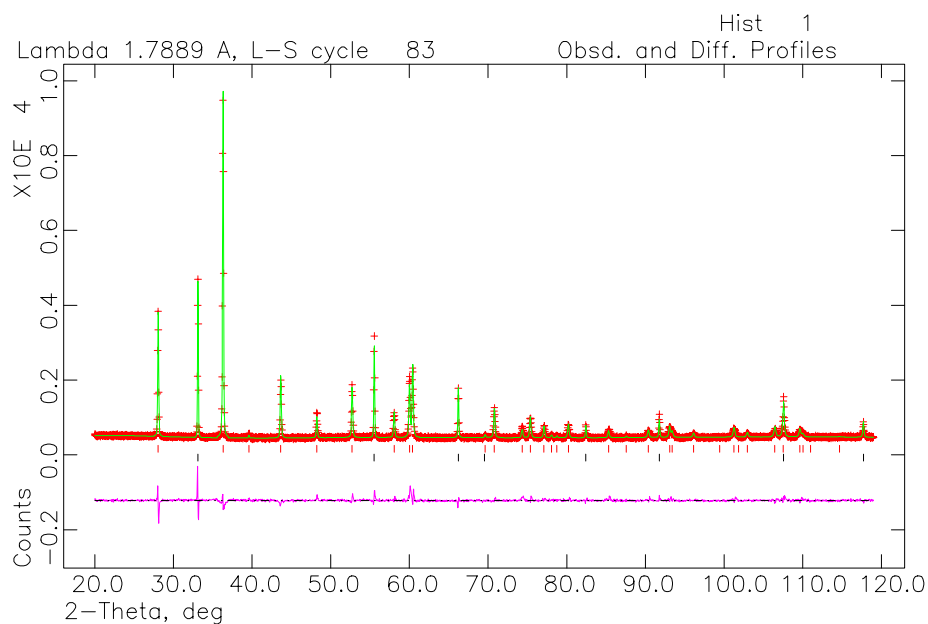


Figure A5.14: Rietveld refinement of the diffraction pattern for $\text{Mg}_{0.4}\text{Cd}_{0.6}\text{CO}_3$ with Si standard. Purple line shows the difference between the calculated and observed intensities. $R^2 = 0.0570$, $\Gamma = 0.1498 \times 10^2$

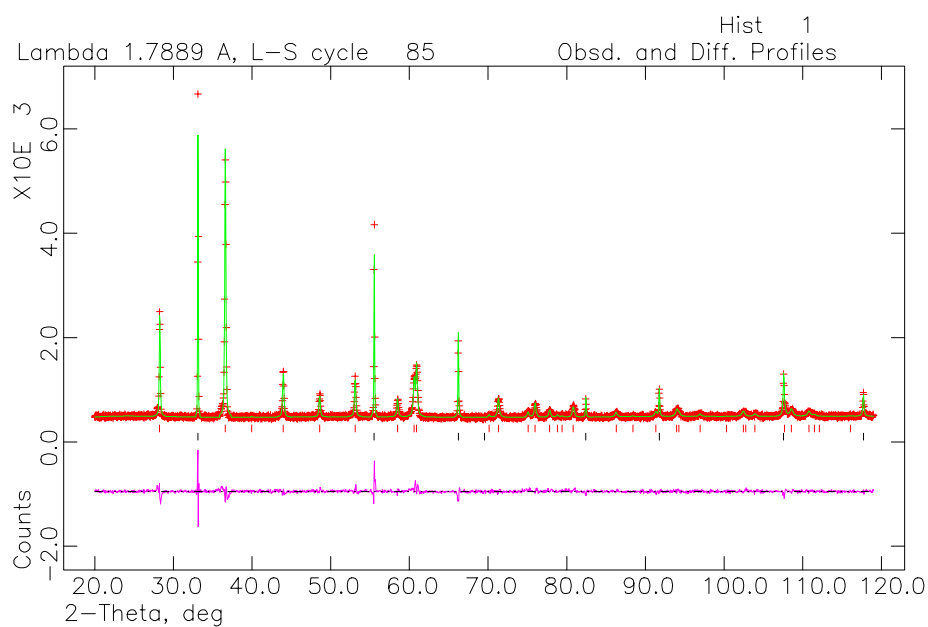


Figure A5.15: Rietveld refinement of the diffraction pattern for $\text{Mg}_{0.5}\text{Cd}_{0.5}\text{CO}_3$ with Si standard. Purple line shows the difference between the calculated and observed intensities. $R^2 = 0.0495$, $\Gamma = 0.2961 \times 10^2$

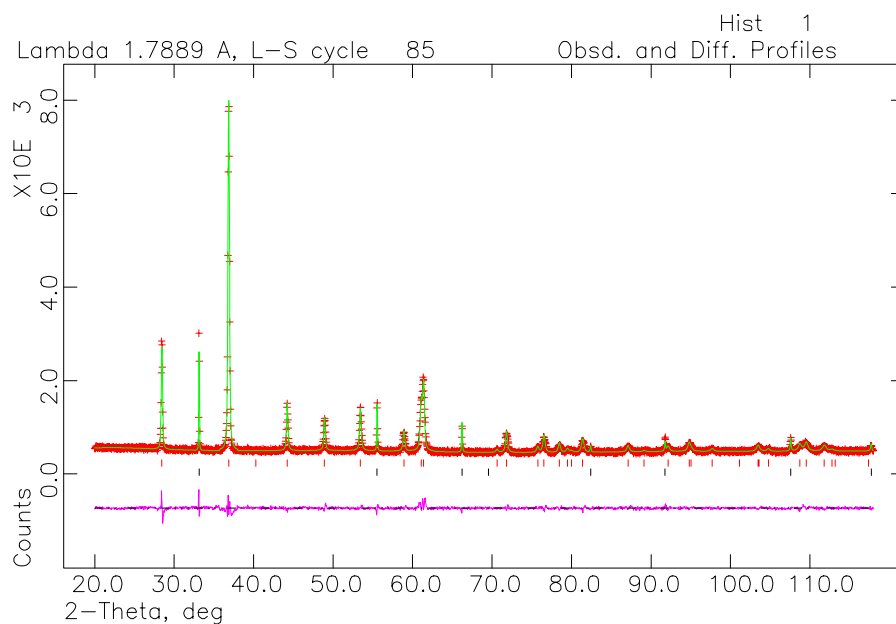


Figure A5.16: Rietveld refinement of the diffraction pattern for $\text{Mg}_{0.6}\text{Cd}_{0.4}\text{CO}_3$ with Si standard. Purple line shows the difference between the calculated and observed intensities. $R^2 = 0.0459$, $\Gamma = 0.3248 \times 10^2$

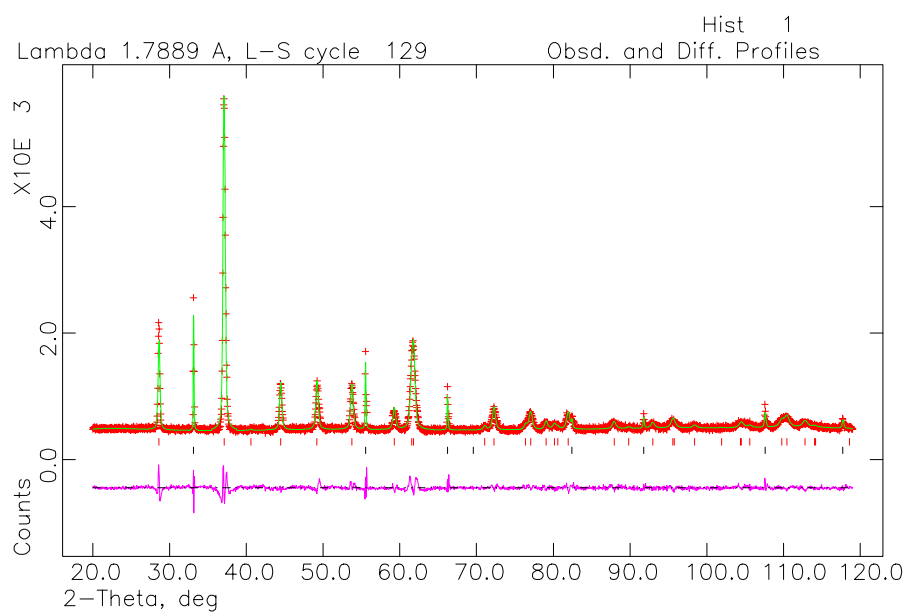


Figure A5.17: Rietveld refinement of the diffraction pattern for $\text{Mg}_{0.7}\text{Cd}_{0.3}\text{CO}_3$ with Si standard. Purple line shows the difference between the calculated and observed intensities. $R^2 = 0.0568$, $\Gamma = 0.4615 \times 10^2$

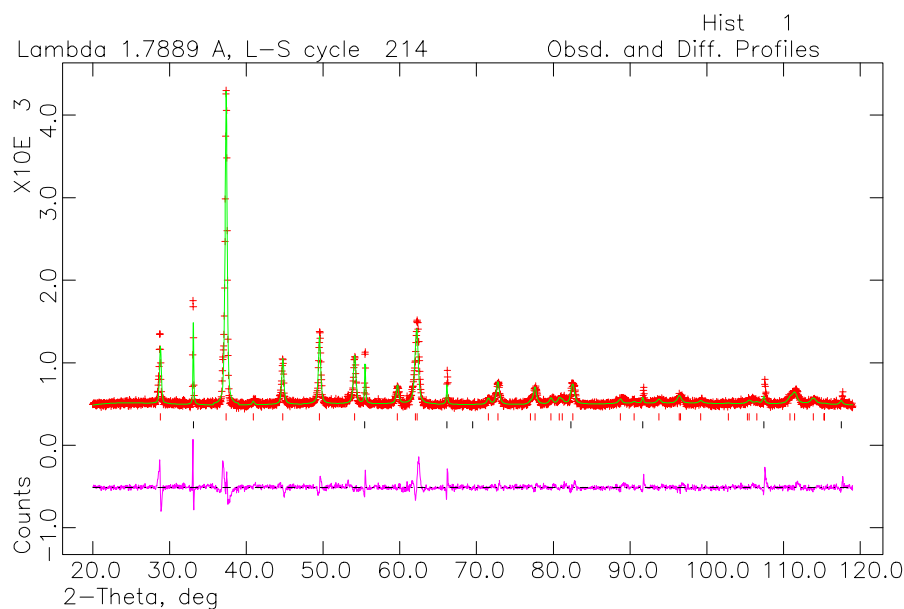


Figure A5.18: Rietveld refinement of the diffraction pattern for $\text{Mg}_{0.8}\text{Cd}_{0.2}\text{CO}_3$ with Si standard. Purple line shows the difference between the calculated and observed intensities. $R^2 = 0.0658$, $\Gamma = 0.4998 \times 10^2$

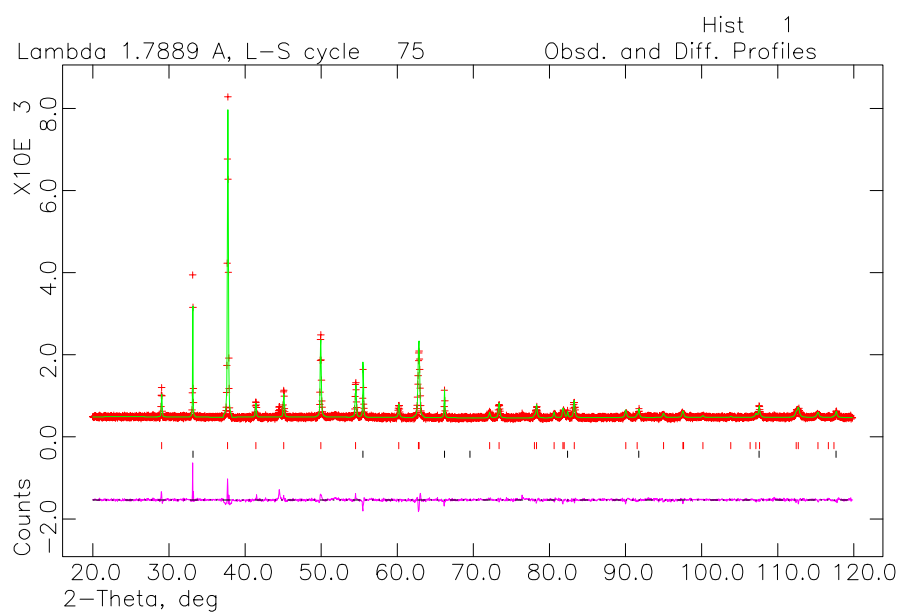


Figure A5.19: Rietveld refinement of the diffraction pattern for $\text{Mg}_{0.9}\text{Cd}_{0.1}\text{CO}_3$ with Si standard. Purple line shows the difference between the calculated and observed intensities. $R^2 = 0.0572$, $\Gamma = 0.1819 \times 10^2$

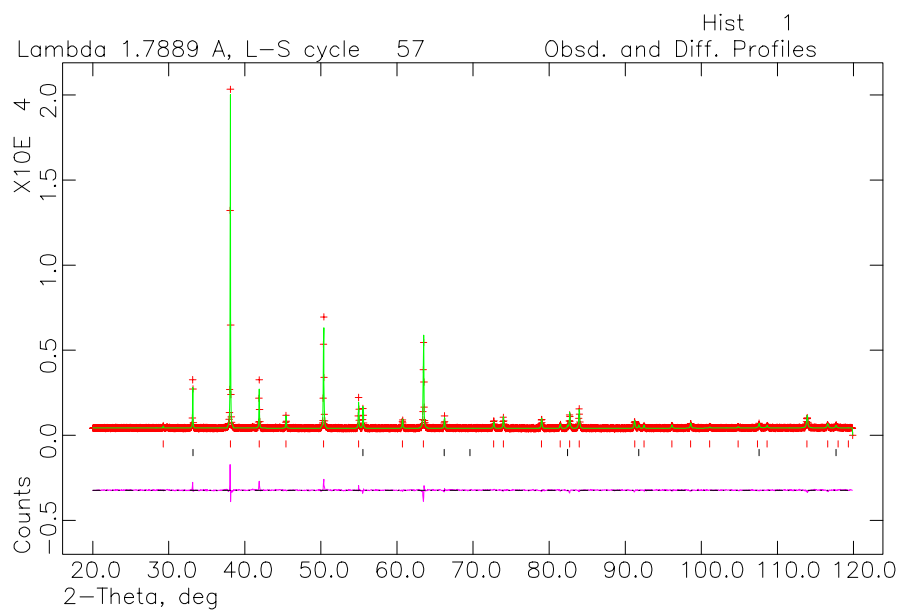


Figure A5.20: Rietveld refinement of the diffraction pattern for MgCO_3 with Si standard. Purple line shows the difference between the calculated and observed intensities. $R^2 = 0.0554$, $\Gamma = 0.1052 \times 10^2$

Sample synthesised at 600°C, 1GPa, 19 hours.

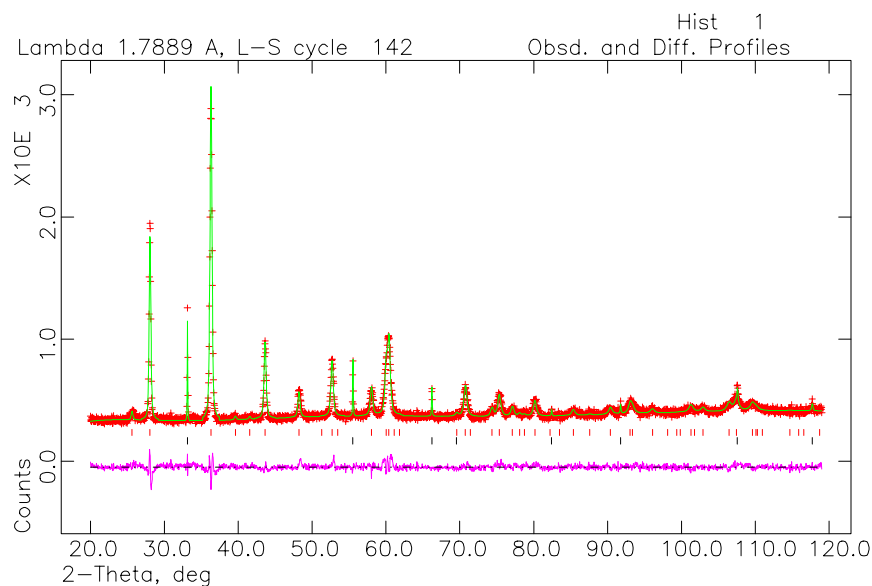


Figure A5.21: Rietveld refinement of the diffraction pattern for $\text{Mg}_{0.4}\text{Cd}_{0.6}\text{CO}_3$ with Si standard. Purple line shows the difference between the calculated and observed intensities. $R^2 = 0.0479$, $\Gamma = 0.4962 \times 10^2$

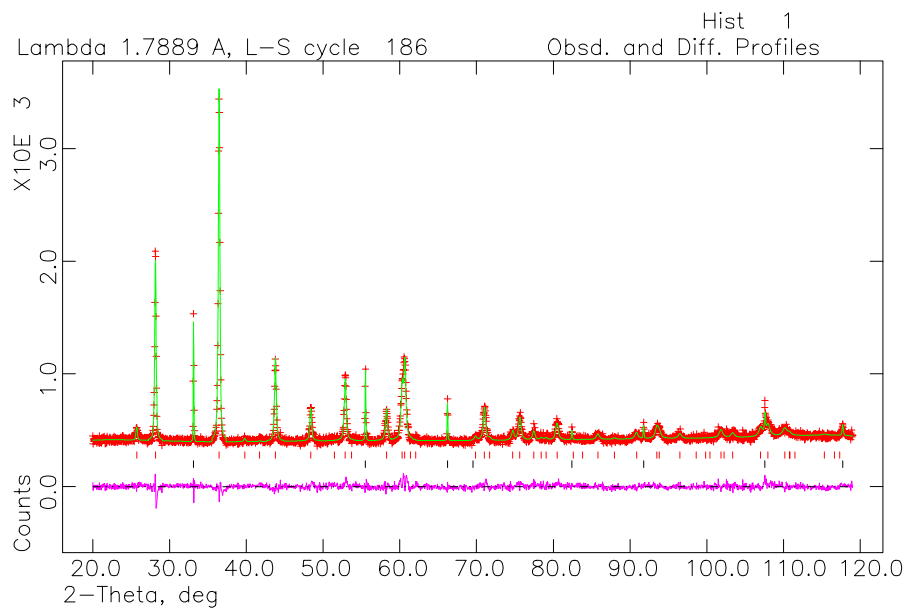


Figure A5.22: Rietveld refinement of the diffraction pattern for $\text{Mg}_{0.45}\text{Cd}_{0.55}\text{CO}_3$ with Si standard. Purple line shows the difference between the calculated and observed intensities. $R^2 = 0.0440$, $\Gamma = 0.4035 \times 10^2$

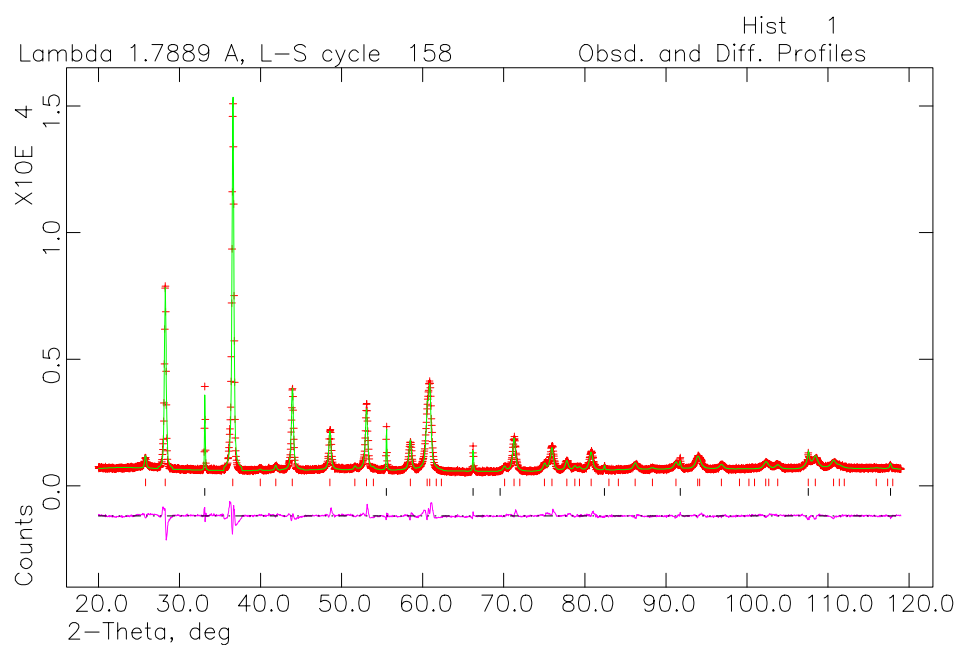


Figure A5.23: Rietveld refinement of the diffraction pattern for $\text{Mg}_{0.5}\text{Cd}_{0.5}\text{CO}_3$ with Si standard. Purple line shows the difference between the calculated and observed intensities. $R^2 = 0.0727$, $\Gamma = 0.4790 \times 10^2$

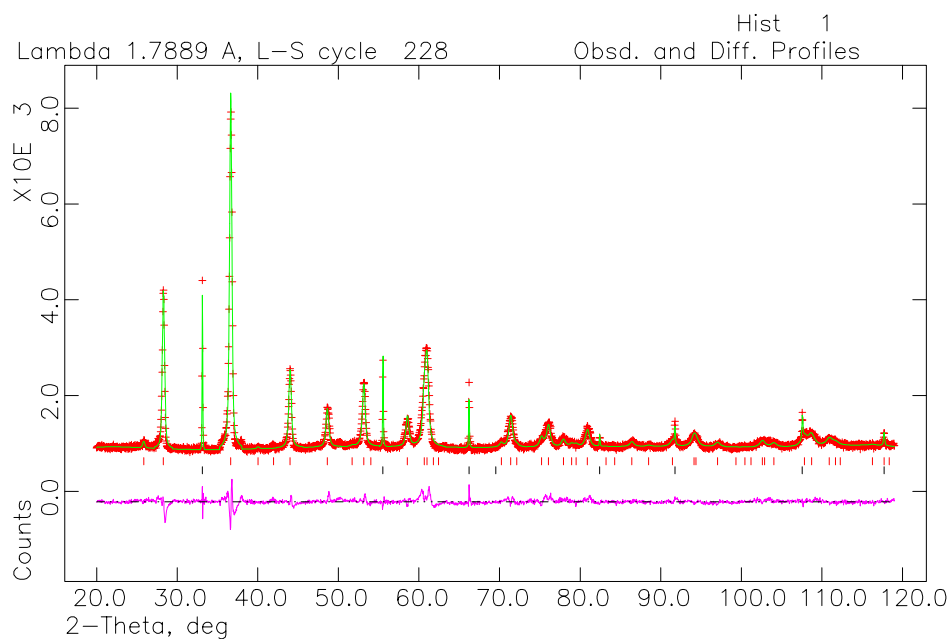


Figure A5.24: Rietveld refinement of the diffraction pattern for $\text{Mg}_{0.55}\text{Cd}_{0.45}\text{CO}_3$ with Si standard. Purple line shows the difference between the calculated and observed intensities. $R^2 = 0.0451$, $\Gamma = 0.6052 \times 10^2$

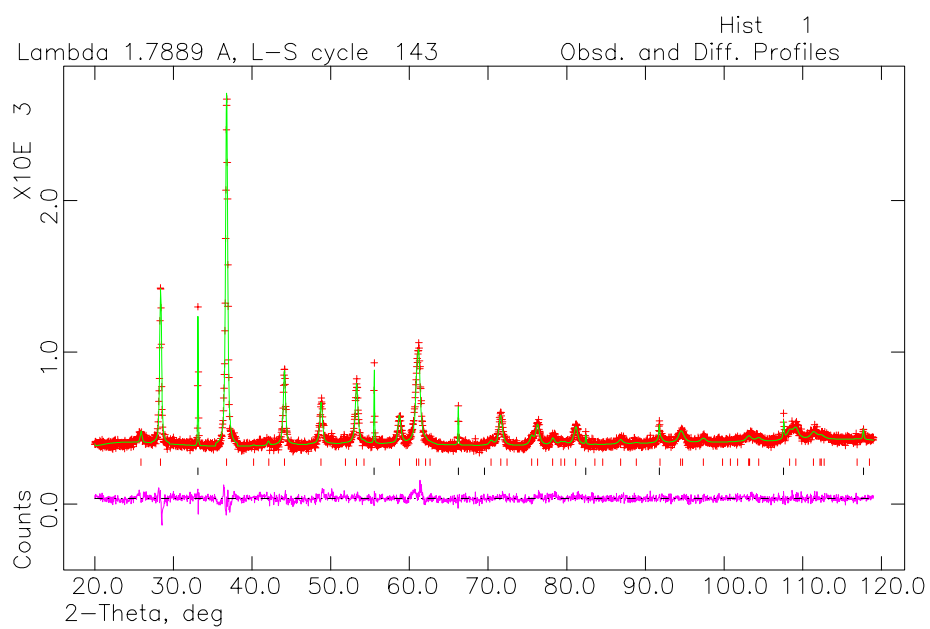


Figure A5.25: Rietveld refinement of the diffraction pattern for $\text{Mg}_{0.6}\text{Cd}_{0.4}\text{CO}_3$ with Si standard. Purple line shows the difference between the calculated and observed intensities. $R^2 = 0.0436$, $\Gamma = 0.6123 \times 10^2$

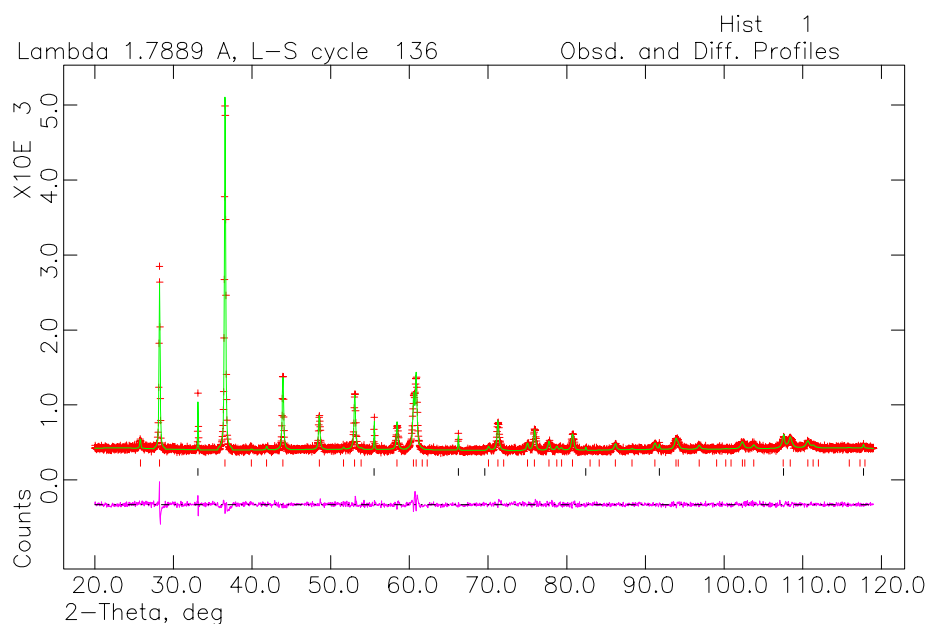


Figure A5.26: Rietveld refinement of the diffraction pattern for $\text{Mg}_{0.5}\text{Cd}_{0.5}\text{CO}_3$ with Si standard. Synthesised at 650°C for 120 hours and 1 GPa. Purple line shows the difference between the calculated and observed intensities. $R^2 = 0.0448$, $\Gamma = 0.3337 \times 10^2$

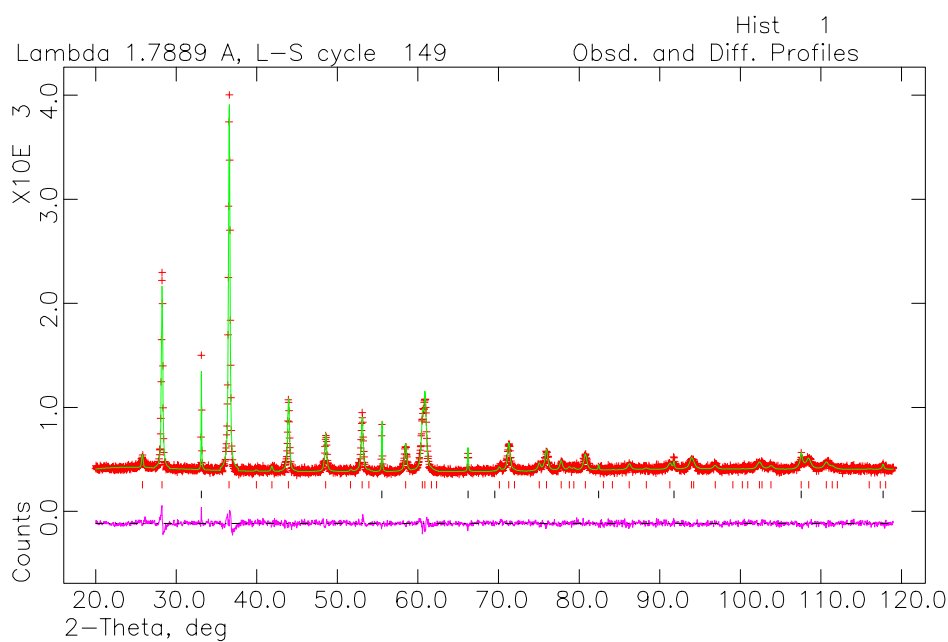


Figure A5.27: Rietveld refinement of the diffraction pattern for $\text{Mg}_{0.5}\text{Cd}_{0.5}\text{CO}_3$ with Si standard. Synthesised at 600°C for 96 hours and 1 GPa. Purple line shows the difference between the calculated and observed intensities. $R^2 = 0.0427$, $\Gamma = 0.4688 \times 10^2$

Samples synthesised at 500°C, 1GPa, 96 hours.

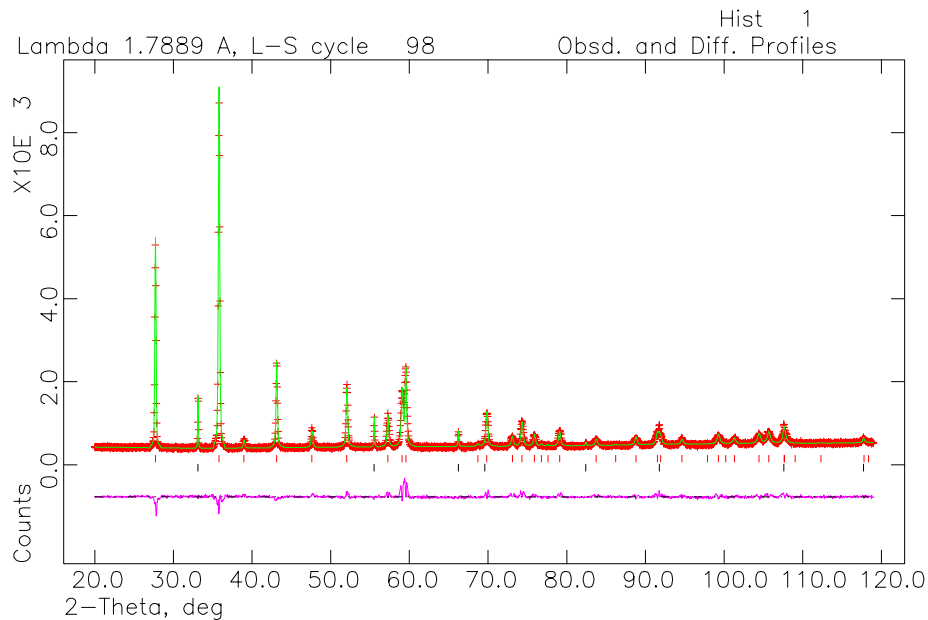


Figure A5.28: Rietveld refinement of the diffraction pattern for $\text{Mg}_{0.2}\text{Cd}_{0.8}\text{CO}_3$ with Si standard. Purple line shows the difference between the calculated and observed intensities. $R^2 = 0.0585$, $\Gamma = 0.2969 \times 10^2$

Figure A5.29: Rietveld refinement of the diffraction pattern for $\text{Mg}_{0.3}\text{Cd}_{0.7}\text{CO}_3$ with Si standard. Purple line shows the difference between the calculated and observed intensities. $R^2 = 0.0509$, $\Gamma = 0.9153 \times 10^2$

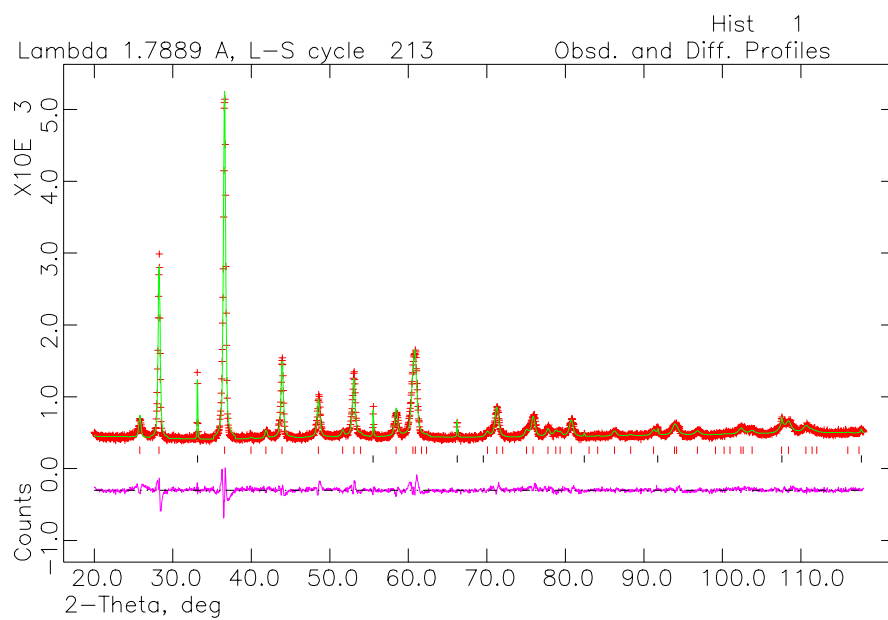


Figure A5.30: Rietveld refinement of the diffraction pattern for $\text{Mg}_{0.5}\text{Cd}_{0.5}\text{CO}_3$ with Si standard. Purple line shows the difference between the calculated and observed intensities. $R^2 = 0.0569$, $\Gamma = 0.5828 \times 10^2$

Samples synthesised at 700°C, 1GPa, 24 hours.

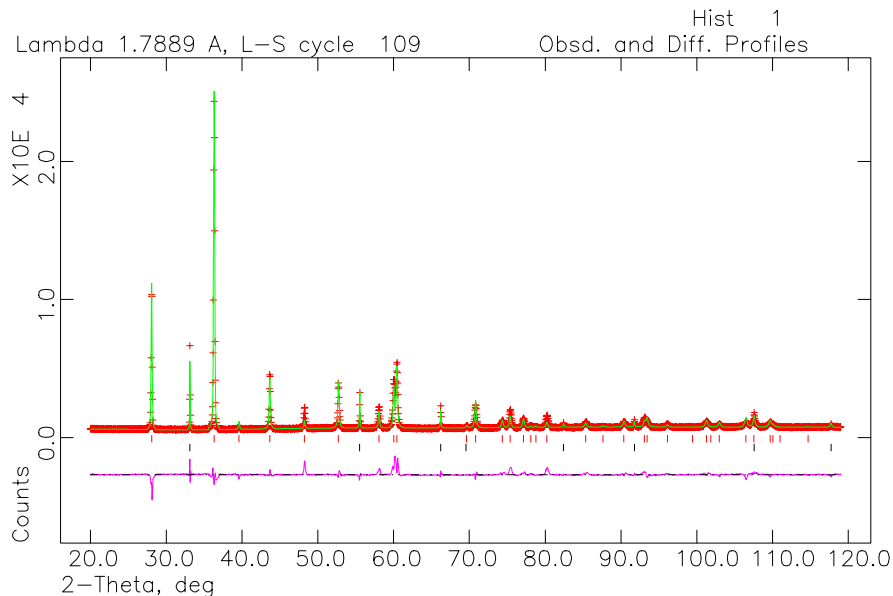


Figure A5.31: Rietveld refinement of the diffraction pattern for $\text{Mg}_{0.4}\text{Cd}_{0.6}\text{CO}_3$ with Si standard. Purple line shows the difference between the calculated and observed intensities. $R^2 = 0.0978$, $\Gamma = 0.2332 \times 10^2$

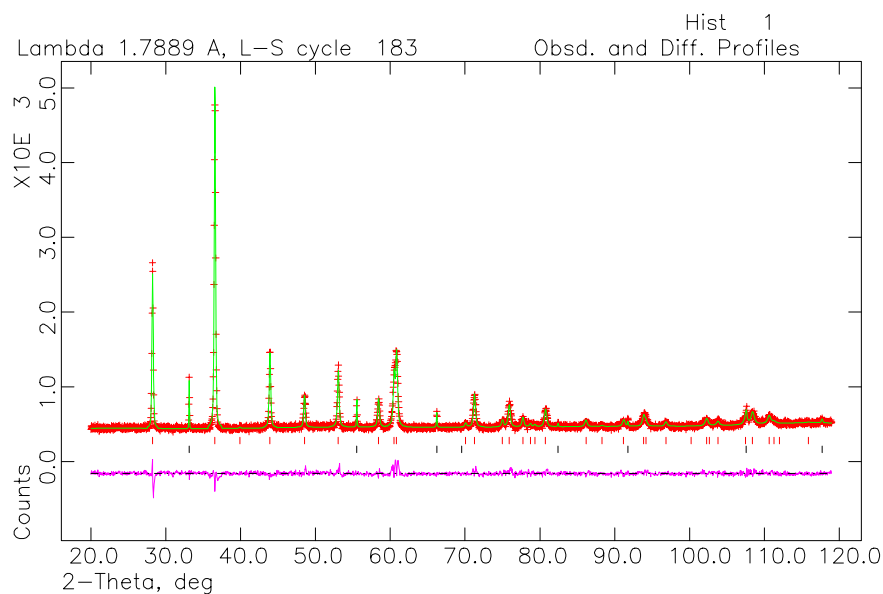


Figure A5.32: Rietveld refinement of the diffraction pattern for $\text{Mg}_{0.5}\text{Cd}_{0.5}\text{CO}_3$ with Si standard. Purple line shows the difference between the calculated and observed intensities. $R^2 = 0.0440$, $\Gamma = 0.3204 \times 10^2$

Experiments disordered from the sample for Figure A5.30

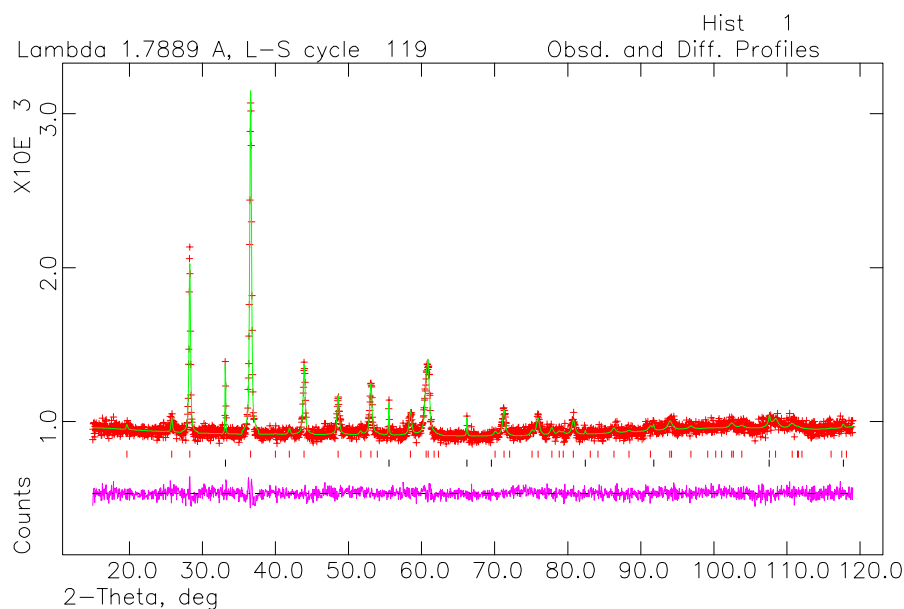


Figure A5.33: Rietveld refinement of the diffraction pattern for $\text{Mg}_{0.5}\text{Cd}_{0.5}\text{CO}_3$ with Si standard. Disordered at 600°C, 1GPa for 20 minutes. Purple line shows the difference between the calculated and observed intensities. $R^2 = 0.0261$, $\Gamma = 0.5469 \times 10^2$

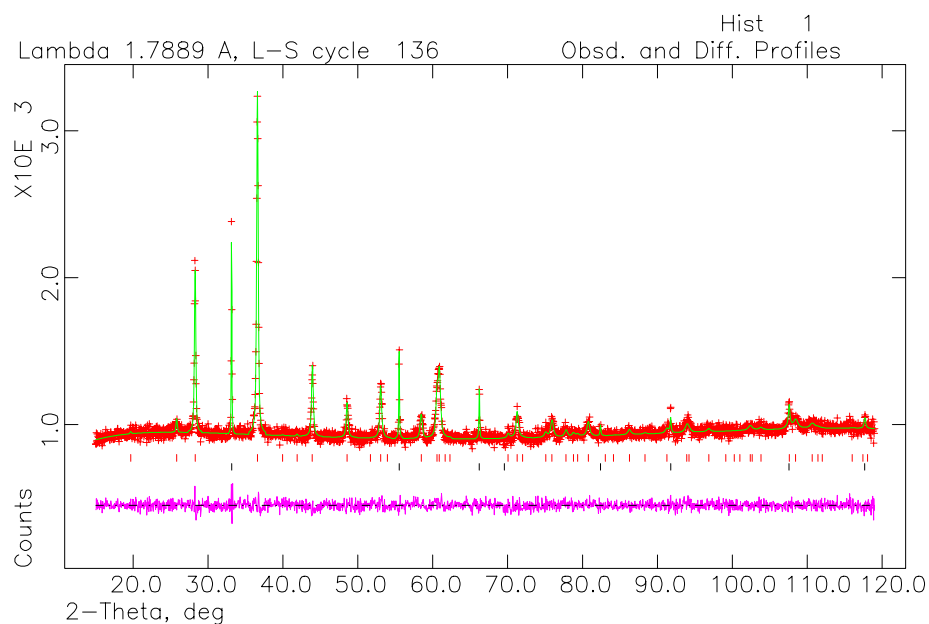


Figure A5.34: Rietveld refinement of the diffraction pattern for $\text{Mg}_{0.2}\text{Cd}_{0.8}\text{CO}_3$ with Si standard. Disordered at 600°C, 1GPa, 48 hours. Purple line shows the difference between the calculated and observed intensities. $R^2 = 0.0256$, $\Gamma = 0.4851 \times 10^2$

Erklärung

Hiermit erkläre ich, daß ich die vorliegende Arbeit selbständig verfaßt und keine anderen als die von mir angegebenen Quellen and Hilfsmittel benutzt habe.

Ferner erkläre ich, daß ich nicht anderweitig mit oder ohne Erfolg versucht habe, eine Dissertation einzureichen. Ich habe keine gleichartige Doktorprüfung an einer anderen Hochschule endgültig nicht bestanden.

Bayreuth, den 25 Juni 2004

Fiona Bromiley